STUDY OF THE EFFECTS OF NUCLEAR STRUCTURE AND RELATIVE ORIENTATIONS IN HEAVY ION REACTIONS

THESIS

SUBMITTED FOR THE AWARD OF THE DEGREE OF

DOCTOR OF PHILOSOPHY

BY

BIRBIKRAM SINGH

REGN. NO.- 9031551

SCHOOL OF PHYSICS AND MATERIALS SCIENCE

THAPAR UNIVERSITY

PATIALA-147 004, INDIA

April, 2009

Dedicated to My Beloved Parents

CERTIFICATE

This is to certify that this thesis entitled "**Study of the Effects of Nuclear Structure and Relative Orientations in Heavy Ion Reactions**" is being submitted by Mr. BirBikram Singh in fulfillment of the requirements for the award of Degree of Doctor of Philosophy in the School of Physics and Material Science, Thapar University, Patiala, is a record of candidate's own work carried out by him under our supervision. The matter presented in this thesis has not been submitted in part or full for the award of any degree in any other University or Institute.

Supervisors

(Dr. Manoj K. Sharma)
Assistant Professor
School of Physics & Material Science
Thapar University
Patiala-147 004, Punjab
India

(Prof. Raj K. Gupta)
DST Ramanna Fellow
Department of Physics
Panjab University
Chandigarh-160 014
India

Acknowledgements

In the first place, the author record his profound gratitude to his Ph.D. thesis supervisor(s) Dr. Manoj K. Sharma, Assistant Professor, School of Physics and Materials Science, Thapar University, Patiala, and Dr. Raj K. Gupta, Professor of Physics (Retd.) and DST Ramanna Fellow, Physics Department, Panjab University, Chandigarh, for their illuminating guidance and unflinching encouragement to complete this thesis work successfully. Dr. Manoj K. Sharma's constant support, dynamic supervision, valuable and innovative suggestions enabled the author to carry out this work effectively. Dr. Raj K. Gupta with his vast research experience, a constant oasis of ideas and passion for scientific research, has inspired the author and enriched his growth as a student, a researcher and a scientist would be. It is a fortune for the author for being associated with them in research field.

The author offers his special thanks to Prof. O.P. Pandey, Head School of Physics and Materials Science, Thapar University, Patiala, for providing all the necessary facilities in the department. Also, the author wishes to express his thankfulness to all the faculty and staff of the School for their kind support. The author is thankful to Prof. K.K. Raina, Deputy Director, and Prof. N.K. Verma, Dean Student Welfare, for their encouragement and constant moral support to accomplish this task. The author also acknowledges the useful suggestions of the members of his doctoral committee Prof. R. K. Sharma and Dr. Sunil Kumar.

The author acknowledges with thanks the co-operation and encouragement extended by his friends and colleagues in the Heavy Ion Reactions Theory group at Chandigarh, particularly, Dr. Rajesh Sharma, Dr. Dalip Singh, Mr. Sham Kumar Arun, Dr. Narinder Singh, Dr. Makhan Singh Mehta, Dr. Monika Manhas, Mrs. Niyti Sharma and Mr. Raj Kumar for their fruitful discussions and novel views. Thanks will not be complete if author does not mention the names of Mrs. Shefali Kanwar, Mr. Vishal Kumar and other doctoral scholars of School of Physics and Materials Science, Thapar University, Patiala for their support. Thanks are also due to Dr. Ashok Kumar, Dr. Amandeep Sood, Dr. Ameeya Bhagwat and Dr. Sukhjit Singh Dhindsa for their encouragement and support.

The author deeply thanks Prof. I.K. Kataria, Director and Dr. Verinder Kaur, Princi-

pal, Swami Vivekanand institute of Engineering and Technolgy, Patiala, for their encouragement and support. Special thanks are reserved for my ever cheerful, dear students, without whose loving and careing attitude throughout, the life would not be so active and good. The author cheerfully acknowledges the support and wishes of his colleagues Mrs. (Dr.) Archana Gupta, Mr. Naveen Thakur and Ms. Ruchi Aneja.

The author can not forget to thank Madam Gupta for her motherly affection and care, along with Madam Sharma for her best wishes.

Most importantly, the author is indebted to his parents who worked industriously to support the family without complaining, in spite of hardships and spared no effort to provide the best possible environment for him to achieve this target. This work is dedicated to his parents (Mr. Jagdish Singh and Mrs. Ravinder Kaur) for their love and sacrifice. Thanks are also due to all other members of his family for their support. Gratitude and regard is recorded for the inspiration and cheerful encouragement offered by his father-in law Mr. Dalbir Singh and uncle Mr. Sarabjit Singh. Acknowledgements will not be complete if author do not mention the name of his friend Mr. Bikramjit Singh for his moral support and useful discussions.

Last but not the least, the author records a special note of admiration and gratitude for his loving wife Kuljit Kaur and cute son Jagbir Singh whose interests were ignored during the course of this work. Her patience, co-operation and understanding paved the way to achieve this academic goal.

The author feels that the chain of gratitude would be definitely incomplete without thanking the Almighty, the prime mover, for inspiring and guiding him (the humble being) to complete this task successfully.

Patiala
April, 2009.

(BirBikram Singh)

List of Publications

I. International Journals:

1. Decay of $^{246}Bk^*$ formed in similar entrance channel reactions of ^{11}B+^{235}U and ^{14}N+^{232}Th at low energies using the dynamical cluster-decay model,
   BirBikram Singh, Manoj K. Sharma and Raj K. Gupta,
   Phys. Rev. **C 77**, 054613 (2008).

2. Entrance-channel effects in the dynamical cluster decay model for the decay of hot and rotating compound nucleus ^{48}Cr at E^*_{CN} ≈60 MeV,
   BirBikram Singh, Manoj K. Sharma, Raj K. Gupta and W. Greiner,
   Int. J. of Mod. Phys. E (Nucl. Phys.) **15**, 699 (2006).

3. Seeger's liquid drop energy and it's temperature dependence,
   BirBikram Singh, Manoj K. Sharma and Raj K. Gupta,
   Parmana J. Phys.- to be submitted.

4. Role of higher multi-pole deformations and orientations in exotic cluster radioactivity,
   Raj K. Gupta, Sham K. Arun, **BirBikram Singh**, Manoj K. Sharma,
   Phys. Rev. **C .**- to be submitted.

II. In Proceedings of Symposia and Conferences:

1. Role of higher multi-pole deformations and orientations in the ^{208}Pb-daughter cluster radioactivity,
   BirBikram Singh, Sham K. Arun, Shefali Kanwar, Manoj K. Sharma and

Raj K. Gupta,

DAE Nucl. Phys. Symp., IIT Roorkee, Uttarakhand, **53**, 261 (2008).

2. Fission and quasi-fission processes in the decay of hot and rotating compound nucleus $^{246}Bk^{*}$,

   BirBikram Singh, Shefali Kanwar, Manoj K. Sharma and Raj K. Gupta,

   11^{th} Punjab Science Congress, Thapar University, Patiala, February, 2008.

3. Role of deformations and orientations in the cluster decay of ^{242}Cm nucleus,

   BirBikram Singh, Manoj K. Sharma and Raj K. Gupta,

   11^{th} Punjab Science Congress, Thapar University, Patiala, February, 2008.

4. Identification of sub-structure in the fission of $^{246}Bk^{*}$ formed in $^{11}B+^{235}U$,

   BirBikram Singh, Manoj K. Sharma, Shefali Kanwar and Raj K. Gupta,

   DAE Nucl. Phys. Symp., Sambalpur University, Burla, Orissa , **52**, 429 (2007).

5. Evaporation residues, fission and capture cross-sections using the dynamical cluster-decay model,

   Raj K. Gupta, Manoj K. Sharma, Monika Manhas, **BirBikram Singh** and Niyti Sharma,

   Fourth **International conference on** "Fission and Properties of Neutron-Rich Nuclei" Sanibel Island, Florida, November 11-17, 2007.

6. Role of deformation and orientations in the fission decay of $^{246}Bk^{*}$,

   BirBikram Singh and Manoj K. Sharma,

   National Conference on Emerging Trends in Engineering Materials, TIET, Patiala, February 1-3, 2007.

7. Fission cross-sections of $^{246}Bk^{*}$ formed in $^{14}N+^{232}Th$ reaction, using dynamical cluster-decay model,

   BirBikram Singh, Manoj K. Sharma and Raj K. Gupta,

   DAE-BRNS Nucl. Phys. Symp., MSR University of Baroda, Vadodra, **51**, 345 (2006).

8. Decay of heavier compound systems using Dynamical Cluster Decay Model,
   BirBikram Singh, Manoj K. Sharma and Raj K. Gupta,
   International workshop on "Nuclear Structure Physics at the Extremes: New Directions", H P Univ. Shimla (2005).

9. Role of Angular Momentum in the Decay of Hot ^{48}Cr,
   BirBikram Singh and Manoj K. Sharma,
   National Conf. on Adv. in Condensed matter Physics, TIET, Patiala, Pages 138-143, (2005).

10. Entrance Channel Effects using the Dynamical Cluster Decay Model: Decay of ^{48}Cr,
    Manoj K. Sharma, **BirBikram Singh**, Dalip Singh and Raj K. Gupta,
    DAE Nucl. Phys. Symp., B H Univ. Banaras, **47 B**, 276 (2004).

11. Fission and Cluster Decay of ^{48}Cr Formed in Heavy Ion Reactions,
    Manoj K. Sharma and **BirBikram Singh**,
    DAE Nucl. Phys. Symp., Bombay, **46 B**, 270 (2003).

Contents

List of Figures

List of Tables

Abstract

The work presented in this thesis deals with the study of heavy ion reaction dynamics using the Dynamical Cluster-decay Model (DCM). DCM is used to study the decay of excited (hot and rotating) compound systems formed in low energy heavy ion reactions, including the deformations and orientations degrees of freedom for reactants/products. To study the ground state decays, the exotic cluster radioactivity, we have used the Preformed Cluster-decay Model (PCM), which also includes the deformation and orientation effects of daughter and cluster nuclei. Both DCM and PCM are based on Quantum Mechanical Fragmentation Theory (QMFT).

Chapter 1 outlines a brief introduction to the experimental and theoretical studies related to heavy ion reaction dynamics and the process of cluster radioactivity. An overview of current status of the related research in nuclear physics and various models have been discussed in this chapter. The role of angular momentum, excitation energy, entrance channel effects together with the effects of deformations and orientations in the fusion-fission process have been discussed briefly.

Chapter 2 gives the details of the methodology used in this thesis. Brief overview of the QMFT is given. The methods of calculating the fragmentation potentials, collective potentials and kinetic energy part of the Hamiltonian are discussed, together with the solution of the stationary Schrödinger wave equation. The details are given for the effect of deformed and oriented nuclei in the proximity, Coulomb and angular momentum potentials. The PCM, which has been used for the calculations of decay half-lives of radioactive nuclei to various clusters formed in ^{208}Pb-daughter cluster radioactivity,

is given. Here also the deformation and orientation effects of daughter and clusters are duly incorporated. Finally, the DCM which is used to calculate the decay properties such as decay cross sections, kinetic energies etc. of compound nuclei have been discussed in detail.

In **Chapter 3**, the temperature dependent binding energies are calculated, which is highly significant keeping in mind the temperature dependence of collective potential used in DCM, to study the decay of excited compound systems. We have refitted the bulk $\alpha(0)$ and neutron proton asymmetry a_a constants, in the Seeger's semi-empirical mass formula at T=0, for all available isotopes of the periodic table upto Z=118. These constants are then used to calculate the temperature dependent liquid drop energies, in reference to the work of Davidson et al., which itself is based upon Seeger's semi-empirical mass formula.

In **Chapter 4**, the entrance-channel effects in the decay of hot and rotating compound nucleus $^{48}Cr^*$, formed in symmetric ^{24}Mg+^{24}Mg and asymmetric ^{36}Ar+^{12}C reactions, are studied as collective clusterization process, for emissions of both the light particles (LPs) as well as the intermediate mass fragments (IMFs), with in the dynamical cluster-decay model (DCM). We find that the little differences observed in the decay of equilibrated compound nucleus $^{48}Cr^*$, formed in the two entrance channels with about the same excitation energy, are *not* in variance with the Bohr's independence hypothesis. In other words, the present study confirms the entrance-channel independence of the decay of compound nucleus $^{48}Cr^*$ formed due to different target-projectile combinations with similar excitation energies. The collective clusterization process is shown to contain the complete structure of the measured fragment cross sections as well as average total kinetic energies.

In **Chapter 5**, based on the extended PCM to include the deformation and orientation degrees of freedom, the phenomenon of cluster radioactivity have been studied. This work has been carried out to investigate the possible role of deformed and oriented nuclei besides well established shell effects in cluster radioactivity. For the purpose we have chosen only those cluster decays for which daughter is always spherical and doubly

magic (N = 126, Z = 82) ^{208}Pb. The chosen deformed parents are ^{222}Ra, $^{226,228}Th$, ^{230}U, ^{231}Pa, $^{232,234}U$, $^{236,238}Pu$ and ^{242}Cm with corresponding observed clusters as ^{14}C, $^{18,20}O$, ^{22}Ne, ^{23}F, $^{24,26}Ne$, $^{28,30}Mg$ and ^{34}Si, respectively. Variance in both the key quantities of PCM, the preformation probability P_0 and penetrability P of clusters with and without invoking deformation and orientation effects has been discussed. The calculated decay half-lives for all such cluster-decays are in good comparison with measured values.

In **Chapter 6**, the decay of ^{246}Bk* nucleus, formed in entrance channel reactions ^{11}B+^{235}U and ^{14}N+^{232}Th at different incident energies, is studied by using the dynamical cluster-decay model (DCM) extended to include the deformations and orientations of nuclei. The main decay mode here is fission. The other (weaker) decay channels are the light particles evaporation (A$\leq$4) and intermediate mass fragments (5$\leq$A$\leq$20). All decay products are calculated as emissions of preformed clusters through the interaction barriers. The calculated fission cross sections σ_{fiss}, taken as a sum of the energetically favoured symmetric and near symmetric fragments ($A_{CN}/2 \pm 7$ and A=106-110 plus complementary fragments) show an excellent agreement with experimental data at all experimental incident c.m. energies for both the reactions, except for top three energies in the case of ^{11}B+^{235}U reaction. The disagreement between the DCM calculations and data at higher incident c.m. energies for the ^{11}B+^{235}U entrance channel is associated with the presence of additional effects of non-compound, quasi-fission (qf) component, in contradiction with the measured anisotropy effects which indicate the other entrance channel ^{14}N+^{232}Th to contain the non-compound nucleus contribution. The prediction of two fission windows, the symmetric fission (SF) and near symmetric or heavy mass fragments (HMFs), suggests the presence of fine structure of fission fragments, which also need an experimental verification. The only parameter of model is the neck length parameter $\triangle R$ whose value is shown to depend strongly on limiting angular momentum, which in turn depends on the use of sticking or non-sticking moment of inertia for angular momentum effects.

Finally, in **chapter 7**, we summarize the results of this work.

Chapter 1

Introduction

Understanding the fundamental nature of matter was an exclusive pursuit of scientists for a long time, almost two hundred years ago. It got great impetus, with the pioneering discoveries of radioactivity and electron during the last decade of 19^{th} century. Since then the microscopic world of atomic nucleus has been explored intensively. This study is named as nuclear physics. In an atom, nucleus is very small, dense region, sitting at its centre, consisting of nucleons (protons and neutrons). The nucleus is a little, positive center that makes up very little of the actual atom but plays an instrumental role in its properties and applications. It is quite an interesting story as to how the atomic nucleus was first discovered, by E. Rutherford in 1911, and perceived. The discovery of the Rutherford-Bohr model of the atom was followed by the advent of quantum mechanics developed by numerous physicists like de Broglie, Schrödinger, Heisenberg, Pauli, Dirac and others. The consistent efforts on the experimental and theoretical fronts finally led to the current understanding of a nucleus and the atom.

In an atomic nucleus, neutrons (neutral particles) and protons (positively charged particles) are held together by a strong nuclear force. Though information on exact nature of this force is still limited and not established analytically, like for the Coulomb force, much progress has been made towards its phenomenological understanding. Various models and theories have been proposed to understand the static and dynamic properties of the atomic nucleus. A light nucleus can contain hundreds of nucleons and with some approximations it can be treated as a classical system, rather than a quantum-mechanical

one, resulting into the liquid-drop model (macroscopic approach). It is assumed that the nucleus has an energy which arises partly from surface tension and partly from electrical repulsion of the protons. This model is able to reproduce many features of nuclei, including the general trend of binding energy per nucleon with respect to mass number, as well as the phenomenon of nuclear fission and fusion. But it fails to explain why nuclei with certain numbers of neutrons and protons (the magic numbers 2, 8, 20, 28, 50, 82, 126, ...) are particularly stable. Also it doesn't account for the different shapes of atomic nucleus. The problem related to magic numbers can be understood using the nuclear shell model (microscopic approach). This model uses the Pauli's principle for describing the structure of the nucleus in terms of energy levels or shells. Some other properties of the nuclei, which can not be explained by above mentioned models can be explained with a unified approach of these two models, called collective or unified model. In this model, nucleus is considered to consist of a core and extra core particles with the core being treated as inert or like a liquid drop. Over the years, in order to keep pace with the rapid accumulation of experimental data, nuclear models are being developed and have become integral part in the development of nuclear physics.

1.1 Cluster radioactivity

The radioactive nuclear decay studies have contributed immensely to the understanding of nuclear phenomena and properties in general, and nuclear structure in particular. The phenomenon of Cluster radioactivity, CR, which is the spontaneous emission of fragments heavier than alpha particle, is now established, since its theoretical prediction in the early 1980 [1] and experimental confirmation in 1984 [2]. It occupies an intermediate position between α - radioactivity and fission, making bridge between these two extreme processes and differ not only in decay mechanisms but also in properties of emitted fragments. The cluster decays of different radioactive nuclei have been observed by many experimental groups around the world some of which include ^{14}C, $^{18,20}O$, ^{23}F, $^{22,24,26}Ne$, $^{28,30}Mg$ and $^{32,34}Si$. All these cluster decays in trans-Lead region have a closed shell daughter, i.e. daughter nucleus is always ^{208}Pb or it's neighbor. Consequently, one may presume that

the nuclear shell structure play very significant role in cluster radioactivity. It is expected that together with shell effects, the nuclear deformations and orientations of nuclei might also play important role in CR. A systematic study in this direction could resolve various issues in cluster radioactivity domain of nuclear physics like the limit of CR and onset of fission, and search for new region of CR.

In the present work, the Preformed Cluster-decay Model (PCM) [3]-[6] is used to study the ^{208}Pb-daughter cluster radioactive decay. The role of deformations and orientations is investigated besides shell structure in cluster radioactivity in the ground state decay of deformed ^{222}Ra and other actinide parents. PCM gives a decent estimation of decay half-life $T_{(1/2)}$ (or the decay constant, λ). The PCM is based on the well known Quantum Mechanical Fragmentation Theory (QMFT) [7],[8]. It is relevant to mention here that the QMFT has been used, advanced and extended by the Chandigarh (India) and Frankfurt (Germany) groups for the last over three decades. It is a unified description of the otherwise two inverse processes, the nuclear fusion and nuclear fission. The QMFT was first given for fission (including cluster radioactivity) and then extended to heavy ion collisions. On the basis of this theory, the cold formation of heavy/super heavy elements was predicted which got experimental confirmation later. Moreover, the fission mass- and charge distribution yields, together with ground state exotic cluster decay is very well explained by it. Here the binary fragmentation is considered as a collective mass transfer process, where different fragments are produced with different quantum mechanical probabilities.

1.2 Heavy ion reactions

Since the first experimental demonstration of nuclear reaction process by Rutherford in 1919, experimental techniques in the field of nuclear physics have improved immensely. Formerly, in the study of nuclear reactions projectiles used were basically the alpha particles from natural radioactive substances. Also, the discovery of neutron in 1932 caused an impetus in the nuclear reaction experiments. Low energy neutrons can easily penetrate Coulomb barrier and cause nuclear reactions. Later on, the advent of highly advanced

particle accelerators techniques have made possible high energy beams of not only protons, deuterons and alpha particles but also heavy ions, to produce nuclear reactions. Highly efficient and precise detector technology, to observe nuclear phenomena, is available. Fast computational methods further aided in precise and accurate measurements of cross sections and angular distribution of the disintegration products in the experiments. As a result, lot of experimental data related to different nuclear phenomena have become available. Nuclear reactions induced by heavy ions have become the principal tool in nuclear physics research.

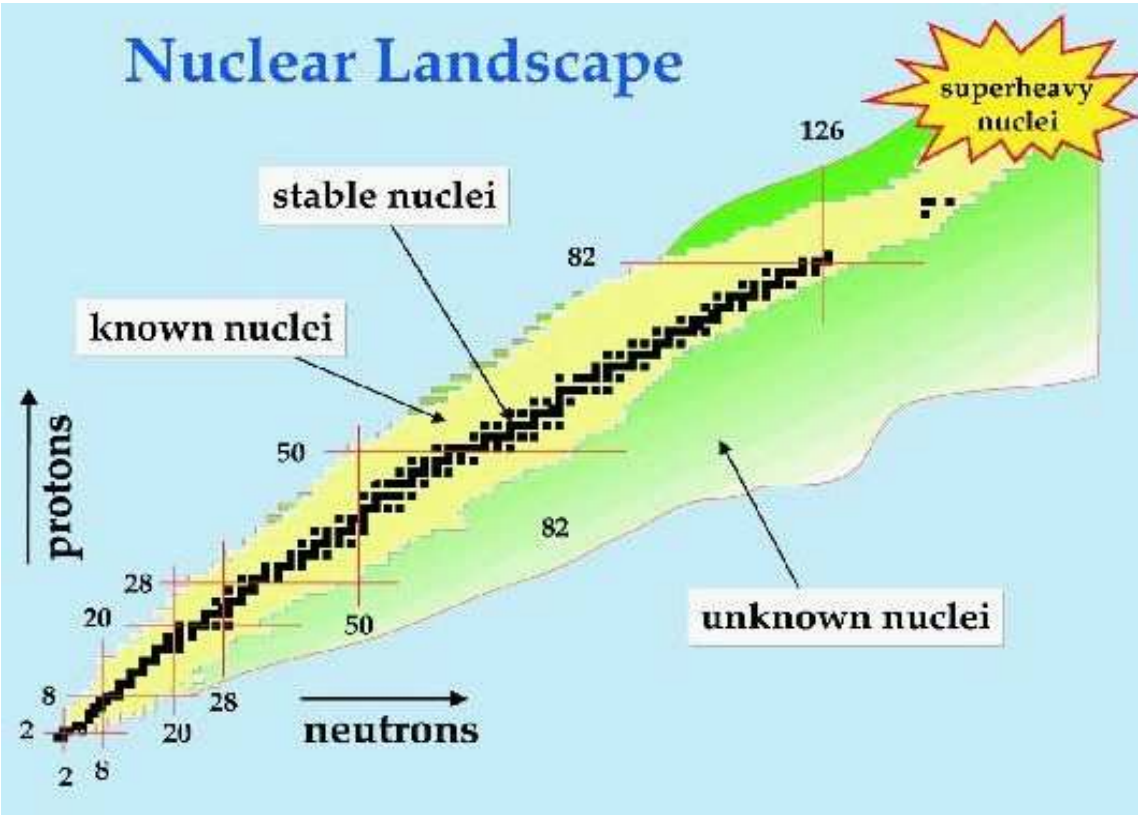

Figure 1.1: A nuclear (Z-N) landscape, the chart of bound as well as unbound nuclear systems. (courtesy: http://www.anl.gov/.../070608_nuclear_landscape-200.jpg)

In the last few decades, nuclear reactions have played a significant role in the discovery of many nuclei away from the valley of stability. The valley of stability (Figure 1.1) comprises bound/ stable nuclear systems in the Z-N landscape, popularly known as "nuclear landscape", a chart plotted as a function of proton number Z and neutron number N. It is relevant to mention here that 7-8 thousand combinations of proton and neutron

are possible (between neutron and proton "drip lines", beyond which nuclear binding is zero) of which our knowledge is restricted to 2-3 thousand only. In other words, number of stable nuclei is very small (shown by black squares) in comparison to large number of possible unstable nuclei. The existence of stable/bound nuclei depends on the sensitive balance between repulsive Coulomb forces and attractive, short range nuclear forces.

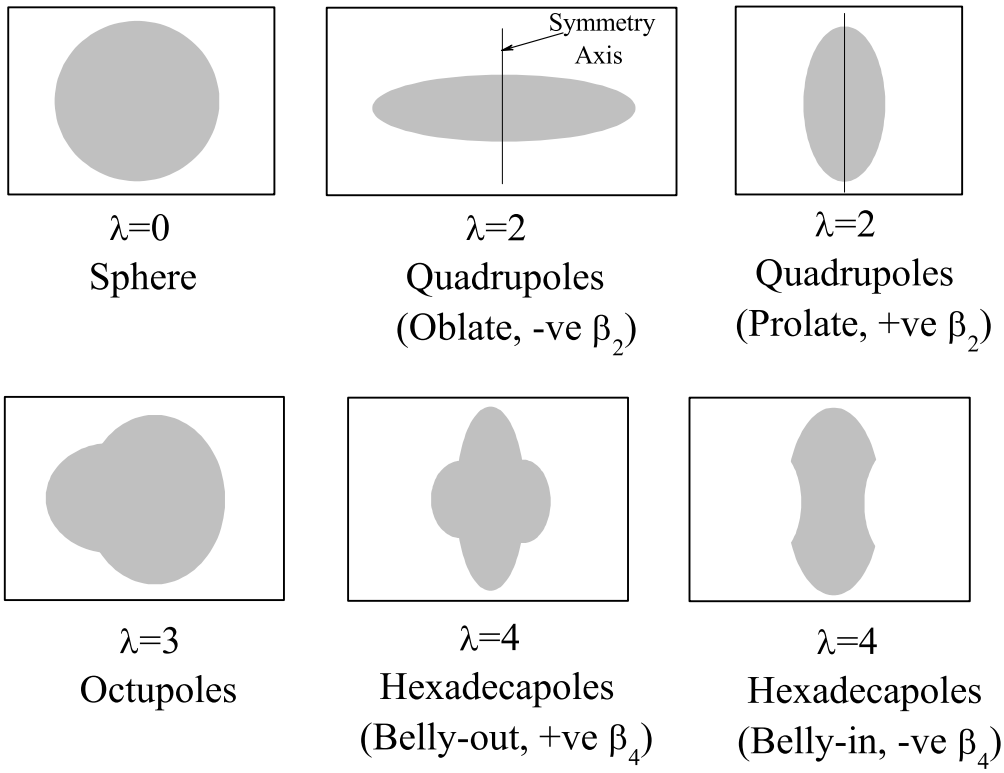

Figure 1.2: Schematic diagram for various multipole deformations in nuclei. For quadrupole deformations, there are two choices i.e. nuclear matter rotates on short axis (oblate) and on long axis (prolate).

Much of current research in nuclear physics relates to the study of nuclei under extreme conditions such as high spin and excitation energy. Nuclei may also have extreme shapes, the higher multi-pole deformations, $\beta_\lambda(\lambda = 2, 3, 4)$ as shown in Figure 1.2 or extreme neutron-to-proton ratios. Experiments can create such nuclei, using artificially induced fusion or nucleon transfer reactions, employing ion beams from an accelerator. With the advent of new generation of accelerators, which are capable of accelerating not only heavy ions but also radioactive ion beams (RIB) to produce exotic nuclei, vast amount of experimental data is being accumulated, from lighter nuclei to some super heavy ones.

All these experimental facilities coupled with theoretical developments, are leading to a better and better understanding of the nucleus and nuclear forces.

A nuclear reaction is described by identifying incident particle/nucleus with specific associated incident energy, target nucleus, and reaction products. Nuclear reactions can be categorized broadly into two types, namely Fusion reactions and Fusion-Fission reactions. These two processes play an important role in the production of new elements, their further studies and applications, etc. For successful formation of heavy nuclei, deep understanding of fusion-fission process of the compound nucleus formed in heavy ion reaction is essential. The study of heavy ion induced reactions has been directed toward this aim since the dream of super heavy elements was seen in the late sixties of last century.

Fusion is a process in which two nuclei are brought together to form a compound nucleus (CN). A substantial energy barrier, due to mutual repulsion between the two nuclei, opposes the fusion reaction. This barrier consists of the Coulomb and the nuclear potentials. However, the long range Coulomb repulsion between the nuclei is offset by stronger, but short range, attractive nuclear force. Then, the problem is to bring the nuclei sufficiently close so that the Coulomb barrier can be crossed over, say, via tunneling. Hence, the two nuclei are required to collide with sufficient kinetic energy to overcome their mutual electrostatic repulsion (or fusion threshold barrier) and subsequently to bring into effect the role of strong but short range attractive nuclear force. In other words, the simplest picture of fusion is that of quantum tunneling through a one dimensional barrier formed by the long range Coulomb potential, the centrifugal potential and the short range nuclear potential. It means that the knowledge of interaction potential, forming barrier, between two nuclei is extremely important in order to have a systematic study of a nuclear reaction.

The inclusion of deformation and orientation effects of the colliding nuclei leads to lowering of its barrier height [9]-[13]. This means that the interaction potential and hence the fusion cross-sections are largely influenced by the nuclear structure effects of the target and projectile nuclei and their relative orientations. The collisions between deformed as well as oriented nuclei have been studied theoretically and experimentally to establish the

effect of deformation and orientation on fusion reactions [9]-[13], [14]-[17]. According to these studies when deformed and oriented nuclei collide, the fusion barrier height varies leading to the barrier height distribution around the spherical Coulomb barrier (Figure 2, [11]). Figure 1.3 shows a schematic configuration of two (equal/ unequal) axially symmetric deformed, oriented nuclei, lying in the same plane ($\phi = 0^0$), for various θ_1 and θ_2 values in the range 0^0 to 180^0. Rest of the details of Figure 1.3 are given in chapter 2.

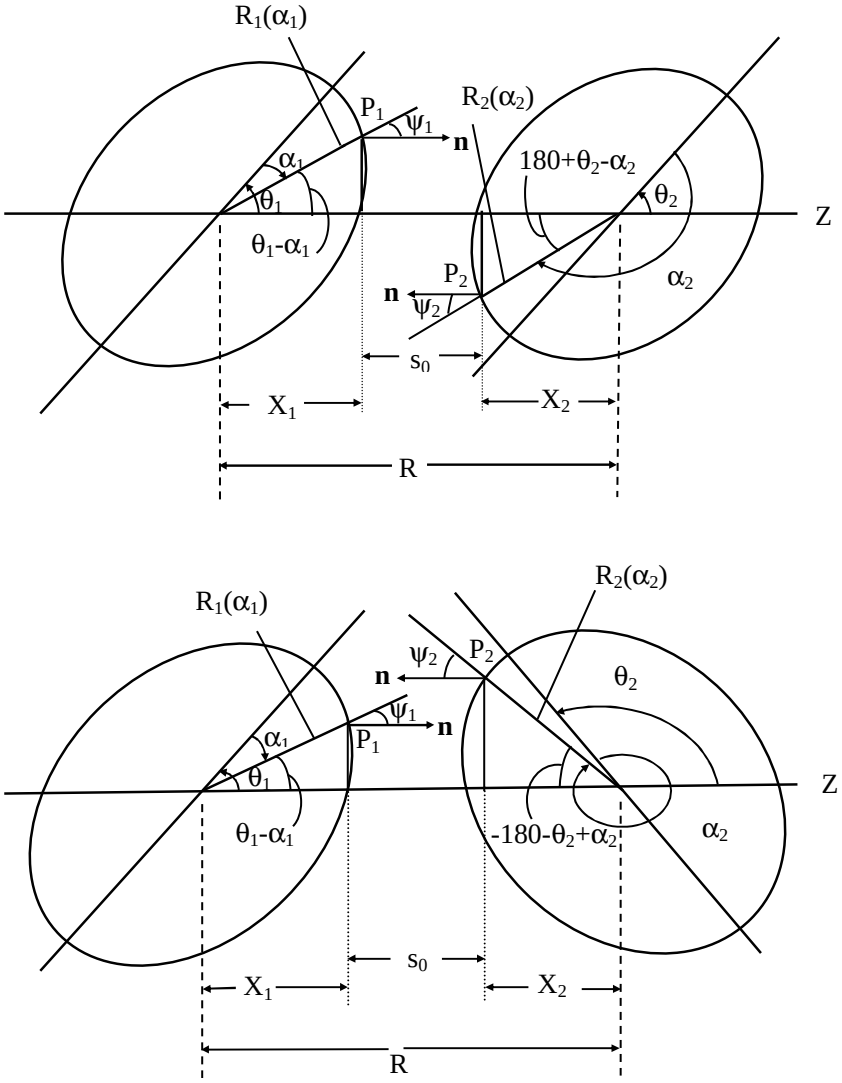

Figure 1.3: Schematic configurations of two (equal/ unequal) axially symmetric deformed, oriented nuclei, lying in the same plane and for various θ_1 and θ_2 values in the range 0^0 to 180^0. The θ's are measured in anti-clockwise from the colliding axis and the angle α's in clockwise from the symmetry axis.

A detailed study [11] based upon Quantum Mechanical Fragmentation Theory

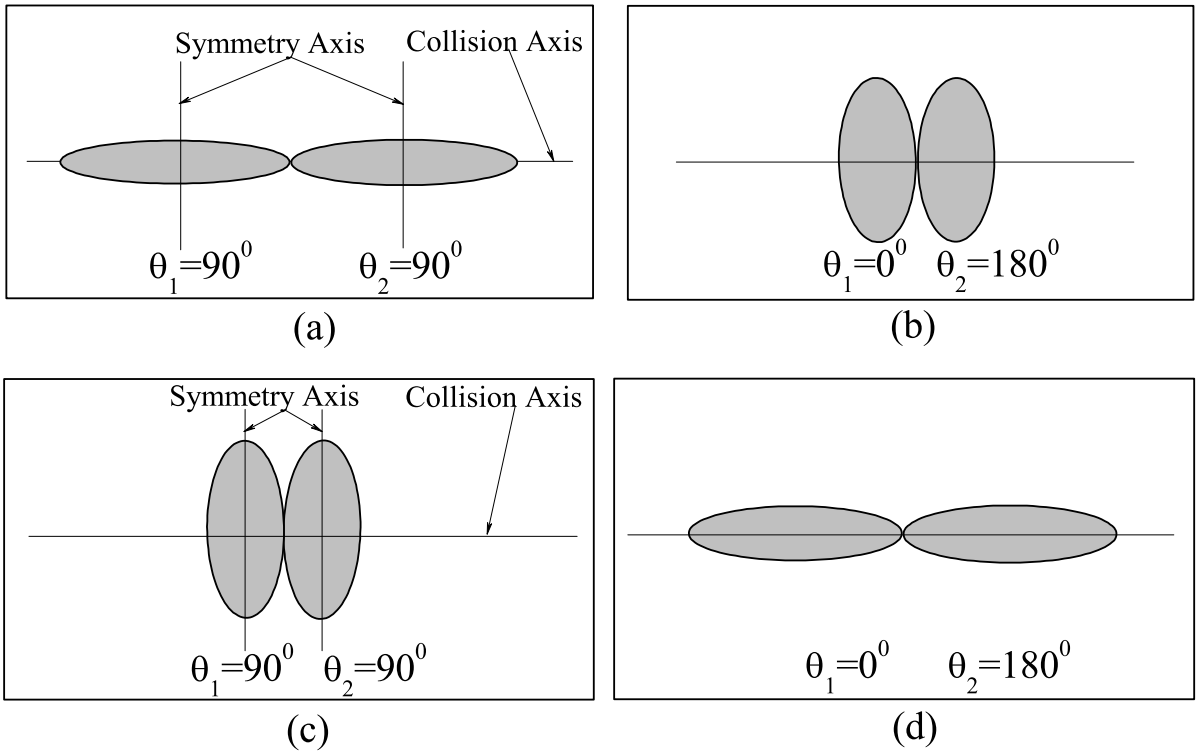

Figure 1.4: Schematic diagrams for deformed nuclei ((a),(b) oblate and (c),(d) prolate only) with corresponding optimum orientations along collision axis for "cold, elongated"((a), (d)) or "hot, compact"((b), (c)) configurations, from Table 1 [11].

(QMFT) by Gupta and collaborators shows that the interaction barrier (height as well as its position) is greatly affected by deformed and oriented colliding nuclei. This study gives the optimum orientations for fusion of deformed nuclei based on the quadrupole deformations alone and also investigated the role of hexadecupole deformation in fusion reactions. The optimum orientations are given for "cold, non-compact" and "hot, compact" fusion configurations corresponding to largest interaction radius/lowest barrier and smallest interaction radius/highest barrier, respectively. The details can be seen in Table 1 of [11]. However a schematic diagram is illustrated in Figure 1.4, only for prolate-prolate and oblate-oblate deformed colliding nuclei along collision axis for both "cold, elongated" and "hot, compact" configurations.

In heavy systems, the heavy ion fusion probability depends on the charge product Z_1Z_2 of projectile and target nuclei. When this charge product approaches $\sim$ 1800, the probability of fusion shows a rapid decrease with increase in Z_1Z_2 [14] due to large Coulomb repulsion. It is interesting to note that in the reaction of a heavy target-projectile

combination, leading to heavier compound system, the crossing of a fusion barrier doesn't guarantee the formation of a CN. However, the system must overcome the saddle point of compound nucleus, which is located inside the fusion barrier between the heavy target and projectile. This hindrance in the fusion process is named as "extra-push" phenomenon and causes significant loss in the kinetic energy. But it has been observed that the favorable compact shape results more easily into CN rather than an elongated touching shape. Here, the favorable compact shape means that the distance between the mass centers of target-projectile at touching should be less than the distance of centers of the nascent fission fragments at the fission saddle point. Hence, the relative distance between the mass centers of two colliding nuclei, with respect to saddle point, affects the fusion of heavy ions considerably.

For a system with large Z_1Z_2 product the contact point usually exists outside the saddle point. But in the fusion of deformed and relatively oriented nuclei the scenario is changed as at touching the distance between mass centers of massive reactants rely on the orientation of the deformed nuclei. It means that the fusion reaction starting from compact touching point results in higher fusion probability than the fusion starting from distant touching point. Thus the fusion process is greatly affected by the relative orientations of the deformed nuclei. In the fusion reactions involving deformed nuclei the quasi-fission and fusion-fission are in competition [15]. In the quasi-fission process, incoming nuclei in a reaction do not loose its identity during the formation of CN and as a result such a non-equilibrated CN decays into fragments which are nearly the same as in the entrance channel i.e. projectile and target like fragments. Several experimental studies show that the collision with tip to tip of deformed projectile-target nuclei lead to quasi-fission and the side collisions results in fusion-fission [14],[15]. The terms like gentle fusion and hugging fusion have been coined theoretically [10], which correspond to typical shapes (prolate, oblate and higher multipoles) of deformed nuclei along with their relative orientations. It is relevant to mention here that the nuclear structure and orientations of the approaching heavy ions seem to affect the mutual long range Coulomb interaction [18], [19] as well as the short range nuclear potential [9],[20].

Heavy ion fusion is not only affected by deformation and relative orientations of the

reactants but also takes into account the nuclear shell structure of projectile and target nuclei. The shell closure of colliding nuclei plays a significant role in the sub-barrier fusion process [17], [21]. It indicates no fusion hindrance for the colliding nuclei with nuclear shell closure structure. The target and projectile with this type of structure makes a compact touching shape and produces an equilibrated compound nucleus.

The nuclear reactions can also be categorized on the basis of energy of projectiles, as low, intermediate and high energy reactions. Projectiles with energies $\leq$ 10 MeV/nucleon and $\geq$ 400 MeV/nucleon cause low and high energy nuclear reactions respectively. Whereas the in between energy range corresponds to the intermediate energy reactions. In low energy reactions average/mean nuclear force field acting between the two nuclei dominate in comparison to high energy reactions where direct nucleon-nucleon interactions takes place. In intermediate energy reactions both the aspects play their role. However, in the present study we have confined ourself to low energy nuclear reaction dynamics only. The present state of art experimental facilities lead to better understanding of nuclear forces with formation of heavy nuclei away from valley of stability. Moreover, one can explore various aspects of nuclear structure and dynamics "at extremes" and thus gain a deeper insight via study of decay products of CN formed in low energy nuclear reactions.

The compound nuclei (CN) formed in low-energy heavy-ion reactions are highly excited and carry large angular momentum (Figure 1.5). The compound systems so formed decay by emitting multiple light particles, LPs (n, p, α) and γ-rays. For light compound systems with $A_{CN} \sim$ 40 - 80, the light-particles (LPs) emission is always accompanied by intermediate mass fragments, the IMFs (with $2 < Z < 10$ and 5$\leq$A$\leq$20). In this mass region the IMFs contribution is very small of the order of 5-10%, in comparison to LPs contribution. However, for the heavy nuclear systems $A_{CN} \sim$ 200, the most probable decay mode of the compound nucleus is fission/ heavy mass fragments (HMFs) (20$\leq$A$\leq$A/2), due to its instability against centrifugal repulsion, with small contribution from neutrons and γ-rays emissions, just in contrast to decay process of light compound systems. Then there are other processes which may contribute to decay products, e.g., orbiting, deep-inelastic and quasi-fission, etc., depending upon the reaction conditions.

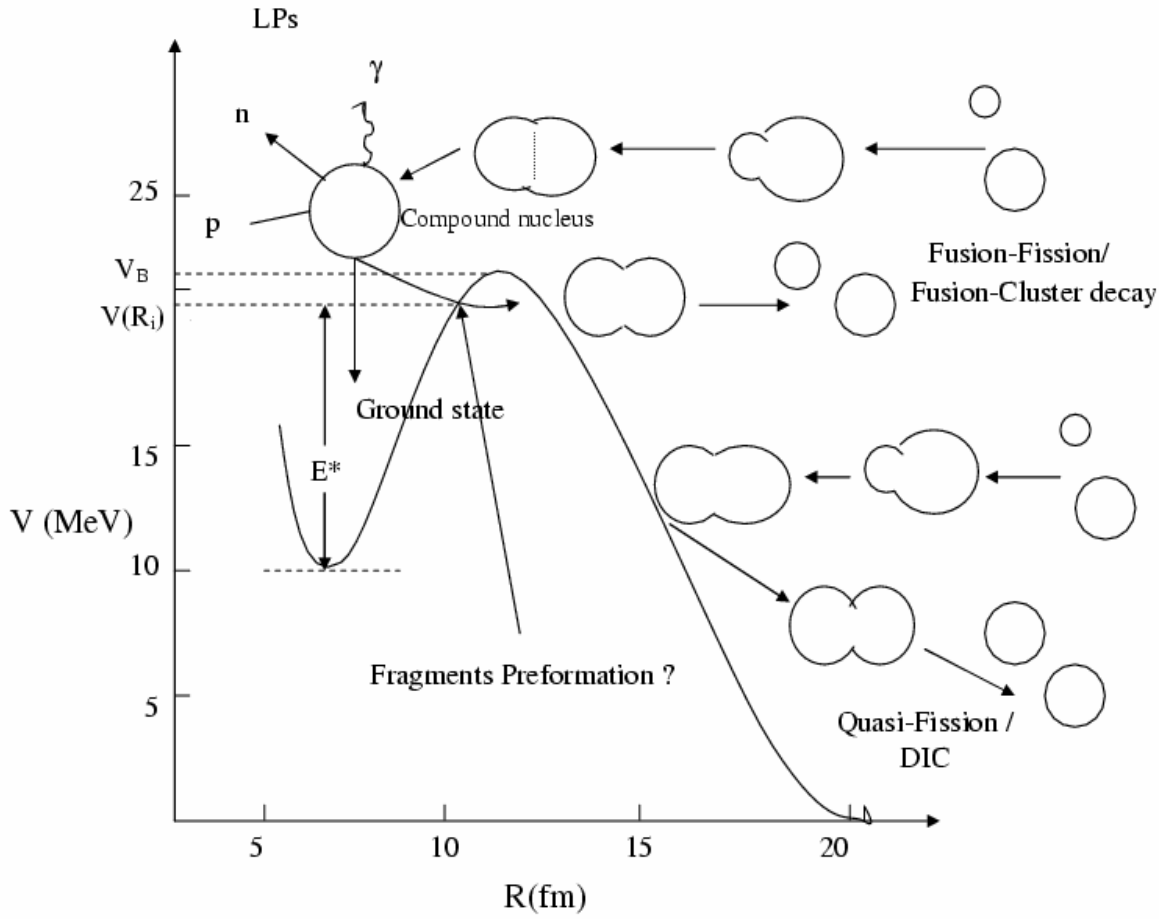

Figure 1.5: Schematic diagram for dynamics of the colliding nuclei playing around Coulomb as well as nuclear interaction potential.

The decay of excited CN formed in heavy ion reactions is affected by the maximum value of angular momentum it can support without fissioning, which in turn depend upon energy of incident projectiles. It is relevant to mention here that value of angular momentum extracted experimentally, is based on the moment of inertia (calculated in non-sticking limit (i.e. $I_{NS} = \mu R^2$)) [22]. It means that fragment emission is punctual. In our recent study we find that sticking limit is more appropriate for the proximity potential (nuclear surface $\leq$ 2 fm apart) which consequently results in to large limiting value of angular momentum [23].

In order to study the decay of a hot and rotating compound system (i.e. having angular momentum, $\ell \neq 0$ and temperature, T $\neq$ 0), we have used the Dynamical Cluster-decay Model (DCM) of Gupta and collaborators [23]-[30] which is a reformulation of PCM [3]-[6] for ground-state decays (i.e. ℓ=0 and T=0). In DCM, decay of excited compound nuclei is

studied as a collective clusterization process for emissions of the LPs, as well as the IMFs and HMFs, in contrast to the statistical models in which each type of emission is treated on different footing. It is relevant to mention here that a statistical Hauser-Feshbach (HF) analysis (LILITA or CASCADE codes) is used to study LPs decay. It's other versions are used to study IMFs/HMFs/fission decay of CN formed in different mass regions like BUSCO code [31] for 2 <Z≤20, extended HF Scission-Point Model [32] and saddle-point "transition-state" fission model [33] for $A < 80$, GEMINI code based on Moretto's fission model [34] fo r $A > 100$. Another advantage of using the DCM is that the structure effect of CN is also included via the preformation of the fragments with relative probabilities, before penetrating the interaction barrier, an useful information which is missing in the statistical fission models.

It is relevant to mention here that the DCM has been applied successfully to study the decay of compound nuclei formed in light mass ($^{56}Ni^*$) and intermediate mass ($^{116}Ba^*$) region [24]-[29]. In the present work, the decay of light and heavy mass CN $^{48}Cr^*$ and $^{246}Bk^*$ respectively have been studied, using DCM, formed in different entrance channels at different centre-of-mass energies $E_{c.m.}$. The results for the same are very well compared with the available experimental data. The role of excitation energy, entrance channel effects together with the effects of deformations and orientations in the fusion-fission process have been investigated extensively.

1.3 Organization of thesis

The thesis is organized as follows.

Chapter 2, gives details of the Preformed Cluster-decay Model (PCM) and the Dynamical Cluster-decay Model (DCM). In PCM and DCM the two contributing factors, the pre-formation probability P_0 of the decaying fragments and their penetrability P across the nuclear interaction barrier describes the decay of nuclei in ground and excited states, respectively. The deformation and orientation effects are duly incorporated in PCM as well as in DCM. These are applied to study the spontaneous cluster radioactivity process

and the decay of hot and rotating compound nucleus formed in heavy ion reactions, respectively. The DCM treats the CN decay of light particles LPs, intermediate mass fragments IMFs and heavy mass fragments HMFs or symmetric fission SF on equal footings, in contrast to statistical models which uses the HF analysis for LPs and binary fission for all other processes.

In Chapter 3, as a first step to be able to use the DCM, for studying the decay of excited compound nucleus, the T-dependent binding energies are obtained. This is essential because the collective potentials used in DCM are T-dependent. The temperature dependent liquid drop energies are calculated in reference to the work of Davidson et al. [35] which itself is based upon a well established Seeger's [36] semi-empirical mass formula. In view of the available large amount of data on ground state binding energies, we have refitted the bulk $\alpha(0)$ and neutron proton asymmetry a_a constants, in the Seeger's semi-empirical mass formula at T=0, for all available isotopes of the periodic table upto Z=118. The ground state binding energies are fitted within 0-1.5 MeV, where T-dependence is given by Davidson et al. (see Figure 3.1 taken from ref. [35]).

In Chapter 4, the entrance-channel effects in the decay of hot and rotating compound nucleus ^{48}Cr are studied, formed in a symmetric ^{24}Mg+^{24}Mg and very asymmetric ^{36}Ar+^{12}C reaction, using the DCM. The role of angular momentum is investigated extensively in the reaction dynamics. The calculations for this low mass CN are done with spherical considerations for the nuclei in the reaction process. This study confirms the entrance-channel independence of the decay of compound nucleus $^{48}Cr^*$ formed via different target-projectile combinations with similar excitation energies as per Bohr's hypothesis. The calculated results are compared nicely with the available experimental data for both the reactions. [37],[38].

In Chapter 5, the role of deformations and orientations of nuclei is studied, for the ground state decays of heavier nuclei. These effects are duly incorporated in PCM for investigating the cluster radioactive decays of parents, which are mostly deformed, namely ^{222}Ra, $^{226,228}Th$, ^{230}U, ^{231}Pa, $^{232,234}U$, $^{236,238}Pu$ and ^{242}Cm. The respective observed clusters are ^{14}C, $^{18,20}O$, ^{22}Ne, ^{23}F, $^{24,26}Ne$, $^{28,30}Mg$ and ^{34}Si. Note that in PCM, not only the shapes of parent, daughter and cluster are important, but also the shapes of all other

possible fragmentations of the decaying parent are important via the calculation of preformation factor P_0. The interesting feature of the study is that in all the chosen cluster decays, the daughter nucleus is always the spherical ^{208}Pb having double shell closure (N = 126, Z = 82). The role of deformations and orientations is investigated, besides shell structure. The Q-value of these decays show interesting structure corresponding to measured decay half-lives, as expected, further emphasizing the role of shell structure. The calculated decay half-lives for all such cluster-decays are in good agreement with measured values [5]. The potential energy surface for the fragmentation process in the ground state decay of parent nucleus changes significantly with the inclusion of deformation and orientation effects. We observe variance in both the key quantities of PCM, the preformation probability P_0 and penetrability P of clusters with and without invoking deformation and orientation effects.

In Chapter 6, the DCM is applied to a heavier nuclear system, the $^{246}Bk^*$ decay, formed in similar entrance channel reactions $^{11}B+^{235}U$ and $^{14}N+^{232}Th$ at various incident centre of mass energies, $E_{c.m.}$. The DCM used include the deformations and orientations of nuclei. The role of temperature, angular momentum and both the entrance channels has been discussed extensively. The decay of $^{246}Bk^*$, formed in both the channels, favoures symmetric mass distributions. This is mainly a fusion-fission decay. The additional effects of non-compound, quasi-fission (qf) component, is shown to be present for the $^{11}B+^{235}U$ entrance channel at higher incident c.m. energies, in contradiction with the measured anisotropy effects which indicate the other entrance channel $^{14}N+^{232}Th$ to contain the non-compound nucleus contribution. The angular momentum and its dependence on the choice of sticking or non-sticking moment of inertia in the calculations has been discussed. The calculated and measured [39] decay cross sections are shown to be in excellent agreement at all $E_{c.m.}$ for both the entrance channels.

Chapter 7, summarizes the overall work of the thesis. Brief notes regarding the significance of the work and conclusion drawn from it are explicitly given in this chapter. There is a definite scope for extension of this work in future.

Bibliography

[1] A. Săndulescu, D.N. Poenaru, and W. Greiner, Sovt. J. Part. Nucl. **11**, 528 (1980).

[2] H.J. Rose and G.A. Jones, Nature **307**, 245 (1984).

[3] R.K. Gupta, in Proc. 5th Int. Conf. on Nuclear Reaction Mechanisms, Varenna, 1988, edited by E. Gadioli (Ricerca Scientifica ed Educazione Permanente, Milano, p.**416** (1988).

[4] S.S. Malik and R.K. Gupta, Phys. Rev. **C 39**, 1992 (1989).

[5] R.K. Gupta and W. Greiner Int. J. Mod. Phys. E **3**, 335 (1994, Suppl.).

[6] S. Kumar and R.K. Gupta, Phys. Rev. **C 55**, 218 (1997).

[7] J. Maruhn and W. Greiner, Phys. Rev. Lett. **32**, 548 (1974).

[8] R. K. Gupta, W. Scheid and W. Greiner, Phys. Rev. Lett. **35**, 353 (1975).

[9] N. Malhotra and R.K. Gupta, Phys. Rev. **C 31**, 1179 (1985).

[10] A. Iwamoto, P. Moller, J.R. Nix, and H. Sogawa, Nucl. Phys. **A596**, 329-354 (1996).

[11] R. K. Gupta, M. Balasubramaniam, R. Kumar, N. Singh, M. Mahhas, and W. Greiner, J. Phys. G: Nucl. Part. Phys. **C 31**, 631 (2005).

[12] M. Manhas and R.K. Gupta, Phys. Rev. **C 72**, 024606 (2005).

[13] R. K. Gupta, M. Manhas, G. Münzenberg, and W.Greiner, Phys. Rev. **C 72**, 014607 (2005).

[14] K. Nishio, H. Ikezoe, S. Mitsuoka and K. Satou, and S.C. Jeong, Phys. Rev. **C 63**, 044610 (2001).

[15] D.J Hinde, M. Dasgupta, J.R. Leigh, J.P Lestone, J.C. Mein, C.R. Morton, J.O. Newton, and H. Timmers, Phys. Rev. Lett. **74**, 1295 (1995).

[16] M. Dasgupta, D.J Hinde, J.R. Leigh and K. Hagino, Nucl. Phys. **A630**, 78C (1998).

[17] Yu. Ts. Oganessian, Heavy Elements and Related New Phenomena, edited by W. Greiner and R.K Gupta, World Scientific, Singapore, **P. 43**, (1999).

[18] C.Y. Wong, Phys. Lett. **26B**, 120 (1968).

[19] L.Wilets, E. Guth, and J.S. Tenn, Phys. Rev. **156**, 1349 (1967); H. Holm, W Scheid, and W. Greiner, Phys. Lett. **24**, 404 (1970); A.S. Jensen and C.W. Wong, Phys. Rev. **C 1**, 1321 (1970); P.W. Riesenfeldt and T.D. Thomas, ibid. **2**, 711 (1970).

[20] M. Seiwert, W. Greiner, V. Oberacker, and M.J. Rhoades-Brown, Phys. Rev. **C 29**, 477 (1984).

[21] H. Ikezoe, S. Mitsuoka, K. Nishio, K. Satou, and I. Nishinaka, J. Nucl. and Radiochemical Sciences, **3**, 39 (2002).

[22] S. Kailas (private communication).

[23] B. B. Singh, M. K. Sharma and R. K. Gupta, Phys. Rev. **C 77**, 054613 (2008).

[24] M. Balasubramaniam, R. Kumar, R. K. Gupta, C. Beck, and W. Scheid, J. Phys. G: Nucl. Part. Phys. **C 29**, 2703 (2003).

[25] R. K. Gupta, Acta Phys. Hung. (New Ser.) Heavy Ion Phys. **18**, 347 (2003).

[26] R. K. Gupta, R. Kumar, N. K. Dhiman, M. Balasubramaniam, W. Scheid, and C. Beck, Phys. Rev. **C 68**, 014610 (2003).

[27] R. K. Gupta, M. Balasubramaniam, R. Kumar, D. Singh, and C. Beck, Nucl. Phys. **A738**, 479c (2004).

[28] R. K. Gupta, M. Balasubramaniam, R. Kumar, D. Singh,C. Beck, and W. Greiner, Phys. Rev. **C 71**, 014601 (2005).

[29] R. K. Gupta, M. Balasubramaniam, R. Kumar, D. Singh, S. K. Arun, and W. Greiner, J. Phys. G: Nucl. Part. Phys. **32**, 345 (2006). R. Kumar and R. K. Gupta, Phys. Rev. **C**, (2009) in press.

[30] B. B. Singh, M. K. Sharma, R. K. Gupta, and W. Greiner, Int. J. Mod. Phys. E **15**, 699 (2006).

[31] J. Gomez del Campo, R. L. Auble, J. R. Beene, M. L. Halbert, H. J. Kim, A. DOnofrio and J. L. Charvet, Phys. Rev. **C 43**, 2689 (1991).

[32] T. Matsuse, C. Beck, R. Nouicer and D. Mahboub, Phys. Rev. **C 55**, 1380 (1997)

[33] R. Vandenbosch and J. R. Huizenga, Nuclear Fission (New York: Academic), (1973).

[34] L. G. Moretto, Nucl. Phys. **A 247**, 211 (1975).

[35] N. J. Davidson, S. S. Hsiao, J. Markram, H. G. Miller, and Y. Tzeng, Nucl. Phys. **A570**, 61c (1994).

[36] P. A. Seeger, Nucl. Phys. **25**, 1 (1961).

[37] A. T. Hasan, S. J. Sanders, K. A. Farrar, F. W. Prosser, B. B. Back, R. R. Betts, M. Freer, D. J. Henderson, R. V. F. Janssens, A. H. Wuosmaa and A. Szanto de Toledo, Phys. Rev. **C 49**, 1031 (1994).

[38] K. A. Farrar, S. J. Sanders, A. K. Dummer, A. T. Hasan, F. W. Prosser, B. B. Back, I. G. Bearden, R. R. Betts, M. P. Carpenter, B. Crowell, M. Freer, D. J. Henderson, R. V. F. Janssens, T. L. Khoo, T. Lauritsen, Y. Liang, D. Nisius, A. H. Wuosmaa, C. Beck, R. M. Freeman, Sl. Cavallaro and A. Szanto de Toledo, Phys. Rev. **C 54**, 1249 (1996).

[39] B. R. Behera, M. Satpathy, S. Jena, S. Kailas, R. G. Thomas, K. Mahata, A. Chatterjee, S. Roy, P. Basu, M. K. Sharan, and S. K. Datta, Phys. Rev. **C 69**, 064603 (2004).

Chapter 2

Methodology

2.1 Introduction

The main aim of this work is to study the heavy ion reaction dynamics, especially the disintegration of excited compound nucleus using the dynamical cluster decay model(DCM) [1]-[7]. It is important to note that deformations and orientation effects of the reaction partners and decay products are explicitly included together with temperature and angular momentum contribution in this model. The ground state/spontaneous cluster decay of radioactive nuclei have also been undertaken within the preformed cluster decay model (PCM) [8]-[16] again having deformations and orientation effects of the clusters as well as daughter nuclei included in it. Note that DCM is a reformulation of PCM for compound nuclei (CN) whose details are given in sections 2.4 and 2.5, respectively. In turn, both PCM and DCM originate from the Quantum Mechanical Fragmentation Theory, (QMFT) [17]-[30] (section 2.2), which, in binary fragmentation, uses a collective mass transfer process.

In QMFT the potential is calculated using macro-microscopic method of Strutinsky [31]. This average two body potential successfully explains the cold and hot fusion reaction dynamics. This theory is based on the fact that the fragments are pre-born prior to the decay of the compound nucleus. The quantum mechanical preformation probability P_0 of the decaying fragments or clusters formed in the mother nucleus can be calculated by solving a stationary Schrödinger equation in mass fragmentation coordinate. Once the

clusters are formed, their penetration probability P across the interaction barrier can be calculated by using the WKB approximation. The calculations of preformation probability P_0 and penetration probability P are discussed in section 2.2.7 and 2.3, respectively. The assault frequency, ν_0, with which the preformed cluster bombard the barrier in ground state decay is discussed in section 2.4.

2.2 Quantum Mechanical Fragmentation Theory

The $QMFT$ [17]-[30] is a unified description of two body channels in both fusion and fission processes. Here the quantum mechanical concept of probability is utilized to investigate the role of shell effects in the fusion, fission and cluster radioactivity. In $QMFT$, nuclear dynamics is explained by the mass parameters defining the kinetic energy of the system while the static properties of nuclear system are determined by the potential energy surfaces. The $QMFT$ is worked out in terms of the following collective coordinates:
(i)Relative separation coordinate R between the two nuclei or, in general, two fragments (or, equivalently, the length parameter $\lambda = L/2R_0$, with L as the length of the nucleus and R_0 as the radius of an equivalent spherical nucleus).
(ii)Mass and charge fragmentation co-ordinates [17],[18],[29], defined by the mass and charge-asymmetry coordinates as

$$\eta = \frac{A_1 - A_2}{A}; \qquad \eta_Z = \frac{Z_1 - Z_2}{Z} \tag{2.1}$$

Similarly, the neutron asymmetry coordinate [18],

$$\eta_N = \frac{N_1 - N_2}{N}, \tag{2.2}$$

can also be used, but it is sufficient to treat only two of them as dynamical co-ordinates since they are related as

$$\eta = \frac{Z}{A}\eta_Z + \frac{N}{A}\eta_N. \tag{2.3}$$

Here $A = A_1 + A_2$, $Z = Z_1 + Z_2$ and $N = N_1 + N_2$. A_i, Z_i and N_i $(i = 1, 2)$ are, respectively, the mass number, the charge number and the neutron number of two fragments. A, Z and N are respectively the mass number, charge number and neutron number of the compound system. The limiting values of η are $0 \leq |\eta| \leq 1$, and thus allows a unified description of a few-nucleon or multi-nucleon (a cluster) transfer, a large-mass transfer, the complete fusion ($|\eta| = 1$) of nuclei and the symmetric ($\eta = 0$), asymmetric and super-asymmetric fission of a nucleus or compound nucleus. The η_Z coordinate gives the associated charge distribution effects.

(iii)The deformation co-ordinates $\beta_{\lambda i}$ (λ=2,3,4... and i=1,2) of the colliding nuclei or fragments.

(iv)The orientation degrees of freedom θ_i (i=1,2) of the deformed nuclei (see Fig. 1.3).

(v)Azimuthal angle ϕ between the principal planes of the two colliding nuclei.

(vi)Neck parameter ε, defined by the ratio $\varepsilon = E_0/E'$ for the interaction region ($R < R_1 + R_2$). R_i (i=1, 2) is the radius of the two nuclei. Here, E_0 is the actual height of the barrier and E' is the fixed barrier of the two center oscillator. $\epsilon = 0$ represents a broad neck formation, whereas $\epsilon = 1$ gives that the neck is fully squeezed in, corresponding to the asymptotic region ($R \geq R_1 + R_2$).

In terms of these collective coordinates and their velocities, the collective Hamiltonian can be written as

$$H = K(\mathbf{R}, \beta, \varepsilon, \eta, \eta_Z; \dot{\mathbf{R}}, \dot{\beta}, \dot{\varepsilon}, \dot{\eta}, \dot{\eta}_Z) + V(\mathbf{R}, \beta, \varepsilon, \eta, \eta_Z). \tag{2.4}$$

Here β is taken as $\beta_{\lambda 1}$ and $\beta_{\lambda 2}$ with λ=2,3,4...., K refers to the kinetic energy and V to the collective potential energy. For fixed β and ϵ, the potential $V(\eta, \eta_Z, R)$, minimized in the η_Z co-ordinate gives the Schrödinger wave equation, in terms of mass parameters η and relative separation R co-ordinates, as

$$H(\eta, R)\psi(\eta, R) = E(\eta, R)\psi(\eta, R) \tag{2.5}$$

with the Hamiltonian,

$$H(\eta, R) = K(\eta) + K(R) + K(\eta, R) + V(\eta) + V(R) + V(\eta, R) \tag{2.6}$$

The mass parameters B_{ij}, defining the kinetic energy term K in the above Eqs. (2.4) and (2.6) are either the consistently calculated cranking masses using the Asymmetric Two-Center Shell Model ($ATCSM$) or the classical hydrodynamical masses, which are shown to have good agreement with microscopic cranking calculations.

The coupling term of the kinetic energy $K(\eta, R)$, proportional to $\frac{\partial^2}{\partial\eta\partial R}$, can be neglected, since the coupled cranking masses are very small [17],[18] ($\mathrm{B}_{R\eta} \ll (B_{RR}B_{\eta\eta})^{1/2}$ and $\mathrm{B}_{R\eta_Z} \ll (B_{RR}B_{\eta_Z\eta_Z})^{1/2}$). Same is true for the coupling term of potential energy $V(\eta, R)$. Therefore, in a decoupled approximation [30], the Schrödinger equation (2.5) can be solved using the Hamiltonian:

$$H = -\frac{\hbar^2}{2\sqrt{B_{\eta\eta}}}\frac{\partial}{\partial\eta}\frac{1}{\sqrt{B_{\eta\eta}}}\frac{\partial}{\partial\eta} - \frac{\hbar^2}{2\sqrt{B_{RR}}}\frac{\partial}{\partial R}\frac{1}{\sqrt{B_{RR}}}\frac{\partial}{\partial R} + V(\eta) + V(R). \tag{2.7}$$

For decoupled Hamiltonian (2.7), Schrödinger wave equation (2.5) can be separated for the two co-ordinates η and R as follows,

$$\left[-\frac{\hbar^2}{2\sqrt{B_{\eta\eta}}}\frac{\partial}{\partial\eta}\frac{1}{\sqrt{B_{\eta\eta}}}\frac{\partial}{\partial\eta} + V(\eta)\right]\psi^{\nu}(\eta) = E^{\nu}_{\eta}\psi^{\nu}(\eta) \tag{2.8}$$

and

$$\left[-\frac{\hbar^2}{2\sqrt{B_{RR}}}\frac{\partial}{\partial R}\frac{1}{\sqrt{B_{RR}}}\frac{\partial}{\partial R} + V(R)\right]\psi^{\nu}(R) = E^{\nu}_{R}\psi^{\nu}(R) \tag{2.9}$$

with

$$\psi(\eta, R) = \psi(\eta)\psi(R) \tag{2.10}$$

and

$$E = E_{\eta} + E_{R} \tag{2.11}$$

The states $\psi^{\nu}(\eta)$ are the vibrational states in the potential $V(\eta)$ and are labelled by the quantum numbers $\nu = 0, 1, 2....$

In the following subsections, we first discuss the various terms of Schrödinger wave equations (2.8) and (2.9) and then give the solution of Eq. (2.8) for the determination of preformation probability $P_0 \propto |\psi^0(\eta)|^2$ in the ground state.

2.2.1 The Scattering Potential $V(R)$

For a fixed η i.e for a given target projectile (A_1, A_2) combination, the scattering potential $V(R)$ in Eq. (2.9) is defined as the sum of the temperature, deformations and orientations dependent Coulomb potential, proximity potential and angular momentum dependent potential, i.e.

$$\begin{aligned} V(R,\ell,T) &= V_c(R, Z_i, \beta_{\lambda i}, \theta_i, \phi, T) + V_p(R, A_i, \beta_{\lambda i}, \theta_i, \phi, T) \\ &+ V_\ell(R, A_i, \beta_{\lambda i}, \theta_i, \phi, T) \end{aligned} \tag{2.12}$$

For spherical-plus-deformed nuclear collisions, only one orientation angle θ is enough, referring to the rotationally-symmetric deformed nucleus. ϕ=0^0 for co-planar nuclei.

2.2.2 The Fragmentation potential $V(\eta)$

The temperature dependent collective potential energy or the fragmentation potential $V(\eta, R, T)$ can be given by

$$\begin{aligned} V(\eta,R,\ell,T) &= -\sum_{i=1}^{2} B_i(A_i, Z_i, \beta_{\lambda i}, T) + V_c(R, Z_i, \beta_{\lambda i}, \theta_i, \phi, T) \\ &+ V_p(R, A_i, \beta_{\lambda i}, \theta_i, \phi, T) + V_\ell(R, A_i, \beta_{\lambda i}, \theta_i, \phi, T) \end{aligned} \tag{2.13}$$

The fragmentation potential $V(\eta)$, appearing in equation (2.8) is calculated at a fixed distance $R = R_1 + R_2 + \delta R$ for consideration of deformed and oriented reaction product with

$$R_i(\alpha_i, T) = R_{0i}(T)[1 + \sum_{\lambda} \beta_{\lambda i} Y_\lambda^{(0)}(\alpha_i)], \tag{2.14}$$

and

$$R_{0i}(T) = (1.28A_i^{1/3} - 0.76 + 0.8A_i^{-1/3}) \times (1 + 0.0007T^2). \tag{2.15}$$

Here λ=2,3,4... and α_i is an angle that the radius vector R_i of the colliding nuclei makes with the symmetry axis (see Fig. 1.3). In terms of Süssmann central radii C_i, $R = C_1 + C_2 + \delta C\ fm$ with $C_i = R_i(1 - \frac{b^2}{R_i^2})$. The diffuseness of the nuclear surface i.e. the surface thickness b, is given by Eq. (2.22).

Further, in Eq. (2.13), within the Strutinsky renormalization procedure [31], we have defined the binding energy B of a nucleus at temperature T as

$$B_i(A_i, Z_i, \beta_{\lambda i}, T) = \sum_{i=1}^{2} V_{LDM}(A_i, Z_i, T) + \sum_{i=1}^{2} \delta U \exp\left(-\frac{T^2}{T_0^2}\right). \tag{2.16}$$

Here, $V_{LDM}(A_i, Z_i, T)$ is the liquid drop part of the binding energy and δU, the shell corrections. $V_{LDM}(A_i, Z_i, T)$ is calculated by using the T-dependent liquid drop model energy V_{LDM} of [32], with its constants at T=0 re-fitted in Chapter 3 to give the recent experimental binding energies [33] and calculated binding energies [34] (only for those nucleides for which experimental data is not available). The "empirical" shell corrections δU are of Ref. [35]. The detailed description for V_{LDM} and δU with their temperature dependence is given in Chapter 3. The shell corrections δU in Eq. (2.16) are considered to vanish exponentially for $E^*_{CN} \geq 60\ MeV$, giving $T_0 = 1.5\ MeV$ [36]. At higher excitation energies the shell corrections vanish completely and only the liquid drop part of energy is present. The shell corrections play an important role in determining or empirical fitting of nuclear masses, because the nuclear masses calculated by using the smooth liquid drop formula show large deviations with respect to the experimental masses. It means that in the experimental masses there exist deep minima at specific neutron and/or proton numbers indicating the presence of shell structure, the so-called magic numbers in nuclei. This characteristic behavior cannot be reproduced by the liquid drop part alone, which means that the introduction of microscopic shell correction in the mass formula is essential. Thus, shell corrections accounts for the removal of deviation from the liquid drop calculations (uniform distribution of nucleons), and are defined, within Strutinsky [31] method as

$$\delta U = U - \tilde{U} \tag{2.17}$$

where, $U = \sum_\nu E_\nu 2n_\nu$ is the sum over all occupied single particle states and

$$\tilde{U} = 2 \int_{-\infty}^{\tilde{\lambda}} E\tilde{g}(E)dE. \tag{2.18}$$

is the average energy for uniform distribution. In general, the microscopic shell correction, together with the liquid drop part, gives a proper description of the binding energy of the nucleus. This method, however, does not give a proper description of light mass nuclei. The difficulty is the inadequacy of shell model for very light nuclei. For this reason, the macro-microscopic calculations of Möller *et al.* [34] are tabulated for $Z \geq 8$ only. For $Z \leq 8$, one could alternatively use the empirical shell correction method of Myers-Swiatecki [35] which again is not very satisfactory for light nuclei ($Z \leq 16$). Gupta and collaborators have modified this empirical method and obtained a better description of the shell corrections for the light as well as heavy mass region, i.e, $1 \leq Z \leq 118$ [2].

The nuclear temperature T (in MeV) is related to the excitation energy E^*_{CN} of the compound nucleus, through a semi-empirical statistical relation as:

$$E^*_{CN} = \frac{1}{9}AT^2 - T \qquad (MeV). \tag{2.19}$$

2.2.3 The Proximity Potential for deformed, oriented and co-planar nuclei

When two surfaces approach each other within a small distance of less than $\sim 2fm$, comparable with the surface thickness of interacting nuclei, or when a nucleus is at the verge of dividing into two fragments, then the two surfaces actually face each other across a small gap or crevice. In both cases, the surface energy term alone could not give rise to the strong attraction that is observed when the two surfaces are brought in close proximity. Such additional attractive forces are called proximity forces and the additional potential due to these forces is called the nuclear proximity potential. Blocki *et al.* [37] have reanalyzed and extended a theorem, originally due to Deryagin [38], according to which the force between two gently curved surfaces in close proximity is proportional

to the interaction potential per unit area between the two flat surfaces. The proximity potential [39] for hot deformed nuclei is given as

$$V_p(A_i, \beta_{\lambda i}, \theta_i, T) = 4\pi \bar{R}(T)\gamma b(T)\Phi(s_0(T)). \tag{2.20}$$

$\Phi(s_0)$ is the universal function, independent of the shapes of nuclei or the geometry of nuclear system, but depends on the minimum separation distance s_0,

$$\Phi(s_0) = \begin{cases} -\frac{1}{2}(s_0 - 2.54)^2 - 0.0852(s_0 - 2.54)^3 \\ -3.437exp(-\frac{s_0}{0.75}) \end{cases} \tag{2.21}$$

respectively, for $s_0 \leq 1.2511$ and $s_0 \geq 1.2511$. Here, s_0 is defined in units of b, i.e. s_0 is s_0/b. This function is defined for negative (the overlap region), zero (touching configuration) and positive values of s_0. s_0, distance of closest approach defined in Fig. 1.3, depends on deformations and orientations of reactants/products (explained later in this section). b is the diffuseness of the nuclear surface given by

$$b = \left[\pi/2\sqrt{3}\ln 9\right]_{t_{10-90}},$$

where t_{10-90} is the thickness of the surface in which the density profile changes from 90% to 10%. The value of b$\sim$1 fm. However, temperature dependent b is given as

$$b(T) = 0.99(1 + 0.009T^2) \tag{2.22}$$

The γ is the specific nuclear surface tension given by

$$\gamma = 0.9517\left[1 - 1.7826\left(\frac{N-Z}{A}\right)^2\right] MeVfm^{-2} \tag{2.23}$$

$\overline{R}$ is the mean curvature radius of the reaction partners and is described in the following for deformed and oriented nuclei.

Fig. 1.3 shows a schematic configuration of two (equal/ unequal) axially symmetric deformed, oriented nuclei, lying in the same plane ($\phi = 0^0$), for various θ_1 and θ_2 values

in the range 0^0 to 180^0. θ_i is the angle of orientation, defined as an angle between the symmetry axis and the axis of collision, with it's rotation measured in anti-clockwise direction from the axis of collision. α_i is an angle between the symmetric axis and the radius vector $R_i(\alpha_i, T)$ of the colliding nuclei, measured in clockwise direction from the symmetry axis of the nucleus.

For the axially symmetric shapes, the nuclear radius parameter (to all higher multipole orders λ=2,3,4,....) is given by Eqs. (2.14) and (2.15). In terms of the radii of curvature R_{i1} and R_{i2} in the principal planes of curvature of each of the two nuclei (i=1,2) at the points of closest approach (defining s_0 in Fig. 1.3), the mean curvature radius $\bar{R}$ for deformed, oriented nuclei is given by

$$\begin{aligned} \frac{1}{\bar{R}^2} &= \frac{1}{R_{11}R_{12}} + \frac{1}{R_{21}R_{22}} + \left[\frac{1}{R_{11}R_{21}} + \frac{1}{R_{12}R_{22}}\right] sin^2\phi \\ &+ \left[\frac{1}{R_{11}R_{22}} + \frac{1}{R_{21}R_{12}}\right] cos^2\phi. \end{aligned} \tag{2.24}$$

Here, ϕ is the azimuthal angle between the principal planes of curvature of two nuclei (for co-planar nuclei ϕ=0^0). The four principal radii of curvature are

$$\begin{aligned} R_{i1}(\alpha_i) &= \frac{\left[R_i^2(\alpha_i) + R_i'^2(\alpha_i)\right]^{3/2}}{R_i^2(\alpha_i) + 2R_i'^2(\alpha_i) - R_i(\alpha_i)R_i''(\alpha_i)} \\ R_{i2}(\alpha_i) &= \frac{R_i(\alpha_i)sin\alpha_i}{cos(\pi/2 - \alpha_i - \delta_i)}. \end{aligned} \tag{2.25}$$

where, $R_i'(\alpha_i)$ and $R_i''(\alpha_i)$ are the first and second order derivatives of $R_i(\alpha_i)$ with respect to α_i, respectively. For the derivation of the radius of curvature R_{i1}, see [40], and it follows from Fig. 2.1, and Ref. [41], that $R_{i2} = h/cos\omega_i$, with $h = R_i(\alpha_i)sin\alpha_i$ and $\omega_i = \pi/2 - \alpha_i - \delta_i$. Also, for $\mathbf{n}$ to be a normal vector

$$tan\delta_i = -\frac{R_i'(\alpha_i)}{R_i(\alpha_i)}. \tag{2.26}$$

Note that $R_{i1}(\alpha_i) = R_{i2}(\alpha_i)$, respectively, for $\alpha_1 = 0^0$ or 180^0 and $\alpha_2 = 180^0$ or 360^0. For a configuration of deformed, oriented nuclei, the minimum distance s_0 (Fig. 1.3) in Eq.

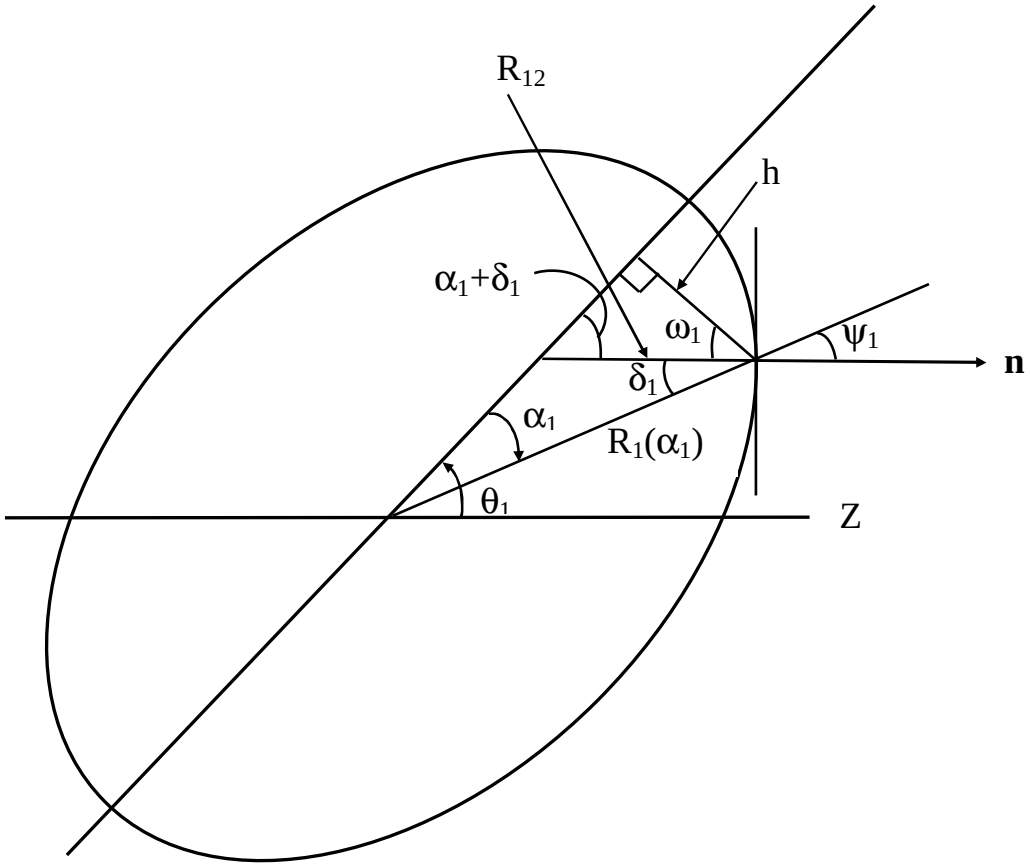

Figure 2.1: An axially symmetric (quadrupole) deformed and oriented nucleus, showing the nuclear radius parameter $R_1(\alpha_1)$ and the geometry associated with the principal radius of curvature $R_{12}(\alpha_1)$.

(2.21) is

$$s_0 = R - X_1 - X_2 \tag{2.27}$$

with the projections X_i along the collision Z-axis given as

$$\begin{aligned} X_1 &= R_1(\alpha_1)cos(\theta_1 - \alpha_1) \\ X_2 &= R_2(\alpha_2)cos(180 + \theta_2 - \alpha_2) \end{aligned} \tag{2.28}$$

with the minimization conditions on s_0,

$$\frac{\partial s_0}{\partial \alpha_1} = \frac{\partial s_0}{\partial \alpha_2} = 0, \tag{2.29}$$

resulting in

$$\begin{aligned} \tan(\theta_1 - \alpha_1) &= -\frac{R_1'(\alpha_1)}{R_1(\alpha_1)} \\ \tan(180 + \theta_2 - \alpha_2) &= -\frac{R_2'(\alpha_2)}{R_2(\alpha_2)}. \end{aligned} \tag{2.30}$$

Comparing Eqs. (2.26) and (2.30), we get

$$\begin{aligned} \delta_1 &= \theta_1 - \alpha_1 \\ \delta_2 &= 180 + \theta_2 - \alpha_2, \end{aligned} \tag{2.31}$$

to be used in Eq. (2.25). Thus, for the given θ_1 and θ_2, X_1 and X_2 are obtained for the angles α_1 and α_2 satisfying the minimization conditions Eq. (2.30). From a detailed study [39], based upon QMFT by Gupta and collaborators, the optimum orientations are given for "cold, non-compact" and "hot, compact" fusion configurations corresponding to largest interaction radius/lowest barrier and smallest interaction radius/highest barrier respectively. The details can be seen in Table 1 of [39]. These optimum orientations have been used in the present study for cluster radioactive decay and for the decay of heavy excited CN.

Note that the conditions Eq. (2.30) refer to perpendiculars (normal vectors) at the points P_1 and P_2. In other words, if the distance s_0 were to be shortest, the perpendicular conditions Eq. (2.30) must be used which would apparently give equations Eq. (2.28) for X_i.

The eq. (2.20) is valid for zero (touching configuration) and positive values of s_0, but is also used for negative s_0. As the two nuclei overlap ($s_0 < 0$), a crevice is formed and, in an adiabatic approximation, the system adjusts its shape parameters such that the two colliding nuclei form a single indented body in the form of a single hyperboloid of one sheet with a hyperboloidal crevice, as shown in Fig. 2.2 (a). For such a necked system, shown in Fig. 2.3 (b), following Blocki *et al.* [37], the proximity potential is obtained by

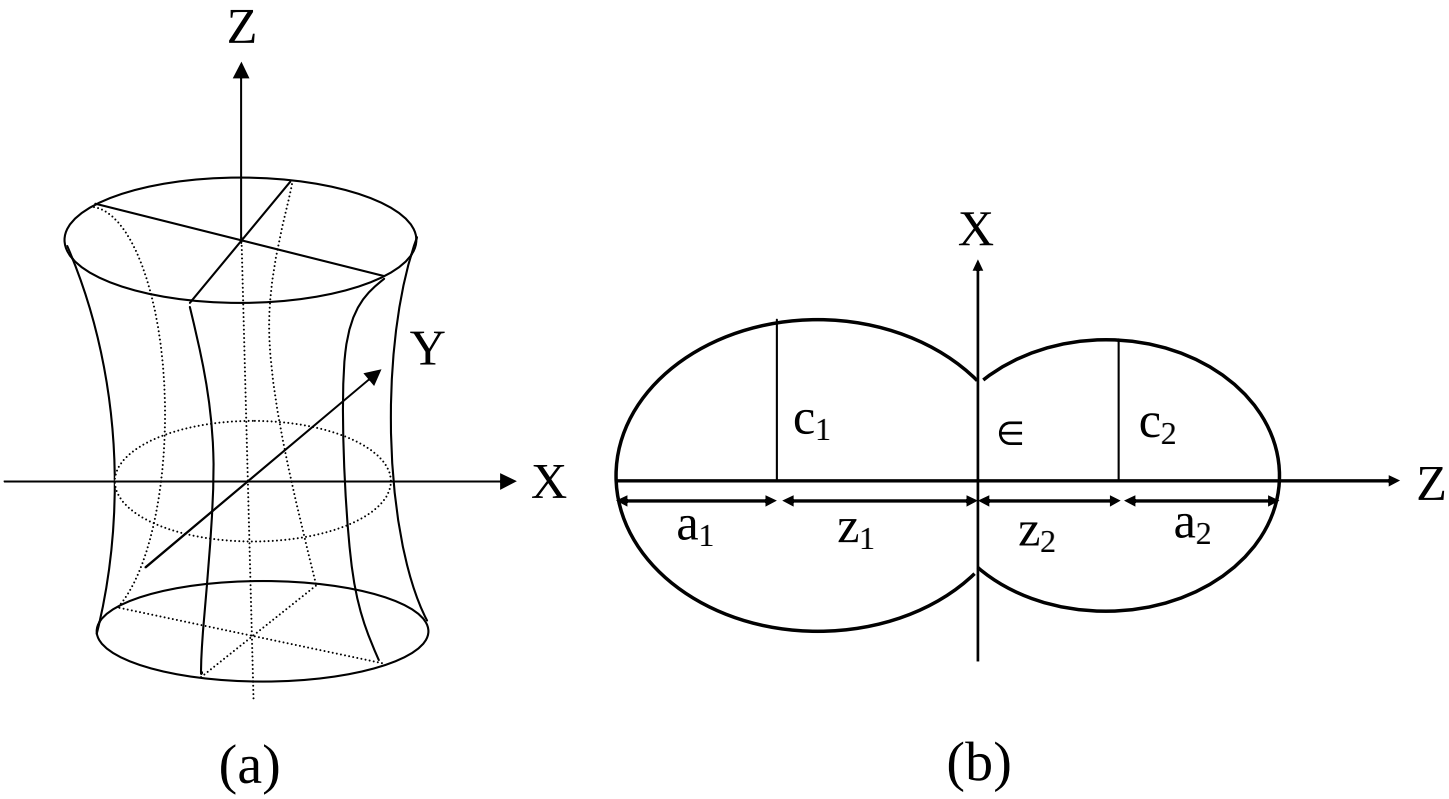

Figure 2.2: (a) Schematic representation of a hyperboloid of revolution in one sheet. (b) Sample nuclear shape formed in two center shell model.

Gupta and collaborators [13],[42] as

$$V_P(s_0) = \pi\gamma b^2 \Phi_1(s_0 = 0) \frac{(c_1^2 + c_2^2 - 2\epsilon^2)}{(z_1^2 + z_2^2)} \tag{2.32}$$

where $\Phi_1(s_0 = 0)$=-2.0306 is the first moment of the universal function Φ at $s_0 = 0$, and c_i, z_i and ϵ are the shape parameters in Fig. 2.2 (b). Apparently, for two equal nuclei, $z_1 = z_2$ and $c_1 = c_2$.

2.2.4 The Coulomb potential

Coulomb potential describes the force of repulsion between two interacting nuclei due to their charges. It acts along the line joining the two nuclei. The Coulomb potential [39] for two interacting hot, deformed and oriented nuclei is given as

$$V_c(Z_i, \beta_{\lambda i}, \theta_i, T) = \frac{Z_1 Z_2 e^2}{R(T)} + 3 Z_1 Z_2 e^2 \sum_{\lambda, i=1,2} \frac{R_i^\lambda(\alpha_i, T)}{(2\lambda + 1) R(T)^{\lambda+1}}$$

$$Y_\lambda^{(0)}(\theta_i)\Big[\beta_{\lambda i} + \frac{4}{7}\beta_{\lambda i}^2 Y_\lambda^{(0)}(\theta_i)\Big], \tag{2.33}$$

with R_i from Eq. (2.14). $Y_\lambda^{(0)}(\theta_i)$ are the spherical harmonics function.

2.2.5 Rotational Energy due to angular momentum

The rotational motion gives an additional energy due to the angular momentum ℓ, defined as

$$V_\ell(R, A_i, \beta_{\lambda i}, \theta_i, T) = \frac{\hbar^2 \ell(\ell+1)}{2I_s(T)} \tag{2.34}$$

with $I(T)$=I_{NS}=μR^2, is the non-sticking limit of moment of inertia with $\mu = \frac{A_1 A_2}{A_1+A_2} m$ as the reduced mass. m is the nucleon mass. In the complete sticking limit, the moment of inertia I is given as,

$$I_s(T) = \mu R^2 + \frac{2}{5} A_1 m R_1^2(\alpha_1, T) + \frac{2}{5} A_2 m R_2^2(\alpha_2, T). \tag{2.35}$$

with R_i from Eq. (2.14). However, for the relative separation of interest here, we use the sticking limit. It is relevant to mention here that value of angular momentum extracted experimentally, is normally based on the moment of inertia calculated in non-sticking limit (i.e. $I_{NS} = \mu R^2$)) [43]. It means that fragment emission is punctual. In our study, however, we find that sticking limit is more appropriate for the proximity potential (nuclear surface $\leq$ 2 fm apart) which consequently results in much larger limiting value of angular momentum [7].

2.2.6 Classical Hydrodynamical Mass Parameters

The kinetic energy part of the Hamiltonian in Eq. (2.8) enters through the mass parameters $B_{\eta\eta}$. We use here the classical hydrodynamical mass parameters of Kröger and Scheid [44]. The model of Kröger and Scheid is based on the hydrodynamical flow, as shown in Fig. 2.3. This model gives a simple analytical expression, whose predictions are shown to compare nicely with the microscopic cranking model calculations. For the $B_{\eta\eta}$

mass we get,

$$B_{\eta\eta} = \frac{AmR^2}{4}\left[\frac{v_t(1+\gamma)}{v_c(1+\delta^2)} - 1\right] \tag{2.36}$$

with

$$\gamma = \frac{R_c}{2R}\left[\frac{1}{1+\cos\vartheta_1}\left(1-\frac{R_c}{R_1}\right) + \frac{1}{1+\cos\vartheta_2}\left(1-\frac{R_c}{R_2}\right)\right] \tag{2.37}$$

$$\delta = \frac{1}{2R}\left[(1-\cos\vartheta_1)(R_1-R_c) + (1-\cos\vartheta_2)(R_2-R_c)\right] \tag{2.38}$$

$$v_c = \pi R_c^2 R \tag{2.39}$$

and $v_t = v_1 + v_2$, is the total conserved volume. The angles ϑ_1 and ϑ_2 and geometry

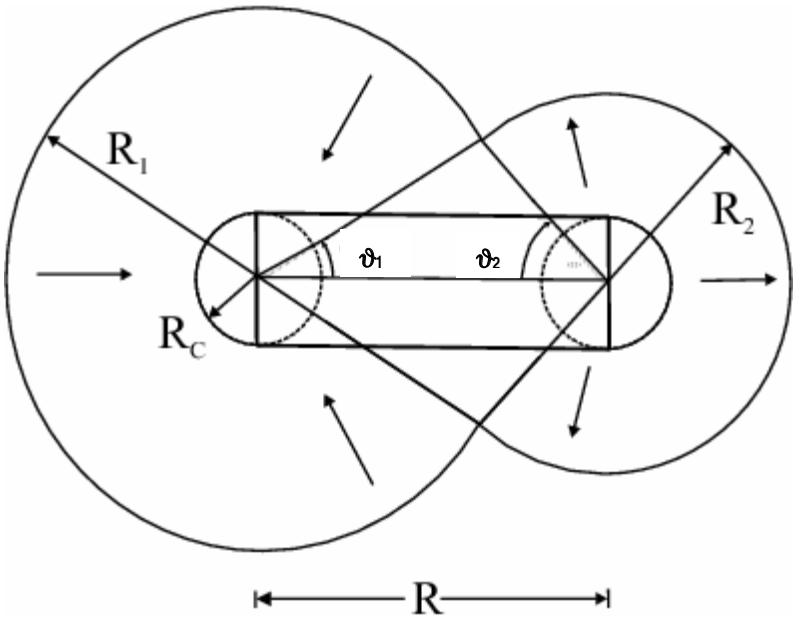

Figure 2.3: The geometry of the classical hydrodynamical model of Kröger and Scheid for calculating the mass parameter $B_{\eta\eta}$.

of the model are shown in Fig. 2.3. For $\vartheta_1 = \vartheta_2 = 0$, $\delta = 0$ which corresponds to two touching spheres. $R_c(\neq 0)$ is the radius of a cylinder of length R, having a homogeneous flow in it; whose existence is assumed for the mass transfer between the two spherical fragments. We have generalized this formalism for deformed nuclei by using the radii R_1 and R_2 for hot deformed nuclei, given by Eq. (2.14).

2.2.7 Preformation Probability P_0

Once the Hamiltonian Eq. (2.7) is established, the Schrödinger equation in mass fragmentation co-ordinate η can be solved. On solving Eq. (2.8) numerically, $|\psi^{\nu}(\eta)|^2$ gives the probability P_0 of finding the mass fragmentation η at a fixed R on the decay path,

$$P_0(A_2) \propto |\psi^{\nu}(A_2)|^2 \tag{2.40}$$

For fission studies, like the spontaneous fission and fission through the barrier, the motion in R at the saddle point is adiabatically slow as compared to the η motion. Therefore, the potential is minimized in the neck ε and deformation coordinates β_1 and β_2 at each R and η values. Starting from the nuclear ground state in spontaneous fission or cluster decay, and to have complete adiabaticity, only the lowest vibrational state $\nu = 0$ is occupied. Then, the mass (or charge) distribution yield, proportional to the probability $|\psi^{(0)}(\eta)|^2$ (or $|\psi^{(0)}(\eta_Z)|^2$) of finding a certain mass (or charge) fragmentation η (or η_Z) at a position R on the decay path, when scaled to, say, mass A_2 of one of the fragments ($d\eta = \frac{2}{A}$) is given by:

$$Y(A_2) = |\psi_R^{(0)}(A_2)|^2 \frac{2}{A} \sqrt{B_{\eta\eta}(A_2)}). \tag{2.41}$$

However, if the system is excited or we allow interaction between various degrees of freedom, higher values of ν would also contribute. These enter via the excitation of higher vibrational states, and through the temperature dependent potential V and masses B_{ij}.

The effect of adding temperature on potential V and masses B_{ij} is to reduce the shell effects in them, resulting finally in the liquid drop potential V_{LDM} and smoothed (averaged) masses $\bar{B}_{ij}$ for the systems to be very hot. Apparently, cold fission means taking both the potential V and masses B_{ij} with full shell effects included in them and hot fission means using the V_{LDM} and smoothed (averaged) masses $\bar{B}_{ij}$. The possible consequence of such excitations are included here by assuming a Boltzmann like occupation of excited states

$$|\psi(\eta)|^2 = \sum_{\nu=0}^{\infty} |\psi^{\nu}(\eta)|^2 \exp\left(-\frac{E_{\eta}^{\nu}}{T}\right) \tag{2.42}$$

Note that we are dealing here with a directly measurable quantity, the mass (or charge)

asymmetry, which works dynamically as mass (or charge) transfer coordinate. Thus, the calculated yields $Y(A_i)$ (or $Y(Z_i)$) are directly comparable with experiments. It may be stressed that there is no free parameter in these calculations. The nuclear shape, once minimized in the neck ε and deformation coordinates β_1 and β_2 at a given R ($\approx R_{saddle}$), remains fixed for both the mass and charge distributions of fission or decay fragments.

2.3 Penetration Probability P

For R-motion, instead of solving the Schrödinger Eq.(2.9), Gupta and collaborators used the WKB approximation to calculate the penetration probability P. For each η-value, the potential $V(R)$ for $R \geq R_t$ is calculated by using Eq.(2.12) and for $R < R_t$ it is parameterized simply as a polynomial of degree two in R, as

$$V(R) = \begin{cases} a_1 R + a_2 R^2 & for \quad R_0 \leq R \leq R_t \\ V_c + V_p + V_\ell & for \quad R \geq R_t \end{cases} \tag{2.43}$$

A typical scattering potential, for ^{232}U$\rightarrow^{208}$Pb+^{24}Ne is shown in Fig. 2.4. This is calculated by using Eq. (2.12) for the case of ℓ=0. The path of the penetration and the related quantities are shown. The constants a_i ($i = 1, 2$) occurring in the polynomial, are determined by using the following boundary conditions.

1. At $R = R_0$, $V(R) = Q$
2. At $R = R_t$, $V(R) = V(R_t)$

In order to avoid the use of undetermined part of the potential, i.e., $V(R_0 \leq R \leq R_t)$, the first (inner) turning point R_a is chosen at the touching configuration, R_a= R_t, and the outer turning point is taken at R_b to give the Q-value of the reaction, i.e., $V(R_b) = Q$. This means that the transmission probability P consists of three contributions

1. The penetrability P_i from R_t to R_i,
2. the (inner) de-excitation probability W_i at R_i and

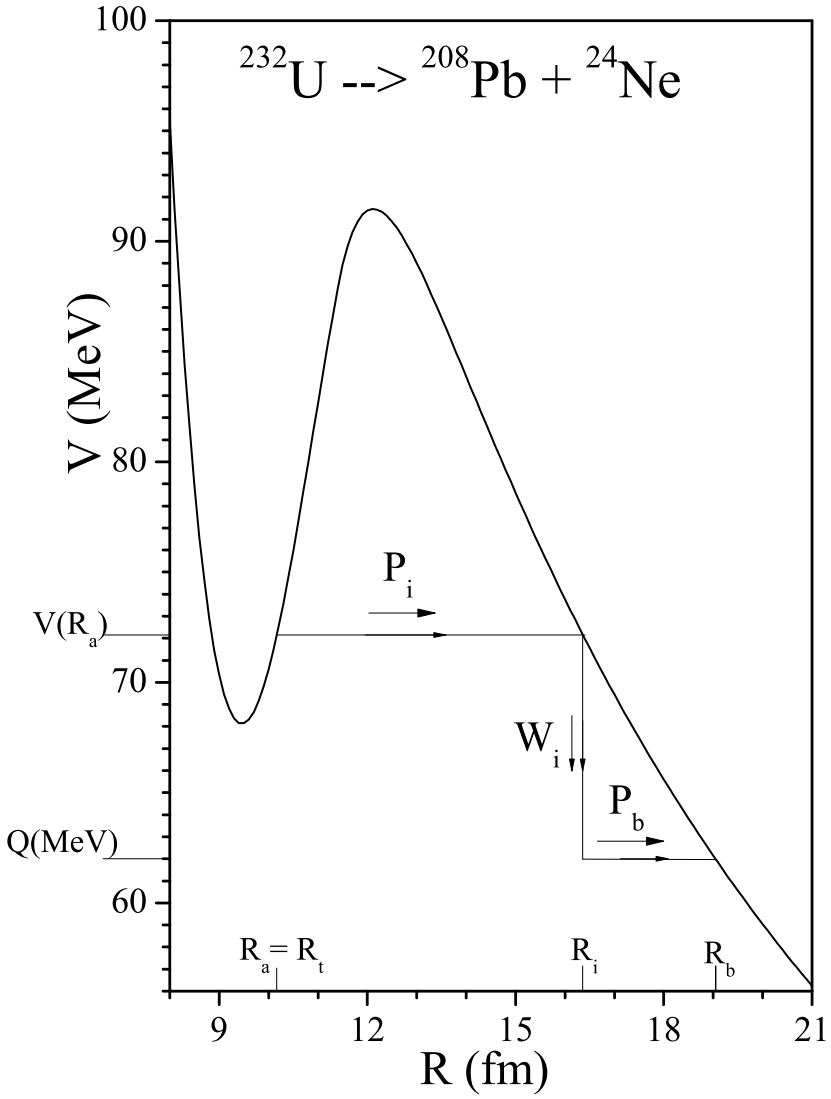

Figure 2.4: The scattering potentials for the ^{24}Ne cluster decay of parent nucleus ^{232}U daughter being ^{208}Pb i.e. ^{232}U$\rightarrow^{208}$Pb+^{24}Ne, with characteristic quantities marked in it.

3. the penetrability P_b from R_i to R_b

giving the penetration probability as

$$P = P_i W_i P_b. \tag{2.44}$$

The shifting of first turning point from R_t to R_0 gives the penetrability calculations similar to Shi and Swiatecki [45] for spherical nuclei, which is known not to fit the experimental data without the adjustment of assault frequency. Following the excitation model of M. Greiner and W. Scheid [46], the de-excitation probability W_i is given as

$$W_i = \exp(-bE_i) \tag{2.45}$$

This means that the de-excitation process is restricted to only a single transition. If the parameter b were allowed to depend on R_i, it should then become a process of multiple de-excitation and proceed as step-like process. For a heavy cluster decay into the excited states of the daughter nucleus the $b = 0$ is assumed [46], which means

$$W_i = 1, \tag{2.46}$$

so that,

$$P = P_i P_b, \tag{2.47}$$

where P_i and P_b are calculated by using WKB approximation, as

$$P_i = \exp\left[-\frac{2}{\hbar}\int_{R_a}^{R_i}\{2\mu[V(R) - V(R_i)]\}^{1/2}dR\right] \tag{2.48}$$

and

$$P_b = \exp\left[-\frac{2}{\hbar}\int_{R_i}^{R_b}\{2\mu[V(R) - Q]\}^{1/2}dR\right]. \tag{2.49}$$

Here R_a and R_b are, respectively, the first and second turning points. This means that the tunnelling begins at $R = R_a$ and terminates at $R = R_b$, with $V(R_b) = Q$-value for ground state decay.

The integrals of the Eqs.(2.48) and (2.49) are solved analytically by parameterizing the above calculated potential $V(R)$, as follows:

$$V(R) = \begin{cases} a_1 R + a_2 R^2, & R_0 \leq R \leq R_t, \\ V(R_t) + m(R - R_t), & R_t \leq R \leq R_m, \\ V_B - \frac{1}{2}k(R - R_B)^2, & R_m \leq R \leq R_h, \\ V(R_h) - c_1\frac{R-R_h}{R}, & R_h \leq R \leq R_i, \\ V(R_i) - c_2\frac{R-R_i}{R}, & R_i \leq R \leq R_b, \end{cases} \tag{2.50}$$

For a polynomial of degree higher than two, analytical solutions of WKB integrals could not be obtained. The polynomial equation above is true for any inner turning point and hence R_t could be chosen empirically at any point on the polynomial part, as

was shown by Kumar and Gupta [13]. Equation (2.50) means that, the first part of the potential from R_0 to R_t (or R_{emp}) is a polynomial of degree two in R, the second part from R_t to R_m is a straight line of slope $'m'$, the top part between R_m and R_h being an inverted harmonic oscillator and the rest from R_h to R_i and R_i to R_b are the Coulomb potentials of the type $1/R$. Finally, V_B and R_B give the height and position of the barrier. The analytical solution for the integrals are obtained as

$$\int_{R_b}^{R_t} V(R)dR = \int_{R_m}^{R_t} V(R)dR + \int_{R_h}^{R_m} V(R)dR + \int_{R_i}^{R_h} V(R)dR + \int_{R_b}^{R_i} V(R)dR \qquad (2.51)$$

For different components of Eq.(2.47), we have

$$\begin{aligned} P_i \;=\; & exp[-\frac{2}{\hbar}\sqrt{2\mu}\{\frac{\sqrt{a_2}}{2}[t_1(t_1^2-L^2)^{\frac{1}{2}} - t_2(t_2^2-L^2)^{\frac{1}{2}} \\ & -L^2(cosh^{-1}(\frac{t_1}{L}) - cosh^{-1}(\frac{t_2}{L})] \\ & +\frac{2}{3}(\frac{R_m-R_t}{V(R_m)-V(R_t)})[(V(R_m)-V(R_i))^{\frac{3}{2}} - (V(R_t)-V(R_i))^{\frac{3}{2}}] \\ & -\frac{1}{\sqrt{2k}}[V_B - V(R_i)][\Theta_2 - \frac{1}{2}sin2\Theta_2 - \Theta_1 + \frac{1}{2}sin2\Theta_1] \\ & +\sqrt{C_1R_hR_i}[\Theta_3 - \frac{1}{2}sin2\Theta_3]\}] \end{aligned} \qquad (2.52)$$

with

$$a_1 = \frac{R_0(Q-V(R_t))}{R_t(R_t-R_0)}, a_2 = -\frac{a_1}{R_0}, t_1 = R_t - \frac{1}{2}R_0, t_2 = R_{emp} - \frac{1}{2}R_0$$

$$L^2 = \frac{1}{4}R_0^2 + R_t(R_t-R_0)\left[\frac{Q-V(R_i)}{Q-V(R_t)}\right]$$

$$\Theta_1 = \cos^{-1}\frac{R_m-R_B}{\sqrt{\alpha}_2}, \Theta_2 = \cos^{-1}\frac{R_h-R_B}{\sqrt{\alpha}_2}, \Theta_3 = \tan^{-1}\left(\frac{R_i-R_h}{R_h}\right)^{1/2}$$

$$\alpha_2 = \frac{2}{k}[V_B - V(R_i)]$$

$$k = \frac{2\{[(V_B - V(R_m)]^{1/2} + [V_B - V(R_h)]^{1/2}\}^2}{(R_m - R_h)^2}, C_1 = R_i \frac{(V(R_h) - V(R_i))}{R_i - R_h}$$

and

$$P_b = \exp\left[-\frac{2}{h}\sqrt{2\mu}\sqrt{C_2 R_i R_b}\left\{\Theta_4 - \frac{1}{2}\sin 2\Theta_4\right\}\right] \tag{2.53}$$

with

$$\Theta_4 = tan^{-1}\left[\frac{R_b - R_i}{R_i}\right]^{1/2},$$

$$C_2 = \frac{R_b[V(R_i) - V(R_b)]}{R_b - R_i}.$$

Substituting these values in Eqs. (2.48) and (2.49) we get P_i and P_b. Further substituting P_i and P_b in Eq. (2.47) we get the probability of penetration or the tunnelling probability, P.

2.4 The Preformed Cluster-decay Model for ground state decay of nucleus

After the establishment of exotic cluster decay [47] many theoretical models were advanced [8],[9],[45], [48]-[51]. In general, these theoretical attempts were made to understand this process in terms of nuclear α decay or nuclear fission. These models fall into two main categories. i) Unified fission models (UFM), and ii) Preformed cluster-decay models (PCM). In the UFM, the cluster decay is dealt simply as a barrier penetration problem, where as in the PCM it is considered to happen in two steps as mentioned in section 2.1. Preformed Cluster Model of Gupta and [8]-[16] has been developed by adopting the Gamow's theory of α-decay. Here, instead of a square well potential, a more realistic nuclear potential, the nuclear proximity potential, is used and also a preformation probability P_0 is associated with each of the emitted cluster. In Gamow's theory of α-decay [52], the preformation probability for α-decay is assumed to be unity, since only α-cluster is considered. In PCM, preformation probability is different for different clusters and it decreases with the increasing size of the cluster. It is relevant to mention here that theoretically the preformation probabilities for all the possible clusters can be obtained in PCM, whereas,

in the other model due to Blendowske et al. [49],[53] the preformation probabilities are calculated for the cluster mass of up to only $A = 16$.

The decay constant in the PCM of Gupta and collaborators is defined as,

$$\lambda = P_0 \nu_0 P. \tag{2.54}$$

The corresponding half life is given by:

$$T_{\frac{1}{2}} = \frac{ln2}{\lambda}. \tag{2.55}$$

PCM here gives the ground state description (ℓ=0 and T =0) of the decay of parent nuclei, with deformation and orientation effects of daughters and clusters included in it. P_0 is preformation probability of the cluster giving the probability of the formation of the cluster within the mother nucleus, which is also shown to carry the effects of deformations and orientations of outgoing fragments. For a pure Coulomb potential and $P_0 = 1$, the above equation (2.54) will give the Gamow factor 'λ_G'. Thus, in contrast to the unified fission models, the clusters in PCM are considered to be preformed with probability P_0, at a relative separation measured in terms of co-ordinate R before the penetration of the potential barrier. Here ν_0 is the impinging frequency with which the cluster hits the barrier, defined in terms of its velocity v as,

$$\nu_0 = \frac{v}{R_0}, \tag{2.56}$$

where R_0 is the radius of parent nucleus. In terms of the kinetic energy E_2 of the emitted cluster, $v = (2E_2/\mu)^{1/2}$. Since both the emitted cluster and the daughter nucleus are produced in the ground state, the entire positive Q-value is equal to total kinetic energy ($Q = E_1 + E_2$) available for the decay process. This kinetic energy is shared between two fragments and the energy of emitted cluster is thus $E_2 = \frac{A_1}{A}Q$ giving ν_0 in terms of Q-value as

$$\nu_0 = \frac{(2Q/A_2)^{1/2}}{R_0} \tag{2.57}$$

and, $E_1 = Q - E_2$ is the recoil energy of the daughter nucleus.

In equation 2.54, P is the penetration probability that gives the probability of penetration of the barrier formed by the outgoing deformed and oriented fragments.

2.5 The Dynamical Cluster-decay Model for hot and rotating compound nucleus

The dynamical cluster decay model (DCM) [1]-[7] for hot and rotating nuclei (i.e. angular momentum $\ell \neq 0$ and temperature $T \neq 0$) is a reformulation of the preformed cluster model (PCM) of Gupta and collaborators for ground-state decays ($\ell=0$ and $T=0$) in cluster radioactivity (CR) and related phenomena [8]-[16]. Like PCM, DCM is also based on the dynamical (or quantum mechanical) fragmentation theory of cold phenomenon in heavy ion reactions and fission dynamics. In DCM, besides the temperature and angular momentum effects in the decay of excited compound nuclei, the deformation and orientation effects of the decay products are also taken care, especially in the decay of heavy excited CN for which deformations of the decay products seem to play significant role. The DCM, worked out in terms of the collective coordinates of mass asymmetry $\eta = \frac{A_1 - A_2}{A_1 + A_2}$ and relative separation R, respectively, give

(i) the nucleon-division (or -exchange) between outgoing fragments, and

(ii) the transfer of kinetic energy of incident channel ($E_{c.m.}$) to internal excitation (total excitation or total kinetic energy, TXE or TKE) of the outgoing channel. It may be noted that the fixed decay point $R = R_a$ (defined later), at which the process is calculated, depends on temperature T as well as on η (i.e. $R(T, \eta)$). This energy transfer process is defined by the following equation (see Fig. 2.5).

$$E^*_{CN} + Q_{out}(T) = TKE(T) + TXE(T). \tag{2.58}$$

The CN excitation energy $E^*_{CN} = E_{c.m.} + Q_{in}$ is related to temperature T (in MeV) as given by Eq.(2.19).

Using the decoupled approximation to R- and η-motions, the DCM defines the CN

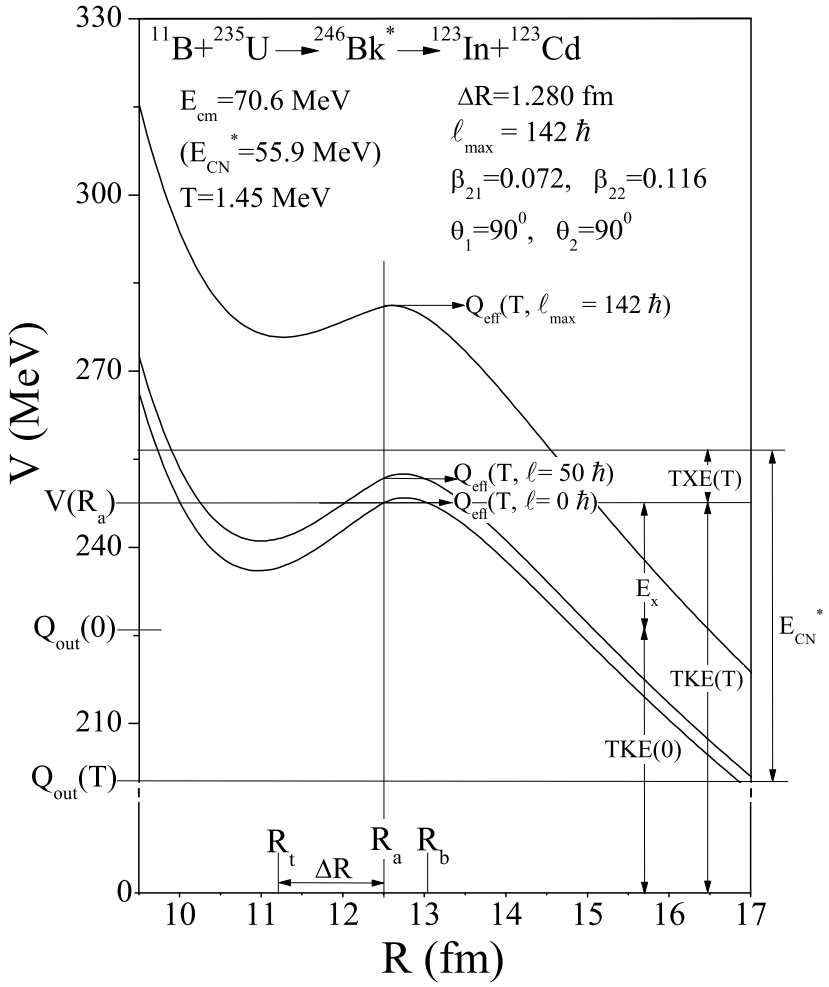

Figure 2.5: The scattering potential for the decay ^{246}Bk* $\rightarrow$^{123}In+^{123}Cd at temperature T=1.45 MeV and different l-values formed in ^{11}B+^{235}U reaction. However, the decay path, defined by $V(R_a, \ell) = Q_{eff}(T, \ell)$ for each ℓ, in this figure is shown to begin at $R_a = R_t + \Delta R$, fixed for the ℓ=0$\hbar$ case.

decay cross section, in terms of partial waves, as [1]-[7]

$$\sigma = \sum_{\ell=0}^{\ell_c} \sigma_\ell = \frac{\pi}{k^2} \sum_{\ell=0}^{\ell_c} (2\ell+1) P_0 P; \qquad k = \sqrt{\frac{2\mu E_{c.m.}}{\hbar^2}} \tag{2.59}$$

where, P_0, the preformation probability, refers to η-motion and P, the penetrability, to R-motion. Here the complex fragments (both light and heavy fragments) are treated as the dynamical collective mass motion of preformed clusters or fragments through the barrier. The structure information of the CN enters the model via the preformation probabilities P_0 (also known as the spectroscopic factors) of the fragments given by the solution of stationary Schrödinger equation in η, at the fixed R=R$_a$, the first turning point of the

penetration path shown in Fig. 2.5 for different ℓ-values,

$$\{-\frac{\hbar^2}{2\sqrt{B_{\eta\eta}}}\frac{\partial}{\partial\eta}\frac{1}{\sqrt{B_{\eta\eta}}}\frac{\partial}{\partial\eta}+V(R,\eta,T)\}\psi^{\nu}(\eta)=E^{\nu}\psi^{\nu}(\eta), \tag{2.60}$$

with ν=0,1,2,3... referring to ground-state ($\nu=0$) and excited-states solutions.

For the decay of a hot CN, we use the postulate for the first turning point

$$R_a(T)=R_t+\Delta R(T) \tag{2.61}$$

where

$$R_t=R_1+R_2 \tag{2.62}$$

$\Delta R(T)$ is the neck-length parameter that assimilates the neck formation effects. This method of introducing a neck length parameter is similar to that used in both the scission-point [54] and saddle-point [55], [56] statistical fission models. The R_i are radius vectors, given by Eqs.(2.14) and (2.15).

The corresponding potential $V(R_a)$ acts like an effective Q-value, Q_{eff}, for the decay of the hot CN at temperature T, to two exit-channel fragments observed in *g.s.* (T=0), defined by

$$\begin{aligned} Q_{eff}(T) &= B(T)-[B_L(T=0)+B_H(T=0)] \\ &= TKE(T)=V(R_a(T)) \end{aligned} \tag{2.63}$$

with B's as the respective binding energies.

The above defined decay of a hot CN into two cold (T=0) fragments, via Eq.(2.63), could apparently be achieved only by emitting some light particle (s) (LPs), like n, p, α, or γ-rays of energy

$$\begin{aligned} E_x &= B(T)-B(0)=Q_{eff}(T)-Q_{out}(T=0) \\ &= TKE(T)-TKE(T=0) \end{aligned} \tag{2.64}$$

which is zero for the g.s. decay, like for exotic CR. Note that the second equality in Eq.

(2.64) is not defined for a negative $Q_{out}(T = 0)$ system since the negative TKE(T=0) has no meaning. Apparently, Eq. (2.64) w.r.t (2.63) suggests that the emission of light-particles starts early in the decay process. The exit channel fragments in Eq. (2.63) are then obtained in the ground-state with TKE(T=0), as can be seen by calculating $E^*_{CN} - E_x$:

$$E^*_{CN} - E_x = -Q_{out}(T) + TKE(T = 0) + TXE(T). \tag{2.65}$$

The excitation energy TXE(T) (not treated here) is used in, the secondary emission of light particles from the fragments which are otherwise in their ground states with TKE(T=0) in the radial motion. Thus, by defining $Q_{eff}(T)$ as in Eq. (2.63), in this model we treat the LP emission at par with the heavy fragments, called intermediate mass fragments ($IMFs$) emission. Thus, in this model a non-statistical dynamical treatment is attempted for not only the emission of $IMFs$ but also of multiple LPs, understood so-far only as the statistically evaporated particles in a CN emission. It may be reminded here that the statistical model interpretation of $IMFs$ is not as good as it is for the LP production [54]-[59].

In terms of $Q_{eff}(T)$, the second turning R_b satisfies (see Fig. 2.5)

$$V(R_a, \ell) = V(R_b, \ell) = Q_{eff}(T, \ell) = TKE(T). \tag{2.66}$$

with the ℓ-dependence of R_a defined by

$$V(R_a, \ell) = Q_{eff}(T, \ell = 0), \tag{2.67}$$

which means that the R_a, given by Eq. (2.67), is the same for all ℓ-values, and that $V(R_a, \ell)$ acts like an effective Q-value, $Q_{eff}(T, \ell)$, given by the total kinetic energy $TKE(T)$. Then, using (2.66), $R_b(\ell)$ is given by the ℓ-dependent scattering potentials, at fixed T is given by Eq.(2.12), which is normalized to the exit channel binding energy $B_L(T) + B_H(T)$. Such a potential is illustrated in Fig. 2.5, for ^{246}Bk* $\rightarrow ^{123}$In+^{123}Cd, at different ℓ-values. The second turning point R_b is marked for the $\ell = 0\hbar$ case of $R_a = R_t + \Delta R(T)$. Note that as the ℓ-value increases, the $Q_{eff}(T)$-value (=TKE(T))

increases and hence $V(R_a, \ell)$ increases, since the decay path for all the ℓ-values begins at $R = R_a$.

Finally, the ℓ_c-value in Eq. (2.59) is the critical ℓ-value, in terms of the bombarding energy $E_{c.m.}$, the reduced mass μ and the first turning point R_a of the entrance channel η_{in}, given by

$$\ell_c = R_a \sqrt{2\mu[E_{c.m.} - V(R_a, \eta_{in}, \ell = 0)]}/\hbar, \tag{2.68}$$

or, alternatively, it could be fixed for the vanishing of fusion barrier of the incoming channel, called ℓ_{fus}, or else the ℓ-value (ℓ_{max}) where the light-particle cross section $\sigma_{LP} \rightarrow 0$. This, however, could also be taken as a variable parameter [55, 60].

Bibliography

[1] R.K. Gupta, R. Kumar, N.K. Dhiman, M. Balasubraniam, W. Scheid, and C. Beck, Phys. Rev. **C 68**, 014610 (2003).

[2] M. Balasubraniam, R. Kumar, R.K. Gupta, C. Beck, and W. Scheid, J. Phys. **G 29**, 2703 (2003).

[3] R.K. Gupta, M. Balasubraniam, R. Kumar, D. Singh, and C. Beck, Nucl. Phys. **A 738**, 479c (2004).

[4] R.K. Gupta, M. Balasubramaniam, R. Kumar, D. Singh, C. Beck, and W. Greiner, Phys. Rev. **C 71**, 014601 (2005).

[5] B. B. Singh, M. K. Sharma, R. K. Gupta, and W. Greiner, Int. J. Mod. Phys. E **15**, 699 (2006).

[6] R.K. Gupta, M. Balasubramaniam, R. Kumar, D. Singh, S. K. Arun and W. Greiner, J. Phys. G: Nucl. Part. Phys. **32**, 345 (2006).

[7] B. B. Singh, M. K. Sharma and R. K. Gupta, Phys. Rev. **C 77**, 054613 (2008).

[8] R.K. Gupta, in Proceedings of the 5th International Conference on Nuclear Reaction Mechanisms, Varenna, 1988, edited by E. Gadioli, (Ricerca Scientifica ed Educazione Permanente, Milano, 1988), p. 416.

[9] S.S. Malik and R.K. Gupta, Phys. Rev. **C 39**, 1992 (1989).

[10] R.K. Gupta, W. Scheid, and W. Greiner, J. Phys. G: Nucl. Part. Phys. **17**, 1731 (1991).

[11] S. Kumar and R.K. Gupta, Phys. Rev. **C 49**, 1922 (1994).

[12] R.K. Gupta and W. Greiner Int. J. Mod. Phys. E **3**, 335 (1994, Suppl.).

[13] S. Kumar and R.K. Gupta, Phys. Rev. **C 55**, 218 (1997).

[14] R.K. Gupta, in *Heavy Elements and Related New Phenomena*, edited by W. Greiner and R.K. Gupta (World Scientific, Singapore, 1999), Vol. **II**, p. 730.

[15] S. K. Arun and R. K. Gupta, DAE Nucl. Phys. (Sambalpur) **52**, 365 (2007).

[16] B. B. Singh, S. K. Arun, M. K. Sharma, S. Kanwar and Raj K. Gupta, DAE Nucl. Phys. (Roorkee) **53**, 261 (2008).

[17] J. Maruhn and W. Greiner, Phys. Rev. Lett. **32**, 548 (1974).

[18] R.K. Gupta, W. Scheid and W. Greiner, Phys. Rev. Lett. **35**, 353 (1975).

[19] A. Săndulescu, R.K. Gupta, W. Scheid and W. Greiner, Phys. Lett. **60B**, 225 (1976).

[20] R.K. Gupta, A. Săndulescu and W. Greiner, Phys. Lett. **67B**, 257 (1977); Rev. Roum. Phys. **23**, 51 (1978).

[21] S. Yamaji, W. Scheid, H.J. Fink and W. Greiner, Z. Phys. **A 278**, 69 (1976).

[22] S. Yamaji, W. Scheid, H.J. Fink and W. Greiner, J. Phys. G: Nucl. Phys. **2**, L189 (1976).

[23] S. Yamaji, K.H. Ziegenhain, H.J. Fink, W. Greiner and W. Scheid, J. Phys. G: Nucl. Phys. **3**, 1283 (1977).

[24] R.K. Gupta, A. Săndulescu and W. Greiner, Z. Naturforsch. **32a**, 704 (1977).

[25] R.K. Gupta, C. Pirvulescu, A. Săndulescu and W. Greiner, Z. Phys. **A 283**, 217 (1977); Sovt. J. Nucl. Phys. **28**, 160 (1978).

[26] R.K. Gupta, Z. Physik. **A 281**, 159 (1977).

[27] A. Săndulescu, H.J. Lustig, J. Hahn, and W. Greiner, J. Phys. G: Nucl. Phys. **4**, L279 (1978).

[28] H.J. Lustig, J.A. Maruhn, and W. Greiner, J. Phys. G: Nucl. Phys. **6**, L25 (1980).

[29] H.J. Fink and W. Greiner and R.K. Gupta and S. Liran and J.H. Maruhn and W. Scheid and O. Zohni, in Proceedings of Int. Conf. on Reaction between Complex Nuclei, Nashville, 1974, 21, (Amsterdam: North Holland), pages 2.

[30] R. K. Gupta, IANCAS Bull. (India), **6**, 2(1990).

[31] V.M. Strutinsky, Nucl. Phys. **A 95**, 420 (1967).

[32] N.J. Davidson, S.S. Hsiao, J. Markram, H.G. Miller, and Y. Tzeng, Nucl. Phys. **A 570**, 61c (1994).

[33] G. Audi, A.H. Wapstra and C. Thiboult, Nucl. Phys. A **729**, 337(2003).

[34] P. Möller, J. R. Nix, W. D. Myers, and W. J. Swiatecki, At. Data Nucl. Data Tables **59**, 185 (1995).

[35] W. Myers and W.J. Swiatecki, Nucl. Phys. **81**, 1 (1966).

[36] A. S. Jensen and J. Damgaard, Nucl. Phys. **A203**, 578 (1973).

[37] J. Blocki, J. Randrup, W. J. Swiatecki, and C. F. Tsang, Ann. Phys. (NY) **105**, 427 (1977).

[38] Deryagin, Kolloid Z. **69**, 155 (1934).

[39] R. K. Gupta, M. Balasubramaniam, R. Kumar, N. Singh, M. Mahhas, and W. Greiner, J. Phys. G: Nucl. Part. Phys. **C 31**, 631 (2005).

[40] A. Gray, *Modern Differential Geometry of Curves and Surfaces with Mathematica*, 2nd Edition, CRC Press, Boca Raton, 1997, p.89.

[41] M. Seiwert, W. Greiner, V. Oberacker, and M.J. Rhoades-Brown, Phys. Rev. **C 29**, 477 (1984).

[42] N. Malhotra and R.K. Gupta, Phys. Rev. **C 31**, 1179 (1985).

[43] S. Kailas (private communication).

[44] H. Kröger and W. Scheid, J. Phys. G **6**, L85 (1980).

[45] Y.J. Shi and Swiatecki, Phys. Rev. **C 54**, 300 (1985).

[46] M. Greiner and W. Scheid, J. Phys. G: Nucl. Phys. **12** L229 (1986).

[47] H.J. Rose and G.A. Jones, Nature **307**, 245 (1984).

[48] G.A. Pik-Pichak, Yad. Fiz. **44**, 1421 (1986).

[49] R. Blendowske and H.Walliser, Phys. Rev. Lett. **61**, 1930 (1988).

[50] B. Buck and A. C. Merchant, J. Phys. G: Nucl. Phys. **15**, 615 (1989).

[51] A. Săndulescu, R. K. Gupta, F. Carstoiu, M. Horoi, and W. Greiner, Int. J. Mod. Phys. **E 1**, 374 (1992).

[52] I. Perlman and J. O. Rasmussen, Alpha Radioactivity, Vol. XLII, Springer,Berlin, 1957.

[53] R. Blendowske, T. Fliessbach, and H.Walliser, Nucl. Phys. A**464**, 75 (1987).

[54] T. Matsuse, C. Beck, R. Nouicer, and D. Mahboub, Phys. Rev. **C 55**, 1380 (1997).

[55] S.J. Sanders, D.G. Kovar, B.B. Back, C. Beck, D.J. Henderson, R.V.F. Janssens, T.F. Wang, and B.D. Wilkins, Phys. Rev. **C 40**, 2091 (1989).

[56] S.J. Sanders, Phys. Rev. **C 44**, 2676 (1991).

[57] J. Gomez del Campo, R.L. Auble, J.R. Beene, M.L. Halbert, H.J. Kim, A. D'Onofrio, and J.L. Charvet, Phys. Rev. C **43**, 2689 (1991); Phys. Rev. Lett. **61**, 290 (1988).

[58] R.J. Charity, M.A. McMahan, G.J. Wozniak, R.J. McDonald, L. G. Moretto, D.G. Sarantites, L.G. Sobotka, G. Guarino, A. Pantaleo, L. Fiore, A. Gobbi and K.D. Hildenbrand, Nucl. Phys. **A 483**, 371 (1988).

[59] C. Beck, R. Nouicer, D. Disdier, G. Duchêne, G. de France, R.M. Freeman, F. Haas, A. Hachem, D. Mahboub, V. Rauch, M. Rousseau, S.J. Sanders, and A. Szanto de Toledo, Phys. Rev. **C 63**, 014607 (2001).

[60] S.J. Sanders, D.G. Kovar, B.B. Back, C. Beck, B.K. Dichter, D. Henderson, R.V.F. Janssens, J.G. Keller, S. Kaufman, T.-F. Wang, B. Wilkins, and F. Videbaek, Phys. Rev. Lett. **59**, 2856 (1987).

Chapter 3

Relevance and need of temperature dependent binding energies

3.1 Introduction

The experimental techniques have improved with time and lot of experimental data related to different nuclear phenomena has become available. In the last about three decades, reactions induced by heavy ions have become the principal tool in nuclear physics research. It has led to phenomenological studies of atomic nuclei, which resulted in better and better understanding of related concepts. A significant amount of information is available regarding synthesis of new heavy and superheavy nuclei, study of the radioactive and chemical properties of new nuclei and their isotopes, production of nuclei far from the beta-stability line, formation and decay of exotic nuclear system, etc. Presently a lot of work is being done on the dynamics of nuclear system at extreme composition, excitation energy, angular momentum, nuclear deformation, etc. In brief the study of nucleus at higher excitation energies carries lot of information, which in turn could be extremely useful for the better understanding of nuclear properties.

The recently developed Dynamical Cluster Decay Model (DCM) [1] - [7], is used to study heavy ion reactions at relevant temperature, angular momentum, deformation and orientation, etc. It is relevant to mention here that this model has been applied successfully to study the decay of compound nuclei formed in light ($^{48}Cr^*$, $^{56}Ni^*$), intermediate

($^{116}Ba^{*}$) and heavy ($^{246}Bk^{*}$) mass region [1] - [7]. The fragmentation potential consists of the macroscopic liquid drop energy V_{LDM} besides Coulomb potential, proximity potential and rotational energy. Therefore, in order to investigate the dynamics of a excited nuclear system, the knowledge of temperature dependence of macroscopic part of nuclear potential becomes essential. This temperature dependent liquid drop potential can be calculated as suggested by Davidson et al. [8]. The predictions of this model find its basis in the well established semi-empirical mass formula of Seeger [9]. Although Seeger's formula was quite successful in explaining the available literature of its time (1961) but our knowledge regarding the understanding of nuclear properties has grown, consequently the constants used in this model need major revival in order to meet the present day requirements.

Since our aim here is not to fit the constants of LDM, but to include the temperature dependence explicitly on the the recent binding energies. Therefore, we have fitted only the bulk $\alpha(0)$ and neutron proton asymmetry a_a constants of Seeger's formula at T=0. This refitting of model parameters is extremely useful in view of availability of enormous amount of binding energy data [10],[11]. This work has been partly done upto Z=56 in [1],[2], for experimental data provided at that time [12]. But we have refitted the bulk α(T) and neutron protron asymmetry a_a constants in reference to improved experimental data [10]. In the present work we have not only improved upon previous fittings, but also have extended the same to Z=118. The domain of this work has been further extended for neutron deficient and neutron excess nuclides (for which experimental binding energies are not available). For these neutron deficient/neutron excess nuclei we have made calculations in reference to the theoretical binding energies made available by Möller-Nix [11]. These fitted constants have been successfully used in the recent calculations to study the decay of heavy compound nucleus $^{246}Bk^{*}$ [7] formed in heavy ion reactions at different incident centre of mass energies for two entrance channels $^{11}B+^{235}U$ and $^{14}N+^{232}Th$.

The methodology followed to fit the available binding energies, is presented in section 3.2. The calculations and fitting results are given in section 3.3. Finally, the results are summarized in section 3.4.

3.2 Temperature dependent binding energies

The binding energy B of a nucleus at temperature T has been defined, within the Strutinsky renormalization procedure, as the sum of liquid drop energy $V_{LDM}(T)$ and shell correction $\delta U(T)$ i.e

$$B(T) = V_{LDM}(T) + \delta U exp\Big(- \frac{T^2}{{T_0}^2}\Big). \tag{3.1}$$

3.2.1 Liquid drop energies and their temperature dependence

The T dependent liquid drop part of the binding energy $V_{LDM}(T)$ is taken from Davidson *et al.* [8], based on the semi-empirical mass formula of Seeger [9], as

$$\begin{aligned} V_{LDM}(A,Z,T) &= \alpha(T)A + \beta(T)A^{\frac{2}{3}} + \left(\gamma(T) - \frac{\eta(T)}{A^{\frac{1}{3}}}\right)\left(\frac{I^2 + 2 \mid I \mid}{A}\right) \\ &\quad + \frac{Z^2}{R_0(T)A^{\frac{1}{3}}}\left(1 - \frac{0.7636}{Z^{\frac{2}{3}}} - \frac{2.29}{[R_0(T)A^{\frac{1}{3}}]^2}\right) + \delta(T)\frac{f(Z,A)}{A^{\frac{3}{4}}}, \end{aligned} \tag{3.2}$$

where

$$I = a_a(Z - N), \quad a_a = 1.0,$$

and, respectively, for even-even, even-odd, and odd-odd nuclei,

$$f(Z,A) = (-1, 0, 1).$$

Note, in Appendix of [1] and Eq. (8) of [2], a_a=0.5, instead of unity.

For $T = 0$, Seeger [9] obtained the constants, by fitting all even-even nuclei and 488 odd-A nuclei available at that time, as

$$\alpha(0) = -16.11\text{MeV}, \quad \beta(0) = 20.21\text{MeV},$$

$$\gamma(0) = 20.65\text{MeV}, \quad \eta(0) = 48.00\text{MeV},$$

with the pairing energy term

$$\delta(0) = 33.0\text{MeV},$$

from Ref. [13]. Evidently, these constants need to be re-fitted since a large amount of data has become available [10],[11] particularly for neutron-rich nuclei. The newly fitted constants give binding energy within < 1.5 MeV of experiments.

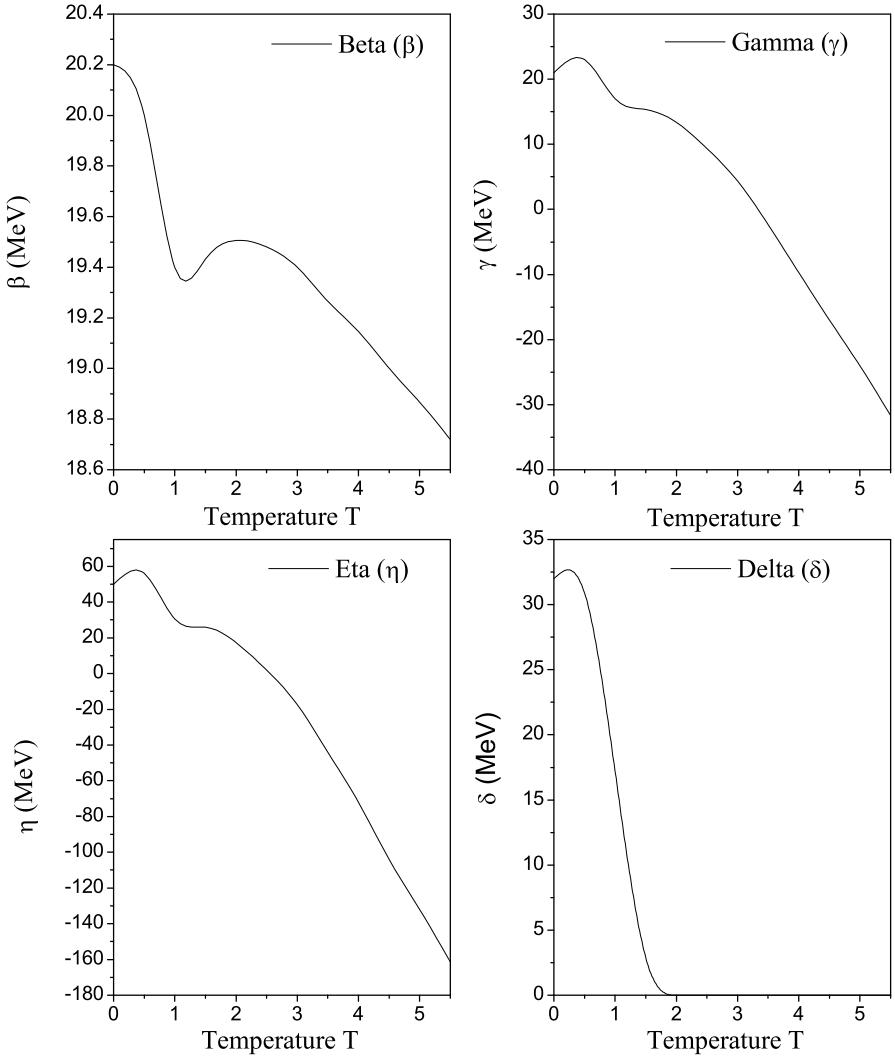

Figure 3.1: The coefficients of the semiempirical mass formula (Eq. 3.2), β(MeV), γ(MeV), η(MeV) and δ(MeV) as a function of the temperature T(MeV) from Davidson et al. [8].

The T-dependent constants in Eq. (3.2) were obtained numerically by Davidson *et al.* [8] for the available experimental information on excited states of 313 nuclei in the mass region $22 \leq A \leq 250$ by determining the partition function $\mathcal{Z}(A, Z, T)$ of each nucleus in the canonical ensemble and making a least squares fit of the excitation energy

$$E_{ex}(A, Z, T) = V_{LDM}(A, Z, T) - V_{LDM}(A, Z, 0)$$

to the ensemble average

$$E_{ex}(A,Z,T) = T^2 \frac{\partial}{\partial T} \ln \mathcal{Z}(A,Z,T).$$

The $\alpha(T)$, $\beta(T)$, $\gamma(T)$, $\eta(T)$ and $\delta(T)$ thus obtained are shown in Figure 3.1 from Ref. [8] for $T \leq 5.5\ MeV$, extrapolated linearly for higher temperatures. For the bulk constant $\alpha(T)$, instead, an empirically fitted expression to a Fermi gas model is used, as

$$\alpha(T) = \alpha(0) + \frac{T^2}{15}.$$

Also, the $\delta(T)$ is constrained to be positive definite at all temperatures, with $\delta(T > 2MeV) = 0$. Finally, the analytical form used for $R_0(T)$ is

$$R_0(T) = 1.07(1 + 0.01T)$$

.

3.2.2 Shell corrections and their temperature dependence

For the shell corrections δU in Eq. (3.1), we use the empirical formula of Myers and Swiatecki [14]. For spherical shapes,

$$\delta U = C \left[\frac{F(N) + F(Z)}{(A/2)^{\frac{2}{3}}} - cA^{\frac{1}{3}} \right] \tag{3.3}$$

where

$$F(X) = \frac{3}{5} \left(\frac{M_i^{\frac{5}{3}} - M_{i-1}^{\frac{5}{3}}}{M_i - M_{i-1}} \right) (X - M_{i-1}) - \frac{3}{5} \left(X^{\frac{5}{3}} - M_{i-1}^{\frac{5}{3}} \right) \tag{3.4}$$

with $X = N$ or Z, $M_{i-1} < X < M_i$ and M_i as the magic numbers 2, 8, 14 (or 20), 28, 50, 82, 126 and 184 for both neutrons and protons. The constants $C = 5.8\ MeV$ and $c = 0.26$. In this work, we use the magic number 14, referred as $MS14$ parameterization. The temperature dependence of shell corrections δU is obtained as given in equation 3.1.

3.3 Calculations

In Table 3.1 we have given the fitted constants for the experimental binding energies [10] and the theoretical binding energies [11] (only for neutron excess and neutron deficient nuclide for which experiment data is not available). The constants chosen to be fitted are the bulk constant $\alpha(0)$, working as an overall scaling factor, and the proton-neutron asymmetry constant a_a, controlling the curvature of the experimental parabola.

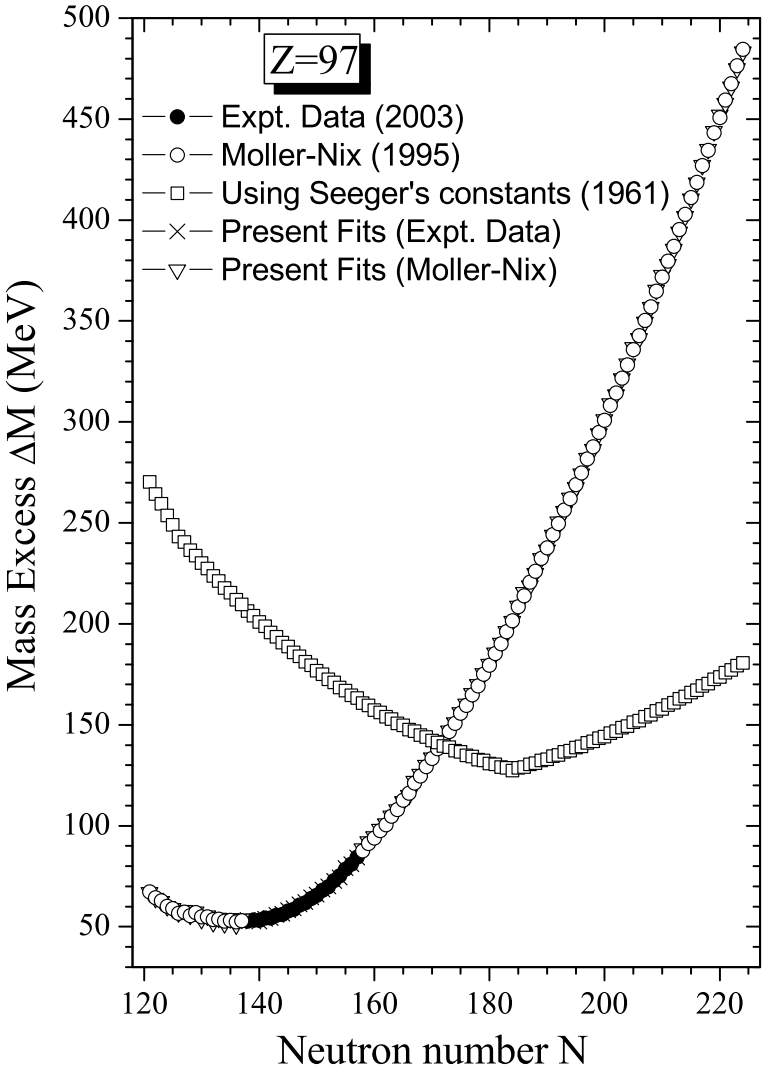

Figure 3.2: The mass excess $\Delta M(= M_A - A = NM_n + ZM_p + B(Z,N) - A)$ in MeV as a function of neutron number N for Z=97, calculated by using the experimental data (solid circle) [10] and theoretical data (open circle) [11], with newly fitted constants (cross and down open triangle) and calculated with the 1961 Seeger's constants [9] (hollow square).

The role of these refitted constants is depicted in Figure 3.2 for Z=97 nuclides. The

Figure **3.2** shows the excellent agreement between the present fits (cross and down open triangle) corresponding to experimental data of [10] (solid circles) and theoretical data [11] (open circle), respectively. The fits are obtained between 0-1.5 MeV of the available binding energies (experimental and theoretical). In Figure 3.2 the calculated binding energies using Seeger's constants are also shown (hollow square), stressing the requirement and extent of fitting.

3.4 Summary

The model parameters, bulk constant $\alpha(0)$ and the proton-neutron asymmetry constant a_a of Seeger's formula at T=0 are refitted in view of availability of a larger data set for binding energies. These fitted constants can be used in order to understand the dynamics of excited nuclear systems. Since our aim here was simply to include the T-dependence on experimental binding energies, and not to obtain the new parameter set of V_{LDM}, we have re-adjusted simply the bulk constant $\alpha(0)$ and the proton-neutron asymmetry constant a_a to obtain B_{expt} within < 1.5 MeV. The temperature dependences of the constants of V_{LDM} in equation 3.2 are shown in Figure 3.1 from [8].

Table 3.1: Re-fitted bulk $\alpha(0)$ and proton-neutron asymmetry a_a constants for Seeger's liquid drop energy for $1 \leq Z \leq 118$, to the experimental (combinations without and with star as super-script upto Z=7 and $Z \geq 8$ respectively) and theoretical binding energies (only for those combinations for which experimental data is not available having $Z \geq 8$, given here without any super-script).

Z	N	$\alpha(0)$	a_a	Z	N	$\alpha(0)$	a_a	Z	N	$\alpha(0)$	a_a
1	2	-15.85	0.100	5	14	-12.92	0.400	10	(8,13)*	-15.89	0.500
	3	-16.93	0.120	6	2	-12.95	0.010		(9-12)*,(15-18)*	-16.16	0.910
	4	-13.37	0.100		3,11	-14.81	0.100		(19-22)*	-16.22	0.882
	5	-13.57	0.120		4,9	-15.65	0.100		(23,24)*	-16.29	0.876
	6	-11.49	0.100		5,7	-16.53	0.100		25,26	-16.25	0.856
2	1	-15.18	0.100		8	-15.92	0.100		27	-16.25	0.848
	2	-16.11	0.100		10	-15.09	0.100		28	-16.25	0.839
	3	-16.90	0.300		12,13	-15.04	0.800		29	-16.25	0.833
	4,5	-14.23	0.300		14	-14.83	0.800		30	-16.25	0.826
	6	-13.12	0.100		15,16	-14.99	0.800		31	-16.25	0.815
	7	-12.87	0.100	7	3	-14.27	0.200	11	(7,8)*	-15.91	0.920
	8	-11.37	0.200		4	-15.12	0.530		(9,21,23)*	-16.21	0.861
3	0	-09.73	0.100		5,9	-16.20	0.800		(10-13)*	-16.27	0.865
	1,4,5	-16.67	0.100		6	-16.53	0.800		14*	-16.06	0.800
	2	-17.00	0.100		7	-16.75	0.800		(15-20,22,24)*	-16.18	0.865
	3	-18.43	0.990		8	-16.35	0.800		(25,26)*	-16.21	0.852
	6	-13.70	0.980		10,11,15	-15.90	0.940		27,28	-16.21	0.833
	7	-14.37	0.400		12,13	-15.70	0.890		29	-16.27	0.832
	8	-13.16	0.100		14	-15.68	0.940		30	-16.27	0.825
	9	-12.99	0.100		16	-15.97	0.940		31	-16.27	0.815
4	1	-12.37	0.010		17,18	-16.10	0.930		32	-16.27	0.809
	2	-14.45	0.100	8	4*	-14.00	0.940		33	-16.27	0.801
	3	-16.12	0.800		5*	-15.30	0.940	12	7*	-15.70	0.967
	4	-17.05	0.980		(6,10,11,13)*	-15.93	0.940		8*	-15.86	0.958
	5	-16.70	0.600		(7,8)*	-16.24	0.500		(9,10)*	-16.07	0.920
	6	-15.50	0.800		(9,15,16)*	-16.17	0.950		(11-13)*	-16.23	0.842
	7	-15.23	0.500		(12,14)*	-15.85	0.940		(14-26)*	-16.18	0.842
	8	-14.24	0.100		(17,19,20)*	-16.09	0.895		(27,28)*	-16.18	0.835
	9	-14.04	0.100		18*	-16.01	0.895		29	-16.33	0.837
	10	-13.28	0.010		21,22	-16.19	0.898		30	-16.03	0.792
	11	-12.96	0.100		23,24	-16.38	0.895		31	-16.03	0.785
	12	-12.23	0.100		25,26	-16.19	0.867		32,34,35	-16.09	0.773
5	1	-13.10	0.100	9	5*	-15.19	0.800		33	-16.03	0.776
	2	-14.53	0.100		(6,12,13)*	-15.78	0.500	13	8*	-15.95	0.950
	3	-16.43	0.100		(7,8,10,11,15,16,18)*	-16.17	0.910		(9,10)*	-16.10	0.930
	4	-16.65	0.600		9*	-16.30	0.900		(11-19)*,(25-28)*	-16.26	0.842
	5	-17.16	0.100		14*	-15.95	0.900		(20-24)*	-16.22	0.845
	6	-16.57	0.600		(17,19,20)*	-16.17	0.895		29*	-16.41	0.850
	7	-16.30	0.100		(21,22)*	-16.17	0.880		30	-16.11	0.799
	8	-15.33	0.100		23-26	-16.25	0.866		31	-16.11	0.787
	9	-15.12	0.100		27	-16.25	0.855		32	-16.11	0.771
	10	-14.40	0.100		28	-16.25	0.846		33-36	-16.00	0.763
	11	-14.10	0.100		29	-16.25	0.839		37,38	-16.08	0.764
	12	-13.41	0.100	10	6*	-15.22	0.500	14	8*	-15.95	0.965
	13	-13.10	0.100		(7,14)*	-15.70	0.500		(9,10)*	-16.04	0.932

Z	N	$\alpha(0)$	a_a	Z	N	$\alpha(0)$	a_a	Z	N	$\alpha(0)$	a_a
14	(11,12)*	-16.17	0.965	18	36-41	-16.21	0.745	23	(26-30)*	-16.39	0.792
	(13-20,27,28)*	-16.27	0.839		42,43,47-49	-16.21	0.741		(31-42)*	-16.40	0.768
	(21-26)*	-16.23	0.841		44-46	-16.21	0.739		43-50	-16.25	0.729
	(29,30)*	-16.31	0.836	19	10	-16.17	0.830		51-53	-16.19	0.718
	31	-16.09	0.776		11,12	-16.20	0.787		54-56	-16.21	0.717
	32-35	-16.05	0.762		(13-21)*	-16.49	0.899		57-60	-16.19	0.712
	36,37	-16.09	0.762		(22-28)*	-16.36	0.813	24	14	-16.30	0.765
	38	-16.09	0.758		(29-32)*	-16.37	0.779		15,16	-16.38	0.765
	39,40	-16.09	0.754		(33-36)*	-16.44	0.783		17	-16.44	0.765
15	8	-16.10	0.970		37-42,45-48	-16.21	0.740		(18-25,42,43)*	-16.45	0.770
	(9-14)*	-16.31	0.939		43,44,49,50	-16.21	0.738		(26-29)*	-16.40	0.795
	(15-24)*	-16.40	0.893		51	-16.21	0.734		(30-41)*	-16.42	0.774
	(25-28)*	-16.12	0.783	20	10	-16.17	0.834		44-46,59-62	-16.17	0.706
	(29-31)*	-16.11	0.762		11	-16.17	0.806		47-51	-16.21	0.720
	32-36	-16.11	0.762		12	-16.17	0.771		52,53	-16.17	0.710
	37,38	-16.09	0.754		13	-16.17	0.718		54-58	-16.17	0.708
	39-42	-16.09	0.749		(14-21)*	-16.49	0.899	25	15,16	-16.38	0.758
16	8	-16.11	0.955		(22-30)*	-16.37	0.789		17,18	-16.48	0.780
	9	-16.11	0.907		(31-34)*	-16.43	0.783		(19-26)*	-16.46	0.760
	(10-14)*	-16.31	0.925		(35-37)*	-16.49	0.789		(27-44)*	-16.42	0.768
	(15-24)*	-16.40	0.893		38-49	-16.22	0.735		45,46	-16.43	0.761
	(25-28)*	-16.31	0.828		50,51	-16.22	0.732		47-52	-16.21	0.715
	(29-30)*	-16.22	0.775		52,53	-16.17	0.723		53-59	-16.17	0.706
	(31-33)*	-16.25	0.773	21	11,12	-16.17	0.770		60-64	-16.17	0.704
	34-38	-16.11	0.751		13,14	-16.29	0.770	26	16-18	-16.44	0.765
	39	-16.20	0.758		(15-21)*	-16.47	0.795		(19-26)*	-16.47	0.770
	40-44	-16.20	0.755		(22,23,31,33,35-39)*	-16.43	0.779		(27-45)*	-16.43	0.768
17	8	-16.11	0.914		(24-30,32,34)*	-16.36	0.774		46*	-16.47	0.770
	9,10	-16.17	0.864		40-50	-16.23	0.733		47	-16.40	0.750
	(11-14,22-28)*	-16.32	0.822		51,52	-16.23	0.729		48-62	-16.17	0.702
	(15-21)*	-16.46	0.893		53-55	-16.17	0.718		63-66	-16.17	0.700
	(29-30)*	-16.27	0.775	22	12	-16.25	0.790	27	17	-16.50	0.782
	(31-34)*	-16.35	0.778		13,14	-16.25	0.765		18,19	-16.50	0.761
	35-40	-16.20	0.755		15	-16.25	0.700		(20-27)*	-16.48	0.755
	41,42	-16.20	0.747		(16-23)*	-16.44	0.775		(28-46)*	-16.44	0.767
	43,44	-16.20	0.745		(24-30)*	-16.39	0.803		(47,48)*	-16.47	0.767
	45,46	-16.20	0.743		(31-41)*	-16.39	0.768		49,50	-16.42	0.750
18	9	-16.17	0.864		42-46,49-51	-16.24	0.729		51-62	-16.18	0.701
	10,11	-16-17	0.811		47,48	-16.24	0.731		63-69	-16.18	0.700
	(12-14)*	-16.40	0.893		52,53	-16.17	0.717	28	18	-16.50	0.774
	(15-19)*	-16.46	0.893		54-56	-16.17	0.715		19	-16.50	0.760
	(20-25)*	-16.43	0.899		57,58	-16.17	0.712		(20-29,46-48)*	-16.48	0.769
	(26-28)*	-16.25	0.775	23	13,14	-16.17	0.721		(30-45)*	-16.45	0.770
	(29-31)*	-16.35	0.785		15,16	-16.44	0.790		(49,50)*	-16.22	0.702
	(32-35)*	-16.35	0.772		(17-25)*	-16.45	0.768		51-55	-16.22	0.702

Z	N	$\alpha(0)$	a_a	Z	N	$\alpha(0)$	a_a	Z	N	$\alpha(0)$	a_a
28	56-60	-16.21	0.702	35	63-74	-16.42	0.707	40	(43-46)*	-16.64	0.805
	61-71	-16.21	0.700		75,76	-16.37	0.703		(47-66)*	-16.59	0.730
29	19-22	-16.54	0.750		77-80	-16.40	0.704		71,72,78-81	-16.51	0.708
	(23-30)*	-16.51	0.720		81,82	-16.40	0.702		73-77	-16.53	0.714
	(31-44)*	-16.51	0.790		83-86	-16.40	0.700		82,83	-16.53	0.709
	(45-51)*	-16.44	0.751	36	27-32	-16.64	0.702		84-87	-16.53	0.707
	52-55	-16.24	0.700		(33-38)*	-16.63	0.652		88-97	-16.24	0.674
	56-73	-16.23	0.700		(39-48)*	-16.59	0.799	41	33-39	-16.73	0.708
30	21-23	-16.55	0.740		(49-64)*	-16.49	0.719		(40-42,70-72)*	-16.70	0.747
	(24-33)*	-16.52	0.700		65-73	-16.44	0.706		(43,44,66-69)*	-16.67	0.746
	(34-40)*	-16.52	0.794		74-76	-16.44	0.709		(45-51)*	-16.64	0.794
	(41-53)*	-16.40	0.730		77-79	-16.49	0.713		(52-65)*	-16.59	0.728
	54-57	-16.28	0.700		80-84	-16.15	0.672		73-80	-16.51	0.708
	58-75	-16.26	0.700		85-88	-16.15	0.674		81-84	-16.51	0.705
31	22-24	-16.56	0.720	37	29-33	-16.66	0.702		85-87	-16.51	0.704
	(25-33)*	-16.57	0.749		(34-39)*	-16.65	0.740		88-99	-16.26	0.674
	(34-45)*	-16.53	0.789		(40-48)*	-16.60	0.799	42	35-39	-16.74	0.711
	(46-53)*	-16.41	0.727		(49-65)*	-16.51	0.720		40	-16.71	0.711
	(54,55)*	-16.44	0.727		66-72	-16.45	0.705		(41,42,72,73)*	-16.72	0.748
	56-63	-16.30	0.700		73-78	-16.45	0.708		(43,44,68-71)*	-16.69	0.748
	64-77	-16.28	0.700		79-84	-16.17	0.672		(45-54)*	-16.66	0.788
32	23-25	-16.58	0.720		85,86	-16.16	0.672		(55-67)*	-16.60	0.728
	(26-33)*	-16.58	0.749		87-91	-16.17	0.674		74-80	-16.53	0.709
	(34-45)*	-16.55	0.795	38	30-34	-16.68	0.702		81-89	-16.53	0.705
	(46-57)*	-16.41	0.719		(35-39)*	-16.67	0.735		90-102	-16.28	0.674
	58	-16.34	0.701		(40-42,64-67)*	-16.63	0.742	43	36-38	-16.75	0.704
	59-80	-16.32	0.701		(43-54)*	-16.58	0.748		39-41	-16.73	0.709
33	24-26	-16.60	0.720		(55-63)*	-16.57	0.734		(42,43,70-72)*	-16.73	0.755
	(27-34)*	-16.60	0.750		68-71	-16.47	0.705		(44,45)*	-16.70	0.748
	(35-46)*	-16.56	0.798		72-79	-16.47	0.708		(46-54)*	-16.66	0.787
	(47-59)*	-16.44	0.721		80-85	-16.21	0.673		(55-69)*	-16.61	0.728
	60-76	-16.38	0.707		86-87	-16.21	0.674		(73-75)*	-16.72	0.748
	77-80	-16.34	0.702		88-93	-16.19	0.674		76-80	-16.55	0.711
	81,82	-16.34	0.700	39	31-36	-16.70	0.702		81-88	-16.55	0.707
34	25-30	-16.60	0.701		(37-40)*	-16.68	0.747		89-103	-16.30	0.674
	(31-36)*	-16.60	0.700		(41-43)*	-16.64	0.805		104	-16.30	0.675
	(37-46)*	-16.57	0.797		(44,45,63-69)*	-16.59	0.730	44	37,38	-16.77	0.704
	(47-60)*	-16.46	0.721		(46-62)*	-16.57	0.730		39-42	-16.73	0.709
	61-73	-16.37	0.701		70,71,81	-16.50	0.708		(43,44,75,76)*	-16.73	0.748
	74-77	-16.37	0.703		72-80	-16.51	0.712		(45,46,72-74)*	-16.71	0.747
	78-84	-16.11	0.675		82-86	-16.22	0.672		(47-56)*	-16.68	0.788
35	26-31	-16.62	0.700		87-95	-16.22	0.674		(57-71)*	-16.62	0.728
	(32-37)*	-16.62	0.760	40	32-37	-16.72	0.702		77-79	-16.57	0.712
	(38-46)*	-16.58	0.799		(38-40)*	-16.70	0.760		80,81	-16.57	0.710
	(47-62)*	-16.48	0.722		(41,42,67-70)*	-16.68	0.747		82-90	-16.57	0.707

Z	N	$\alpha(0)$	a_a	Z	N	$\alpha(0)$	a_a	Z	N	$\alpha(0)$	a_a
44	91-103	-16.32	0.674	48	106-115	-16.39	0.677	53	53,54	-16.83	0.685
	104-106	-16.33	0.676	49	43-46	-16.82	0.678		(55-60)*	-16.82	0.885
45	38-40	-16.76	0.674		47	-16.80	0.695		(61-68)*	-16.80	0.798
	41-43	-16.74	0.674		(48-51,78)*	-16.78	0.752		(69-81)*	-16.72	0.725
	(44,45)*	-16.74	0.700		(52-64)*	-16.75	0.789		(82-91)*	-16.70	0.713
	(46,47,75-77)*	-16.72	0.746		(65-77)*	-16.67	0.727		92-98	-16.64	0.700
	(48-57)*	-16.69	0.787		(79-86)*	-16.67	0.718		99-109	-16.66	0.701
	(58-74)*	-16.63	0.727		87-97	-16.61	0.704		110-118,123-126	-16.49	0.680
	78-80	-16.57	0.710		98-102	-16.39	0.673		119-122	-16.48	0.680
	81-91	-16.57	0.706		103-105	-16.41	0.677	54	49-52	-16.87	0.600
	92-93	-16.59	0.707		106-117	-16.42	0.679		53,54	-16.85	0.600
	94-103	-16.35	0.676	50	44-46	-16.84	0.639		55	-16.84	0.600
	104-108	-16.35	0.677		47,48	-16.82	0.600		(56-60)*	-16.84	0.889
46	40-42	-16.77	0.684		(49-52)*	-16.80	0.990		(61-68)*	-16.81	0.799
	43-44	-16.76	0.689		(53-64)*	-16.76	0.798		(69-83)*	-16.74	0.726
	(45,46)*	-16.76	0.710		(65-77)*	-16.68	0.725		(84-93)*	-16.71	0.712
	(47-48,76-78)*	-16.73	0.746		(78-81)*	-16.68	0.719		94-97	-16.66	0.700
	(49-61)*	-16.71	0.780		(82-87)*	-16.68	0.715		98-113	-16.67	0.700
	(62-75)*	-16.64	0.727		88-97	-16.63	0.706		114,125-128	-16.51	0.680
	79	-16.59	0.711		98-102	-16.43	0.676		115-124	-16.50	0.680
	80-91	-16.59	0.707		103-106	-16.44	0.679	55	51-53	-16.88	0.600
	92-94	-16.59	0.705		107-119	-16.43	0.679		54,55	-16.87	0.600
	95-105	-16.40	0.680	51	46-49	-16.84	0.639		56	-16.86	0.600
	106-110	-16.35	0.676		50,51	-16.82	0.630		(57-63)*	-16.85	0.889
47	41,42	-16.79	0.684		(52-59)*	-16.80	0.885		(64-71)*	-16.83	0.797
	43-45	-16.77	0.690		(60-65)*	-16.77	0.797		(72-76,92-96)*	-16.73	0.713
	(46,81-83)*	-16.78	0.746		(66-78)*	-16.69	0.724		(77-91)*	-16.71	0.712
	(47-49,78-80)*	-16.75	0.745		(79-88)*	-16.69	0.717		97-115	-16.68	0.700
	(50-62)*	-16.72	0.780		89-95	-16.64	0.706		116-124	-16.53	0.682
	(63-77)*	-16.65	0.726		96-100	-16.64	0.704		125-130	-16.53	0.681
	84-93	-16.59	0.705		101-106	-16.64	0.702	56	52-54	-16.90	0.600
	94-95	-16.57	0.701		107-111	-16.45	0.679		55,56	-16.88	0.600
	96-101	-16.39	0.677		112-121	-16.43	0.678		57	-16.87	0.600
	102-105	-16.34	0.672	52	47-50	-16.86	0.680		(58-62)*	-16.87	0.890
	106-113	-16.39	0.679		51,52	-16.84	0.630		(63-71)*	-16.84	0.797
48	42-44	-16.80	0.678		(53-59)*	-16.81	0.885		(72-76,93-97)*	-16.75	0.713
	45,46	-16.78	0.695		(60-66)*	-16.78	0.796		(77-92)*	-16.73	0.712
	(47-49,80-82)*	-16.77	0.745		(67-79)*	-16.70	0.723		98-120	-16.70	0.700
	(50-63)*	-16.74	0.786		(80-90)*	-16.69	0.713		121-131	-16.54	0.681
	(64-79)*	-16.66	0.725		91-98	-16.64	0.702		132,133	-16.54	0.680
	(83,84)*	-16.67	0.720		99-109	-16.64	0.700	57	53-56	-16.91	0.600
	85-88,93-96	-16.61	0.705		110,111,123,124	-16.48	0.680		57,58	-16.89	0.600
	89-92	-16.58	0.702		112-122	-16.47	0.680		59	-16.88	0.600
	97-100	-16.39	0.674	53	48-50	-16.86	0.600		(60-62)*	-16.87	0.735
	101-105	-16.41	0.678		51,52	-16.85	0.685		(63-74)*	-16.85	0.789

Z	N	$\alpha(0)$	a_a	Z	N	$\alpha(0)$	a_a	Z	N	$\alpha(0)$	a_a
57	(75-81)*	-16.77	0.727	62	61,62	-17.00	0.600	66	(72-77)*	-17.00	0.930
	(82-98)*	-16.70	0.698		63-64	-16.98	0.826		(78-85)*	-16.92	0.768
	99-117	-16.71	0.701		65	-16.96	0.826		(86-91)*	-16.84	0.700
	118-132	-16.54	0.680		(66-76)*	-16.95	0.859		(92-107)*	-16.86	0.709
	133-135	-16.55	0.680		(77-85)*	-16.86	0.747		108-124	-16.87	0.713
58	55,56	-16.93	0.600		(86-103)*	-16.78	0.700		125-129	-16.80	0.701
	57	-16.92	0.600		104-106	-16.80	0.705		130-150	-16.53	0.664
	58-60	-16.91	0.600		107-122	-16.80	0.707		151-155	-16.52	0.664
	(61,62,97-99)*	-16.89	0.736		123-134	-16.64	0.684	67	69,70	-17.01	0.826
	(63-66,90-92)*	-16.87	0.746		135-146	-16.44	0.661		71,72	-17.01	0.826
	(67-76)*	-16.86	0.788	63	62	-17.01	0.826		(73-78)*	-17.00	0.930
	(77-89)*	-16.77	0.720		63,64	-17.00	0.826		(79-87)*	-16.93	0.768
	(93-96)*	-16.80	0.720		65,66	-16.98	0.826		(88-93)*	-16.85	0.700
	100-119	-16.74	0.703		(67-74)*	-16.96	0.889		(94-108)*	-16.88	0.712
	120-128	-16.57	0.682		(75-84)*	-16.90	0.777		109-123	-16.90	0.718
	129-137	-16.37	0.661		(85-104)*	-16.79	0.699		124-129	-16.81	0.701
59	56-58	-16.95	0.600		105-109	-16.81	0.706		130-135	-16.58	0.669
	59-61	-16.93	0.600		110-120	-16.81	0.708		136-153	-16.56	0.666
	(62-69)*	-16.91	0.850		121-131	-16.65	0.685		154-157	-16.56	0.667
	(70-80)*	-16.86	0.772		132-148	-16.45	0.661	68	70	-17.05	0.826
	(81-92)*	-16.76	0.710	64	64	-17.01	0.826		71,72	-17.03	0.826
	(93-100)*	-16.75	0.702		65,66	-17.00	0.826		73,74	-17.01	0.826
	101-118	-16.78	0.708		67,68	-16.98	0.826		(75-80)*	-17.00	0.870
	119-130	-16.59	0.683		69	-16.97	0.826		(81-84)*	-16.91	0.724
	131-139	-16.40	0.663		(70-75)*	-16.97	0.889		(85-109)*	-16.89	0.712
60	58-60	-16.97	0.600		(76-85)*	-16.91	0.773		110-123	-16.91	0.718
	61,62	-16.95	0.600		(86-105)*	-16.81	0.701		124-130	-16.83	0.703
	63	-16.92	0.600		106-112	-16.82	0.706		131-156	-16.59	0.668
	(64-76)*	-16.92	0.834		113-120	-16.82	0.708		157-159	-16.58	0.668
	(77-86)*	-16.82	0.735		121-134	-16.67	0.685	69	72,73	-17.04	0.881
	(87-91)*	-16.75	0.702		135-150	-16.48	0.662		74,75	-17.00	0.708
	(92-101)*	-16.75	0.699	65	65,66	-17.02	0.826		(76-85)*	-16.99	0.820
	102-119	-16.79	0.708		67,68	-17.00	0.826		(86-95)*	-16.91	0.720
	120-130	-16.61	0.684		69,70	-16.99	0.826		(96-110)*	-16.90	0.712
	131-141	-16.42	0.663		(71-76)*	-16.99	0.930		111-124	-16.92	0.719
61	59,60	-16.99	0.600		(77-85)*	-16.91	0.767		125-131	-16.85	0.705
	61,62	-16.97	0.600		(86-103)*	-16.82	0.699		132-157	-16.60	0.668
	63,64	-16.95	0.600		(104-106)*	-16.82	0.702		158-161	-16.59	0.668
	(65-77)*	-16.93	0.840		107-115	-16.85	0.711	70	73,74	-17.04	0.778
	(78-85)*	-16.84	0.745		116-121	-16.83	0.709		75	-17.01	0.642
	(86-102)*	-16.75	0.695		122-134	-16.68	0.686		76,77	-17.00	0.786
	103-105	-16.79	0.705		135-153	-16.52	0.665		(78-87)*	-17.00	0.813
	106-118	-16.79	0.707	66	67,68	-17.02	0.826		(88-108)*	-16.91	0.711
	119-128	-16.62	0.684		69,70	-17.01	0.826		(109-111)*	-16.90	0.711
	129-144	-16.43	0.662		71	-16.99	0.826		112-123	-16.93	0.720

Z	N	$\alpha(0)$	a_a	Z	N	$\alpha(0)$	a_a	Z	N	$\alpha(0)$	a_a
70	124-131	-16.86	0.705	76	(96-100)*	-17.02	0.743	81	160-165	-16.85	0.686
	132-164	-16.65	0.672		(101-120)*	-16.98	0.720		176-185	-16.95	0.694
71	75	-17.03	0.603		121-136	-16.92	0.706		186-188	-16.96	0.694
	76-78	-17.03	0.910		137-142	-16.72	0.671	82	93-95	-17.14	0.845
	(79-88)*	-17.00	0.797		143-152	-16.72	0.672		(96-106)*	-17.11	0.786
	(89-113)*	-16.93	0.717		153-163	-16.73	0.674		(107-133)*	-17.02	0.716
	114-124	-16.95	0.723		164-166	-17.02	0.705		134-143	-17.00	0.712
	125-130	-16.87	0.706		167-170	-17.03	0.705		144-159	-16.86	0.685
	131-163	-16.66	0.672		171-177	-16.80	0.683		160-165	-16.87	0.687
	164-166	-16.65	0.672	77	85,86	-17.09	0.845		166-188	-16.86	0.685
72	77-80	-17.03	0.845		(87-94)*	-17.06	0.780		189-191	-16.86	0.684
	(81-93)*	-17.00	0.770		(95-105)*	-17.02	0.740	83	95,96	-17.14	0.845
	(94-116)*	-16.94	0.718		(106-122)*	-16.98	0.718		97-100	-17.15	0.845
	117,118	-16.95	0.721		123-138	-16.93	0.706		(101-113)*	-17.08	0.747
	119-131	-16.88	0.706		139-143	-16.73	0.671		(114-135)*	-17.03	0.717
	132-134,148-152	-16.68	0.672		144-150	-16.73	0.672		136-140	-17.01	0.713
	135-147,153-164	-16.67	0.672		151-167	-16.81	0.683		141-154	-16.88	0.686
	165-168	-16.78	0.683		168-179	-16.77	0.680		155-193	-16.86	0.684
73	78,79	-17.05	0.845	78	87	-17.10	0.845	84	97-98	-17.16	0.845
	80,81	-17.04	0.845		(88-97)*	-17.08	0.798		99-101	-17.17	0.845
	(82-93)*	-17.01	0.772		(98-105)*	-17.05	0.755		102,103	-17.18	0.845
	(94-117)*	-16.95	0.719		(106-124)*	-16.99	0.718		(104-115)*	-17.10	0.751
	118	-16.89	0.704		125-140	-16.94	0.706		(116-136)*	-17.04	0.717
	119-133	-16.89	0.706		141-150	-16.74	0.671		137-140	-16.90	0.685
	134-136	-16.90	0.706		151-166	-16.82	0.683		141-152	-16.90	0.686
	137-160	-16.68	0.672		167-182	-16.76	0.678		153-156	-16.90	0.687
	161-167	-16.79	0.683	79	88,89	-17.11	0.845		157-171	-16.90	0.688
	168-170	-16.79	0.684		(90-98)*	-17.09	0.801		172-193	-16.89	0.686
74	80-83	-17.06	0.845		(99-106)*	-17.06	0.759		194,195	-16.89	0.685
	(84-96)*	-17.02	0.762		(107-126)*	-16.99	0.715	85	99,100	-17.18	0.845
	(97-118)*	-16.97	0.723		127-136	-16.97	0.711		101-103	-17.19	0.845
	119-134	-16.90	0.706		137-164,171-184	-16.83	0.684		104,105	-17.20	0.845
	135-152	-16.70	0.672		165-170	-16.84	0.686		106,107	-17.21	0.845
	153-162	-16.70	0.673	80	90	-17.12	0.845		(108-116)*	-17.11	0.751
	163-173	-16.90	0.693		(91-103)*	-17.09	0.783		(117-138)*	-17.05	0.718
75	81-84	-17.07	0.845		(104-111)*	-17.05	0.743		139-149	-16.91	0.685
	(85-97)*	-17.03	0.766		(112-130)*	-16.99	0.713		150-154,194-197	-16.91	0.686
	(98-102)*	-16.97	0.716		131-139	-16.98	0.711		155-188	-16.91	0.688
	(103-119)*	-16.97	0.721		140-163,168-186	-16.84	0.684		189-193	-16.92	0.688
	120-136	-16.91	0.706		164-167	-16.85	0.686	86	100-102	-17.20	0.845
	137-151	-16.71	0.672	81	92-94	-17.13	0.845		103-105	-17.21	0.845
	152-161	-16.71	0.673		(95-106)*	-17.08	0.765		106-108	-17.22	0.845
	162-175	-16.88	0.691		(107-131)*	-17.01	0.716		(109-120)*	-17.13	0.753
76	83-85	-17.08	0.845		132-140	-16.99	0.712		(121-125,132)*	-17.02	0.700
	(86-95)*	-17.06	0.795		141-159,166-175	-16.85	0.685		(126-131,133-142)*	-17.02	0.706

Z	N	$\alpha(0)$	a_a	Z	N	$\alpha(0)$	a_a	Z	N	$\alpha(0)$	a_a
86	143-152	-16.92	0.684	89	182-189	-16.90	0.684	92	190,191	-16.99	0.690
	153-162	-16.93	0.688		190-192	-16.90	0.683		192-194	-16.99	0.689
	163-189	-16.92	0.688		193-197	-16.90	0.682		195-197	-16.99	0.688
	190-193	-16.92	0.687		198-202	-16.90	0.681		198-201	-16.99	0.687
	194-197	-16.92	0.686		203-206	-16.90	0.680		202-205	-16.99	0.686
	198-200	-16.92	0.685	90	108-113	-17.25	0.830		206-209,212	-16.99	0.685
87	102-106	-17.20	0.845		114,115	-17.26	0.830		210,211,213	-16.99	0.684
	107-109	-17.23	0.845		116,117	-17.27	0.830	93	113-118	-17.25	0.800
	110	-17.24	0.845		118	-17.29	0.834		119-123	-17.26	0.800
	111	-17.25	0.845		(119-126)*	-17.16	0.751		124-126	-17.27	0.800
	(112-117)*	-17.14	0.759		(127-148)*	-17.05	0.700		127	-17.28	0.800
	(118-129)*	-17.09	0.728		149-154,172-176	-17.06	0.702		128,129	-17.29	0.800
	(130-145)*	-17.01	0.700		155-171	-17.06	0.703		130,131	-17.31	0.800
	146-153	-16.95	0.688		177-181	-17.07	0.703		(132-140,146-151)*	-17.09	0.700
	154-163	-16.95	0.690		182-189	-16.92	0.685		(141-145)*	-17.10	0.701
	164-189	-16.95	0.691		190-192	-16.92	0.684		152-155	-17.09	0.701
	190-192	-16.90	0.685		193-196	-16.92	0.683		156-186	-17.10	0.705
	193-195	-16.90	0.684		197-202	-16.92	0.682		187-189	-17.00	0.691
	196-199,201	-16.90	0.683		203-205	-16.92	0.681		190-192	-17.00	0.690
	200,202	-16.90	0.682		206-209	-16.92	0.680		193-195	-17.00	0.689
88	104-107	-17.23	0.845	91	109-115	-17.26	0.830		196-199	-17.00	0.688
	108,109	-17.24	0.845		116,117	-17.27	0.830		200-203	-17.00	0.687
	110,111	-17.25	0.845		118,119	-17.29	0.834		204-206	-17.00	0.686
	112,113	-17.26	0.845		120	-17.30	0.832		207-212	-17.00	0.685
	(114-120)*	-17.15	0.755		(121-129)*	-17.17	0.751		213-215	-17.00	0.684
	(121-130)*	-17.10	0.728		(130-149)*	-17.06	0.699	94	115-119	-17.26	0.801
	(131-146)*	-17.02	0.699		150-155,177-187	-17.07	0.702		120-123	-17.27	0.801
	147-153	-16.96	0.687		156-166,169-175	-17.07	0.703		124-127	-17.28	0.800
	154-160	-16.96	0.689		167,168	-17.07	0.704		128,129	-17.30	0.803
	161-164	-16.96	0.690		188-190	-16.93	0.685		130,131	-17.31	0.800
	165-189	-16.96	0.691		191-193	-16.93	0.684		132,133	-17.33	0.800
	190,191	-16.92	0.686		194-196	-16.93	0.683		(134-153)*	-17.11	0.701
	192-195	-16.92	0.685		197-203	-16.93	0.682		154-158	-17.10	0.701
	196-199	-16.92	0.684		204-209	-16.93	0.681		159-187	-17.11	0.705
	200-202	-16.92	0.683		210,211	-16.93	0.680		188,189	-17.00	0.690
	203,204	-16.92	0.682	92	111-117	-17.27	0.827		190-192	-17.00	0.689
89	106-111	-17.24	0.834		118-121	-17.28	0.820		193-195	-17.00	0.688
	112,113	-17.26	0.845		122,123	-17.31	0.830		196-199	-17.00	0.687
	114	-17.27	0.845		124	-17.31	0.820		200-203	-17.00	0.686
	115	-17.28	0.845		(125-128,134-137)*	-17.09	0.704		204-207	-17.00	0.685
	116	-17.29	0.845		(129-133)*	-17.09	0.707		208-215	-17.00	0.684
	(117-127)*	-17.15	0.749		(138-150)*	-17.08	0.700		216-218	-17.00	0.683
	(128-147)*	-17.04	0.701		151-154	-17.08	0.701	95	117-123	-17.27	0.800
	148-169	-17.05	0.703		155-185	-17.08	0.703		124-127	-17.28	0.800
	170-181	-16.96	0.690		186-189	-16.99	0.691		128,129	-17.29	0.800

Z	N	$\alpha(0)$	a_a	Z	N	$\alpha(0)$	a_a	Z	N	$\alpha(0)$	a_a
95	130,131	-17.31	0.800	97	193,194	-17.03	0.689	99	217-226,228,229	-17.05	0.684
	132,133	-17.33	0.800		195-197	-17.03	0.688	100	126-129	-17.32	0.802
	134,135	-17.35	0.800		198-201	-17.03	0.687		130,131	-17.34	0.802
	(136-150)*	-17.12	0.700		202-205	-17.03	0.686		132,133	-17.35	0.802
	(151-154)*	-17.13	0.704		206-210	-17.03	0.685		134,135	-17.37	0.802
	155-185	-17.14	0.709		211-220	-17.03	0.684		136,137	-17.39	0.804
	186-188	-17.01	0.691		221-224	-17.04	0.684		138,139	-17.41	0.805
	189,190	-17.01	0.690	98	123-127	-17.30	0.800		140,141	-17.43	0.807
	191-193	-17.01	0.689		128,129	-17.31	0.800		(142-154)*	-17.21	0.710
	194-197	-17.01	0.688		130,131	-17.33	0.803		(155-160)*	-17.22	0.714
	198-200	-17.01	0.687		132,133	-17.35	0.805		161-166	-17.18	0.706
	201-204	-17.01	0.686		134,135	-17.37	0.806		167-170	-17.18	0.709
	205-208	-17.01	0.685		136,137	-17.39	0.807		171-186	-17.18	0.710
	209-217	-17.01	0.684		138	-17.38	0.800		187-189	-17.05	0.690
	218-220	-17.01	0.683		(139-153)*	-17.18	0.707		190-192	-17.05	0.689
96	119-124	-17.28	0.800		(154-158)*	-17.18	0.709		193-195	-17.05	0.688
	125-129	-17.29	0.800		159-165	-17.17	0.709		196-198	-17.05	0.687
	130,131	-17.32	0.801		166-187	-17.17	0.710		199-201	-17.05	0.686
	132,133	-17.34	0.803		188-190	-17.05	0.692		202-207	-17.05	0.685
	134,135	-17.36	0.803		191-193	-17.05	0.691		208-218,227	-17.05	0.684
	136	-17.37	0.800		194,195	-17.05	0.690		219-226,228-231	-17.07	0.685
	(137,154-156)*	-17.15	0.707		196-198	-17.05	0.689	101	128,129	-17.33	0.800
	(138-153)*	-17.15	0.705		199-201	-17.05	0.688		130,131	-17.34	0.800
	157-186	-17.15	0.709		202-205	-17.04	0.686		132,133	-17.36	0.803
	187-189	-17.02	0.691		206-211	-17.04	0.685		134,135	-17.37	0.801
	190,191	-17.02	0.690		212-227	-17.04	0.684		136,137	-17.39	0.803
	192-194	-17.02	0.689	99	125-129	-17.31	0.800		138,139	-17.40	0.801
	195-197	-17.02	0.688		130,131	-17.33	0.800		140,141	-17.42	0.802
	198-200	-17.02	0.687		132	-17.34	0.800		142,143	-17.44	0.803
	201-204	-17.02	0.686		133,134	-17.35	0.800		(144-155)*	-17.22	0.710
	205-208	-17.02	0.685		135,136	-17.37	0.801		(156-161)*	-17.22	0.712
	209-217	-17.02	0.684		137,138	-17.39	0.802		162-166	-17.21	0.711
	218-222	-17.02	0.683		139,140	-17.42	0.807		167-186	-17.21	0.714
97	121-127	-17.29	0.800		(141-154)*	-17.19	0.707		187-189	-17.07	0.692
	128,129	-17.30	0.800		(155-159)*	-17.19	0.709		190,191	-17.07	0.691
	130,131	-17.32	0.801		160-166	-17.18	0.709		192,193	-17.07	0.690
	132,133	-17.34	0.802		167-180	-17.18	0.711		194-196	-17.07	0.689
	134,135	-17.36	0.803		181-187	-17.05	0.692		197-199	-17.07	0.688
	136,137	-17.38	0.803		188-191	-17.05	0.691		200-203	-17.07	0.687
	(138,155-157)*	-17.16	0.707		192,193	-17.05	0.690		204-211	-17.07	0.686
	(139-154)*	-17.17	0.708		194,195	-17.05	0.689		212-220,227-233	-17.07	0.685
	158-166	-17.16	0.709		196-199	-17.05	0.688		221-226	-17.07	0.684
	167-186	-17.15	0.709		200-202	-17.05	0.687	102	130,131	-17.35	0.802
	187-189	-17.03	0.691		203-207	-17.05	0.686		132,133	-17.36	0.800
	190-192	-17.03	0.690		208-216,227	-17.05	0.685		134,135	-17.38	0.802

Z	N	$\alpha(0)$	a_a	Z	N	$\alpha(0)$	a_a	Z	N	$\alpha(0)$	a_a
102	136,137	-17.39	0.800	104	165-167	-17.26	0.716	107	144,145	-17.46	0.800
	138,139	-17.40	0.800		168-187	-17.26	0.719		146,147	-17.47	0.800
	140,141	-17.42	0.800		188-191	-17.09	0.690		148,149	-17.49	0.802
	142,143	-17.44	0.802		192,193	-17.09	0.689		150,151	-17.50	0.800
	144,145	-17.45	0.800		194-196	-17.09	0.688		152	-17.51	0.800
	(146-162)*	-17.27	0.723		197-199	-17.09	0.687		(153-168)*	-17.33	0.729
	163-167	-17.22	0.711		200-205	-17.09	0.686		169	-17.30	0.721
	168-182	-17.22	0.714		206-216,227	-17.09	0.685		170-182	-17.30	0.723
	183-188	-17.07	0.691		217-226	-17.09	0.684		183-192	-17.12	0.690
	189,190	-17.07	0.690		228-235	-17.09	0.684		193-195	-17.12	0.689
	191-193	-17.07	0.689	105	136,137	-17.40	0.800		196-198	-17.12	0.688
	194,195	-17.07	0.688		138,139	-17.41	0.800		199-203	-17.12	0.687
	196-199	-17.07	0.687		140,141	-17.43	0.802		204-211,226	-17.12	0.686
	200-203	-17.07	0.686		142,143	-17.44	0.800		212-225,227-232	-17.12	0.685
	204-212	-17.07	0.685		144,145	-17.45	0.800	108	142,143	-17.45	0.802
	213-236	-17.07	0.684		146,147	-17.47	0.801		144,145	-17.46	0.800
103	132,133	-17.37	0.803		148,149	-17.49	0.803		146,147	-17.48	0.802
	134,135	-17.38	0.803		(150-165)*	-17.30	0.725		148,149	-17.49	0.802
	136,137	-17.39	0.800		166,167	-17.27	0.717		150,151	-17.50	0.800
	138,139	-17.41	0.803		168-186	-17.27	0.720		152,153	-17.52	0.802
	140,141	-17.42	0.800		187-191	-17.10	0.690		154	-17.53	0.802
	142,143	-17.44	0.803		192-194	-17.10	0.689		(155-169)*	-17.33	0.727
	144,145	-17.45	0.800		195-197	-17.10	0.688		170-183	-17.32	0.725
	146,147	-17.47	0.802		198-201	-17.10	0.687		184-193	-17.13	0.690
	(148-163)*	-17.27	0.721		202-208	-17.10	0.686		194-195	-17.13	0.689
	164-166	-17.25	0.716		209-218,227-234	-17.10	0.685		196-199	-17.13	0.688
	167-170	-17.24	0.716		219-226	-17.10	0.684		200-203	-17.13	0.687
	171-188	-17.24	0.717	106	138,139	-17.42	0.800		204-218,220-223,225-226	-17.13	0.686
	189-190	-17.08	0.690		140,141	-17.43	0.800		219-224,227-231	-17.13	0.685
	191-193	-17.08	0.689		142,143	-17.44	0.800	109	144,145	-17.47	0.803
	194-196	-17.08	0.688		144,145	-17.46	0.802		146,147	-17.48	0.803
	197-199	-17.08	0.687		146,147	-17.47	0.800		148,149	-17.49	0.802
	200-205	-17.08	0.686		148,149	-17.49	0.802		150,151	-17.51	0.803
	206-215,227	-17.08	0.685		150,151	-17.50	0.800		152,153	-17.52	0.803
	216-226	-17.08	0.684		(152-165)*	-17.33	0.731		154	-17.53	0.803
	228-236	-17.08	0.684		(166-167)*	-17.33	0.731		155	-17.34	0.724
104	134,135	-17.39	0.804		168-186	-17.29	0.722		(156-162)*	-17.34	0.727
	136,137	-17.40	0.804		187-191	-17.11	0.690		(163-170)*	-17.33	0.726
	138,139	-17.41	0.801		192-194	-17.11	0.689		171-183	-17.33	0.726
	140,141	-17.43	0.804		195-197	-17.11	0.688		184-194	-17.14	0.690
	142,143	-17.44	0.801		198-201	-17.11	0.687		195-197	-17.14	0.689
	144,145	-17.46	0.804		202-209	-17.11	0.686		198-200	-17.14	0.688
	146,147	-17.47	0.801		210-233	-17.11	0.685		201-209	-17.14	0.687
	148	-17.48	0.801	107	140,141	-17.43	0.800		210-218,222-227	-17.14	0.686
	(149-164)*	-17.30	0.727		142,143	-17.45	0.802		219-221	-17.15	0.688

Z	N	$\alpha(0)$	a_a	Z	N	$\alpha(0)$	a_a
109	228-230	-17.14	0.685	113	198-201	-17.18	0.689
110	146,147	-17.48	0.800		202-221	-17.18	0.688
	148,149	-17.49	0.800		222-226	-17.18	0.687
	150,151	-17.50	0.800	114	155-170	-17.39	0.730
	152,153	-17.52	0.802		(171-175)*	-17.35	0.722
	154-156	-17.35	0.725		176-182,188-190	-17.38	0.729
	(157-164)*	-17.35	0.728		183-187	-17.38	0.730
	(165-172)*	-17.34	0.727		191-197	-17.19	0.690
	173-187	-17.34	0.727		198-201	-17.19	0.689
	188-194	-17.15	0.690		202-221	-17.19	0.688
	195-197	-17.15	0.689		222-225	-17.19	0.687
	198-201	-17.15	0.688	115	157-171	-17.40	0.731
	202-211,218-223	-17.15	0.687		(172-176)*	-17.35	0.720
	212-217,224-227	-17.15	0.686		177-181	-17.39	0.730
	228,229	-17.15	0.685		182-189	-17.39	0.731
111	148,149	-17.49	0.800		190-197	-17.20	0.690
	150,151	-17.51	0.804		198-215	-17.20	0.689
	152	-17.51	0.800		216-224	-17.20	0.688
	153-160	-17.36	0.726	116	159-167	-17.41	0.731
	(161-164)*	-17.37	0.733		168-172	-17.41	0.733
	(165-172)*	-17.35	0.728		(173-176)*	-17.42	0.740
	173-183	-17.35	0.727		177-179	-17.41	0.733
	184-188	-17.16	0.689		180-189	-17.40	0.732
	189-197	-17.16	0.690		190-197	-17.21	0.690
	198-207	-17.16	0.688		198-219	-17.21	0.689
	208-225	-17.16	0.687		220-223	-17.21	0.688
	226-228	-17.16	0.686	117	161-171	-17.42	0.733
112	150,151	-17.51	0.802		172,173,176	-17.42	0.735
	152-164	-17.37	0.726		(174,175)*	-17.42	0.739
	(165-173)*	-17.35	0.726		177-181	-17.41	0.733
	174-188	-17.36	0.728		182-189	-17.41	0.734
	189-195	-17.17	0.690		190-198	-17.22	0.690
	196-199	-17.17	0.689		199-222	-17.22	0.689
	200-213	-17.17	0.688	118	163-174,176	-17.44	0.739
	214-224	-17.17	0.687		(175)*	-17.42	0.739
	225-227	-17.17	0.686		177-181	-17.43	0.737
113	153-164	-17.38	0.728		182-188	-17.42	0.736
	165-169	-17.37	0.727		189-194	-17.23	0.690
	(170-174)*	-17.35	0.724		195-197	-17.23	0.687
	175-188	-17.37	0.729		198-221	-17.23	0.689
	189-197	-17.18	0.690				

Bibliography

[1] R. K. Gupta, R. Kumar, N. K. Dhiman, M. Balasubramaniam, W. Scheid and C. Beck, Phys. Rev. C **68**, 014610 (2003).

[2] M. Balasubramaniam, R. Kumar, R. K. Gupta, C. Beck and W. Scheid, J. Phys. G: Nucl. Part. Phys. **29**, 2703 (2003).

[3] R. K. Gupta, M Balasubramaniam, R. Kumar, D. Singh and C. Beck Nucl. Phys. A**738**, 479c (2004).

[4] R. K. Gupta, M. Balasubramaniam, R. Kumar, D. Singh, C. Beck and W. Greiner, Phys. Rev. C **71**, 014601 (2005).

[5] R. K. Gupta, M. Balasubramaniam, R. Kumar, D. Singh, S. K. Arun and W. Greiner, J. Phys. G: Nucl. Part. Phys. **32**, 345 (2006).

[6] B. B. Singh, M. K. Sharma, R. K. Gupta and Walter Greiner Int. J. Mod. Phys. E **15**, 699 (2006).

[7] B. B. Singh, M. K. Sharma and R. K. Gupta, Phys. Rev. C **77**, 054613 (2008).

[8] N. J. Davidson, S. S. Hsiao, J. Markram, H. G. Miller and Y. Tzeng, Nucl. Phys. A **570**, 61c (1994).

[9] P. A. Seeger, Nucl. Phys. **25**, 1 (1961).

[10] G. Audi, A.H. Wapstra and C. Thiboult, Nucl. Phys. A **729**, 337 (2003).

[11] P. Möller, J. R. Nix, W. D. Myers and W. J. Swiatecki, At. Nucl. Data Tables **59**, 185 (1995).

[12] G. Audi and A.H. Wapstra Nucl. Phys. A **595**, 4 (1995).

[13] S. DeBenedetti, Nuclear Interactions (New York: Wiley) (1964).

[14] W. Myers and W.J. Swiatecki, Nucl. Phys. **81**, 1 (1966).

Chapter 4

Decay of the hot and rotating compund nucleus ^{48}Cr at $\mathbf{E}^*_{CN}$ ≈60 MeV

4.1 Introduction

The compound nucleus ^{48}Cr* is produced in a symmetric ^{24}Mg+^{24}Mg [1] as well as very asymmetric ^{36}Ar+^{12}C reaction [2], using different center-of-mass energies ($E_{c.m.}$=44.4 and 47.0 MeV, respectively), such that the excitation energy E^*_{CN} (= 59.4 and 59.5 MeV, respecively) is nearly the same. This nucleus offers as an ideal example for studying the entrance-channel effects, since it belongs to the well established mass region $40 \leq A_{CN} \leq 80$ of fusion-fission phenomenon, and has also the observed data showing additional non-statistical reaction mechanisms, like the resonances, deep-inelastic or orbiting processess associated with such effects [3],[4]. According to the independence hypothesis of Bohr [5], the excitation process leaves the compound nucleus (formed with fixed angular momentum and excitation energy) in a sufficiently complex state that the subsequent decay is statistical and independent of the formation process. The statistical model analysis in terms of the transition-state model (TSM) [6], applied to the above mentioned data, shows [1],[2] that the mass and kinetic energy distributions are better reproduced for the symmetric-channel ^{24}Mg+^{24}Mg than that for the asymmetric-channel ^{36}Ar+^{12}C. For the

asymmetric channel, the calculated mass asymmetry is lower than that of the data, possibly due to the non-statistical processes. The entrance-channel effects are also found to be present in heavy compound systems (A_{CN} ∼160) [7]-[10], which are understood in terms of the increased fusion/ formation times for more symmetric channels due to the added nuclear dissipative effects in the calculations [11],[12].

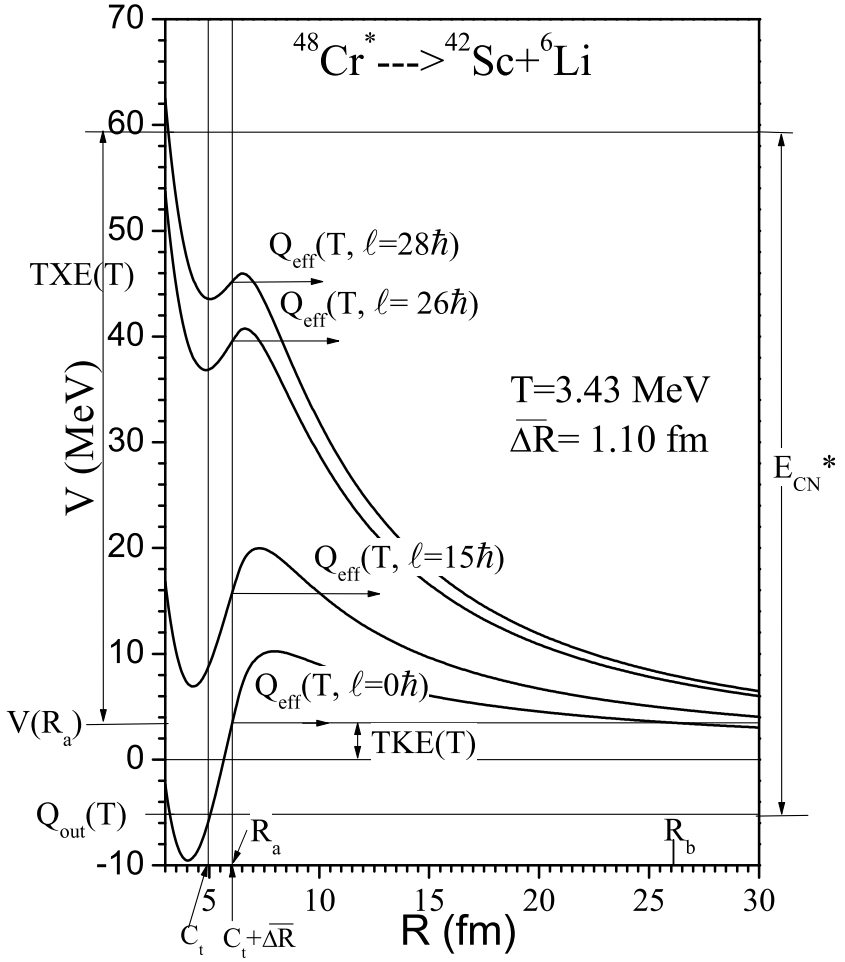

Figure 4.1: The scattering potential for the decay $^{48}Cr^{*} \rightarrow ^{42}Sc+^{6}Li$ at temperature T=3.43 MeV and different l-values.

In this work, we study for the first time the entrance channel effects in the decay of $^{48}Cr^{*}$, formed via the symmetric and very asymmetric entrance channels, using the dynamical cluster-decay model (DCM) of Gupta and collaborators [13]-[19]. Another interest of this study is the extension of the application of DCM to the decay of a further lighter compound nucleus; the lightest compound system studied so far on DCM is $^{56}Ni^{*}$. Light compound nuclei formed in low-energy (E/A ≤ 10 MeV/nucleon) heavy-ion reactions are highly excited and carry large angular momenta. The compound systems

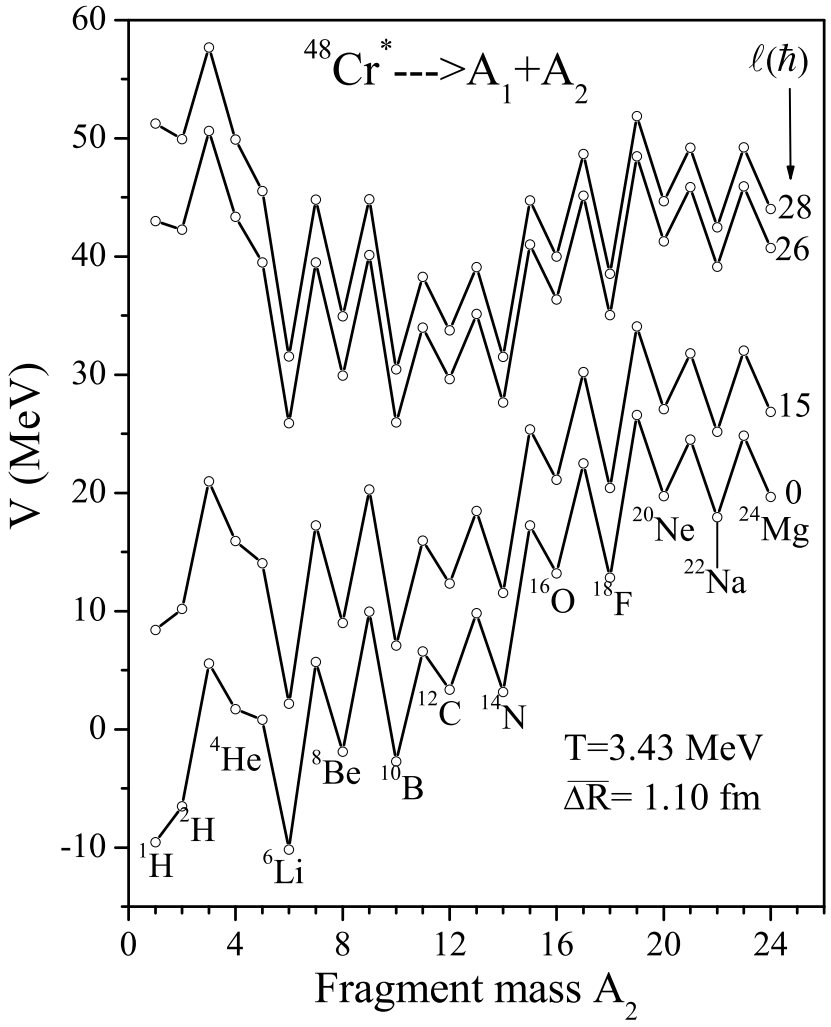

Figure 4.2: Fragmentation potential for the decay of ^{48}Cr* at T=3.43 MeV, $R = C_t + \overline{\Delta R}$ ($\overline{\Delta R}$=1.10 fm), and at different l-values.

so formed decay by emitting multiple light particles (n, p, α) and γ-rays,. For light compound systems with $A_{CN} \leq 40$, the light-particles (LP) emission is always accompanied by intermediate mass fragments, the IMFs (with $2 < Z < 10$ and $5 \leq A \leq 20$), whose contribution, though small of the order of 5-10%, is to be included in the compound nucleus fusion cross sections. The temperature and spin dependent potentials must also be mass-asymmetry dependent. Therefore, the structure effects of the compound system also become important. DCM is a decent dynamical treatment to the decay of hot and rotating compound nuclei. It is based on a collective clusterization process for emissions of the LPs, as well as the IMFs, in contrast to the statistical models in which both type of emissions are treated on different footings. Moreover, the structure effect of compound

nucleus is also included via the preformation of the fragments with relative probabilities, before penetrating the interaction barrier, an useful information which is missing in the statistical fission models.

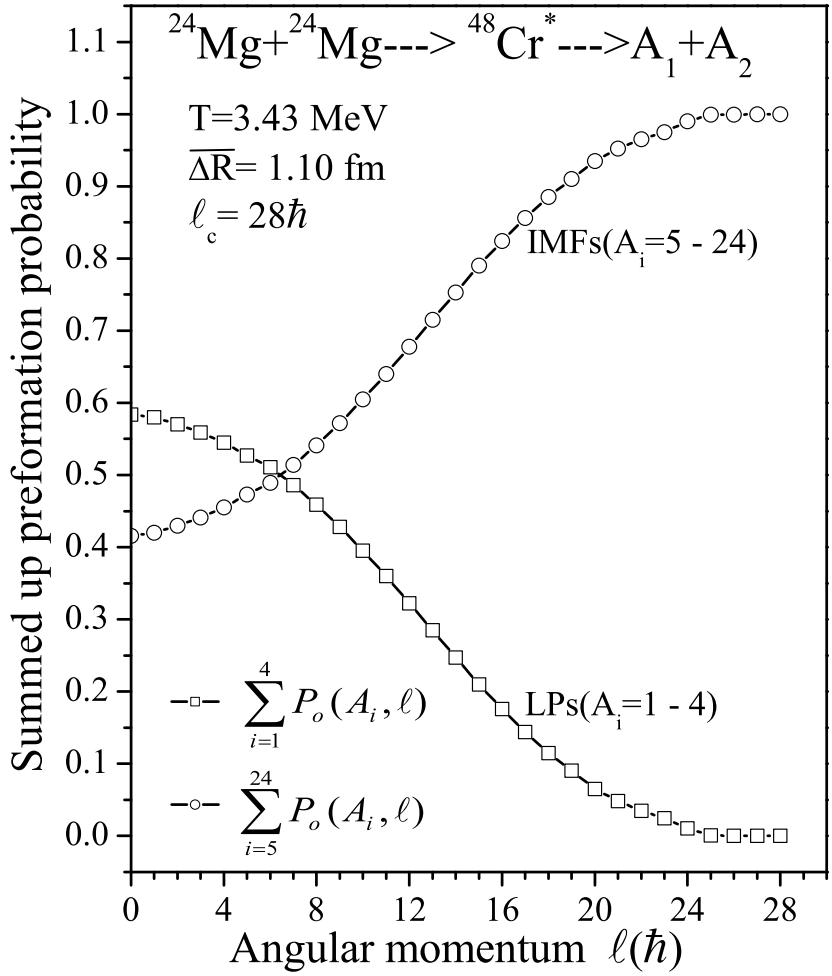

Figure 4.3: The summed up preformation probability P_0 for the LPs and IMFs, shown as a function of l ($\hbar$) for the decay of compound system ^{48}Cr* formed in the symmetric ^{24}Mg+^{24}Mg channel.

Like ^{56}Ni*, ^{48}Cr is also a negative Q-value (Q_{out}) system and would decay only if it is produced in heavy ion reactions with enough compound nucleus excitation energy, such that

$$E^{*}_{CN} = \mid Q_{out}(T) \mid + TKE(T) + TXE(T). \tag{4.1}$$

Here $E^{*}_{CN} = E_{c.m.} + Q_{in}$ and, $TXE(T)$ and $TKE(T)$ are the total excitation energy and total kinetic energy of the decay fragments, respectively. Such a distribution of E^{*}_{CN} is shown in Fig. 4.1. The Q-value of the entrance (incoming) channel Q_{in}=15.0 and 12.5

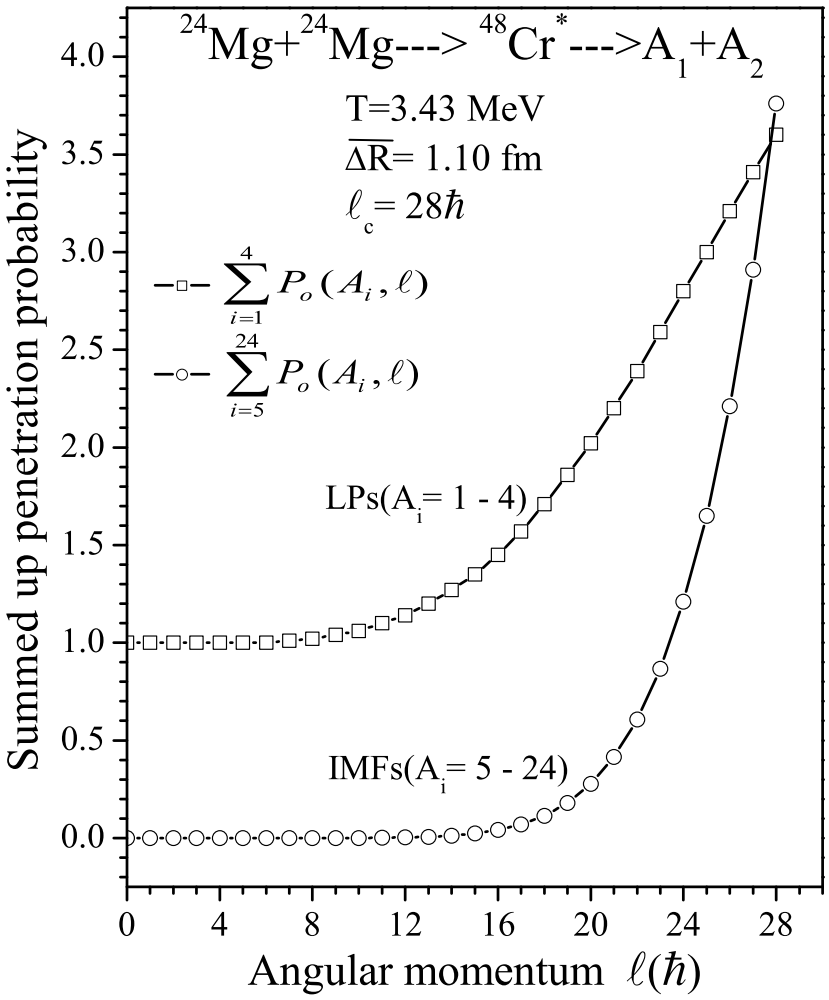

Figure 4.4: Same as for Fig. 4.3, but for penetration probability P.

MeV, respectively, for ^{24}Mg+^{24}Mg and ^{36}Ar+^{12}C reactions. The temperature T=3.43 MeV for the two reactions, obtained by using the expression given by eq. 2.19. Experimental data for both the symmetric (^{24}Mg+^{24}Mg) and asymmetric (^{36}Ar+^{12}C) reactions are available for both the LPs and IMFs mass yields and average TKE [1],[2]. The LP and IMF emission cross section, estimated in these experiments, are respectively 1065±65 mb and 150 mb for ^{24}Mg+^{24}Mg reaction, and 1215±67 mb and 25 mb for ^{36}Ar+^{12}C reaction. The total fusion cross section is then the sum of this cross section due to the LP emission and the fission-like IMF emission cross section.

The decay of compound nucleus ^{48}Cr* formed in ^{24}Mg+^{24}Mg and ^{36}Ar+^{12}C reactions is presented in section 4.2. The idea of the calculations is to look for the entrance-channel effects, if any. However, role of angular momentum in the decay of light mass compound nucleus ^{48}Cr* is also investigated explicitly. The calculations to study the decay of this

light mass compound nucleus are done with spherical considerations for the decaying fragments in the reaction process, for both the reactions. Our results are summarized in the Section 4.3.

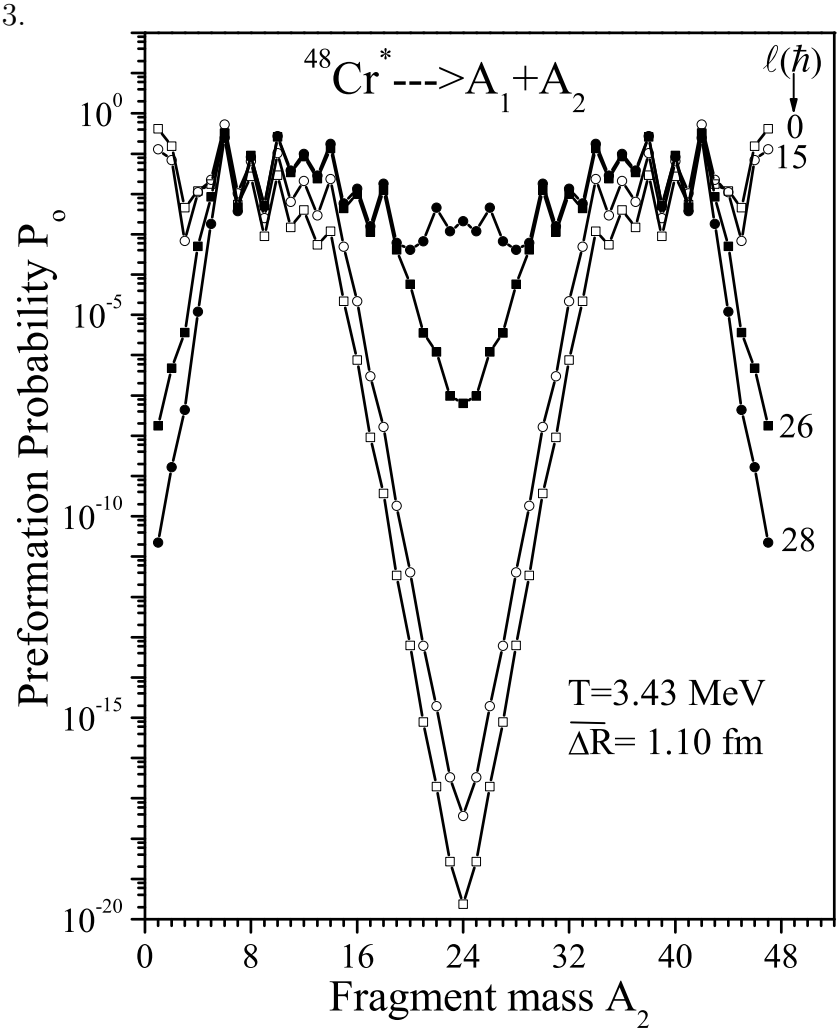

Figure 4.5: Preformation probability P_0 as a function of fragment mass A_i for the decay of $^{48}Cr^{*}$, calculated by using the fragmentation potential of Fig. 4.2.

4.2 Calculations

The total or critical angular momentum of the compound system formed depends on the entrance-channel mass asymmetry η_{in} and the entrance-channel c.m. energy $E_{c.m.}$ (Eq. 2.68), which are different for the symmetric and asymmetric entrance-channels so as to obtain nearly the same compound nucleus excitation energy E^{*}_{CN}. For $^{48}Cr^{*}$ system, l_c=28 and 26$\hbar$, respectively, for the symmetric $^{24}Mg+^{24}Mg$ and asymmetric $^{36}Ar+^{12}C$

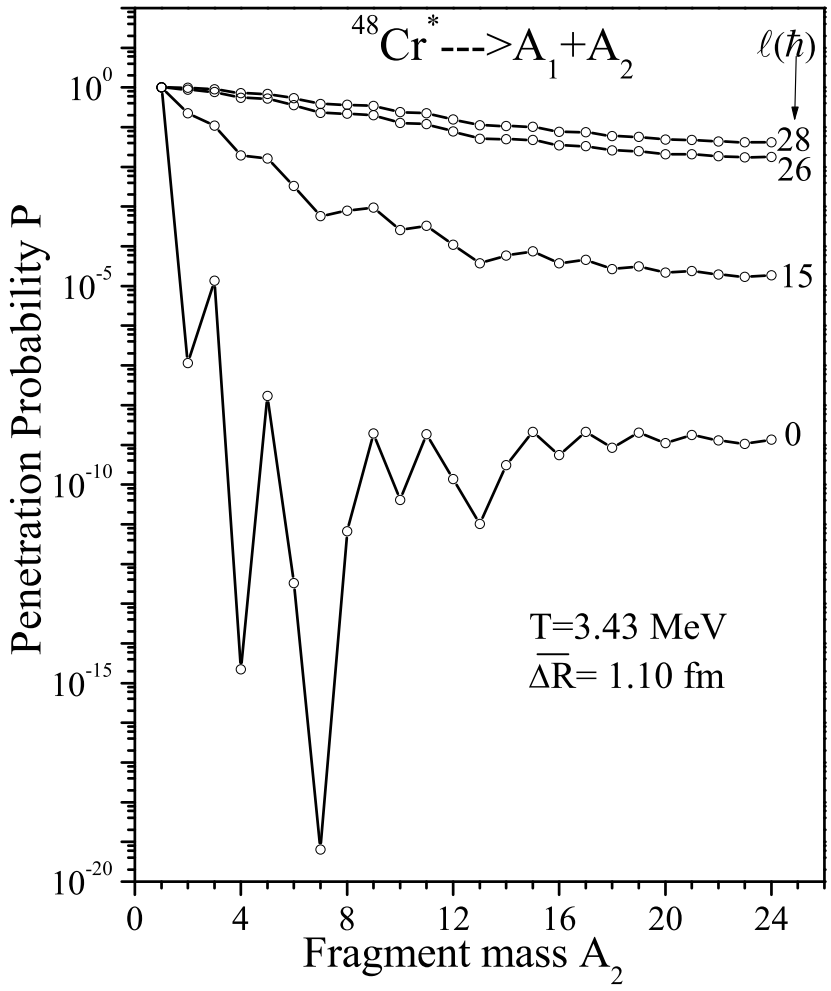

Figure 4.6: Penetration probability P as a function of fragment mass A_2 for the decay of $^{48}Cr^{*}$.

entrance-channels.

Fig. 4.2 gives the calculated fragmentation potential for the decay of $^{48}Cr^{*}$ into various mass fragments (LPs and IMFs) at T=3.43 MeV of the experimental data, and different l-values. We notice that the structure of the potential energy surface does not change much in going from l=26 (the l_c-value for $^{36}Ar+^{12}C$) to 28$\hbar$ (the l_c-value for $^{24}Mg+^{24}Mg$), even though the characteristic behaviour of the fragmentation potential for LPs and IMFs are different at the lower versus higher l-values. At lower l-values, the LPs are energetically more favourable (lower in energy), whereas the same is true of IMFs at higher l-values. This result is further illustrated in Figs. 4.3 and 4.4, respectively, for the summed up preformation probability P_0 and penetration probability P, for the case of l_c=28$\hbar$. The $\sum P_0$ is larger for LPs at lower l's whereas it is larger for IMFs at higher l's. The $\sum P$,

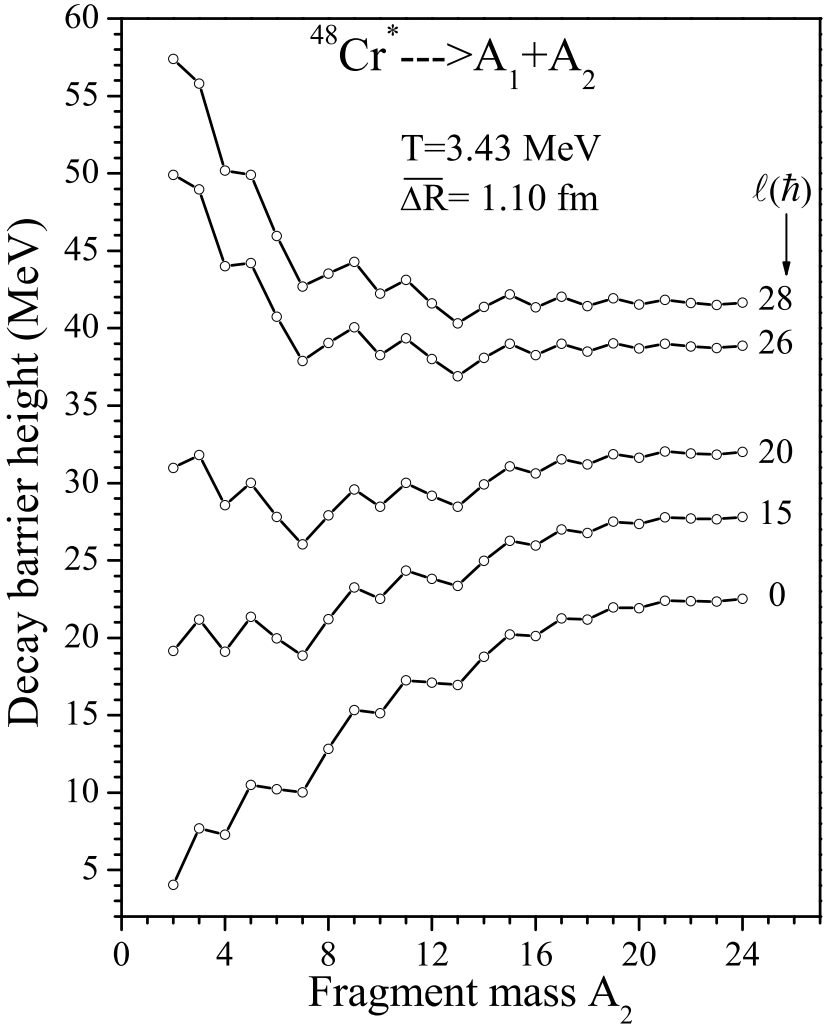

Figure 4.7: The (decay) barrier heights for the decay of $^{48}Cr^{*}$ into various fragments (LPs and IMFs), calculated at different l-values.

however, becomes larger for IMFs only for $l > 26\hbar$, the l_c-value for the symmetric-channel case.

The calculated P_0 as a function of fragment mass is shown in Fig. 4.5 for different l-values. Comparing Figs. 4.3 and 4.5, we notice that, though the summed up P_0 does not change much, its magnitude as a function of fragment mass shows a considerable change, for both the LPs and heavy mass fragments ($20 \leq A_2 \leq 24$), when l-value is changed by two units in the neighbourhood of l_c. However, these results of the entrance-channel effects in P_0 are contrary to the behaviour presented by penetrability P in Fig. 4.6, i.e., the $P(A_2)$ does not change much by changing l_c by two units. In the following, we look for the consequences of these results for the cross-sections.

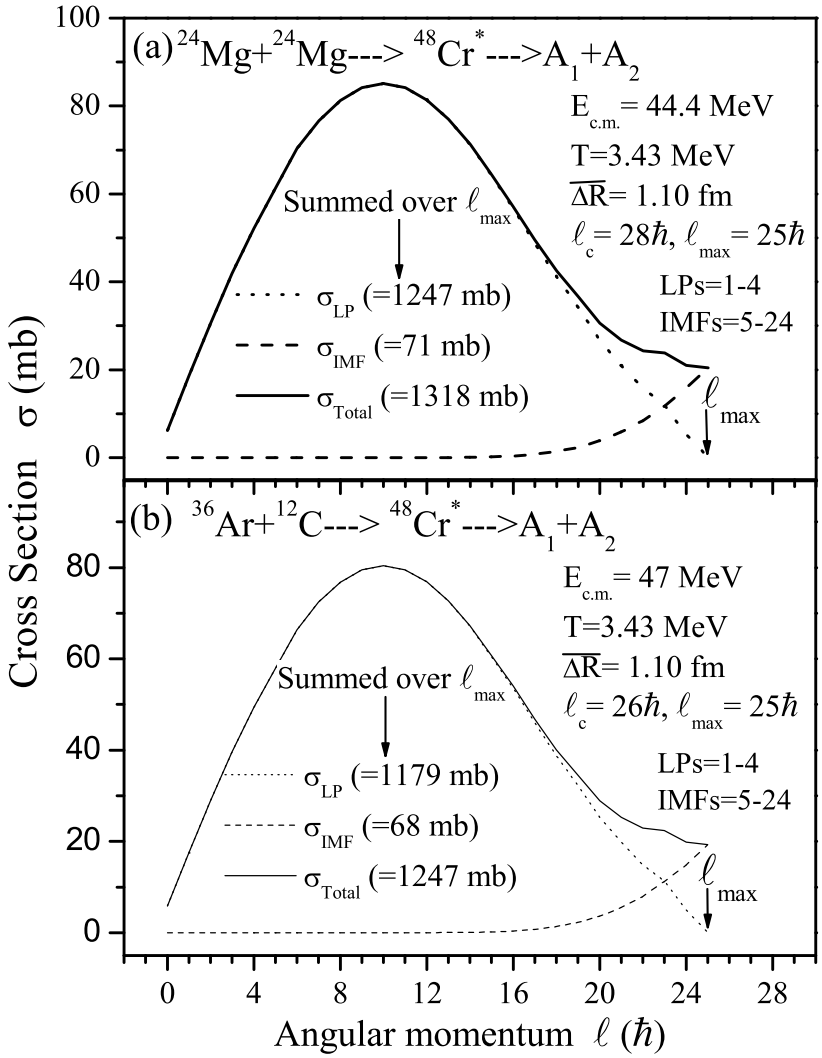

Figure 4.8: Variation of the σ_{LP}, the σ_{IMF} and their sum σ_{Total} as a function to ℓ for the decay of compound system ^{48}Cr* formed in (a) symmetric and (b) asymmetric entrance channels. Here, LPs=1-4 and IMFs=5-24, in both the cases.

In Fig. 4.7, we have plotted the (decay) barrier heights $V_B(A_2, l)$ for ^{48}Cr*. We find that, in agreement with the earlier fission barrier calculations of Royer [20], for low spins the V_B decreases, and hence the decay probability increases, with the increase of mass asymmetry (i.e. for LPs), whereas the same for higher spins increases with the increase of mass asymmetry. Interestingly, this result remains the same for l_c=26 and 28$\hbar$, i.e. is independent of whether the compound nucleus ^{48}Cr* is formed from symmetric ^{24}Mg+^{24}Mg or asymmetric ^{36}Ar+^{12}C channel. Figure 4.8 shows the calculated cross-sections for the decay of compound nucleus ^{48}Cr*, formed via the two entrance-channels ^{24}Mg+^{24}Mg and ^{36}Ar+^{12}C, into the LPs, the σ_{LP} (equivalently, σ_{evr} in the

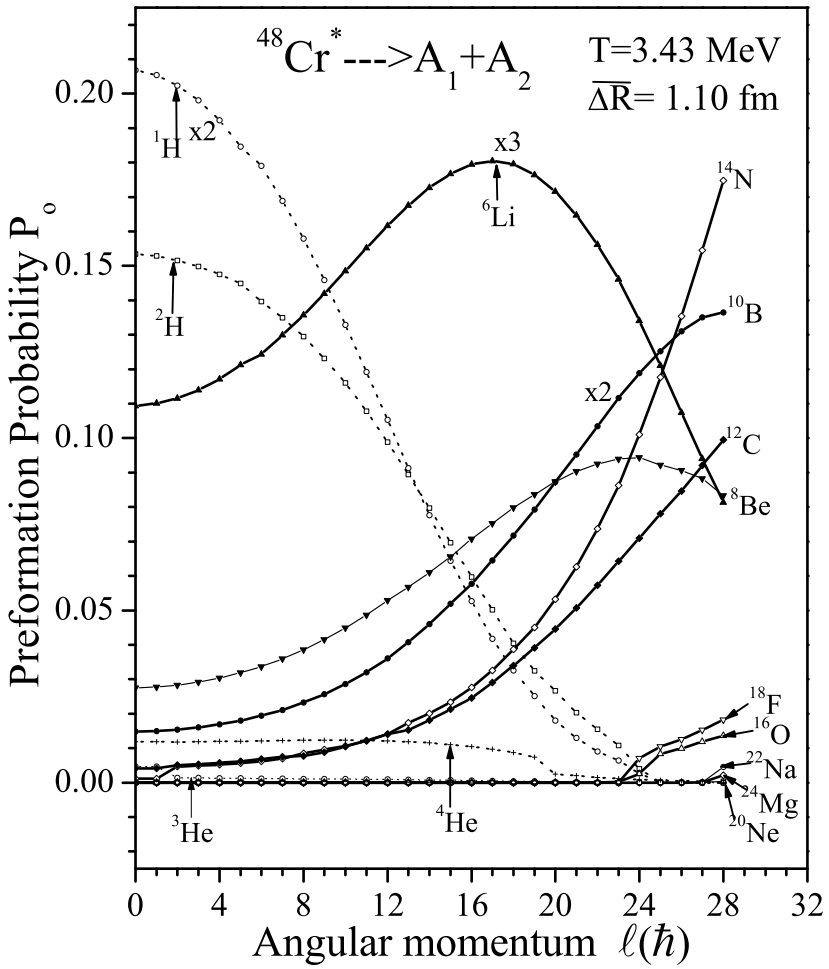

Figure 4.9: Variation of P_0 with ℓ, for both the LPs and even-A,N = Z IMFs, using the fragmentation potentials in Fig. 4.2.

language of statistical model), and IMFs, σ_{IMF}, and their sum, the total cross-section σ_{Total}. The summed up cross-sections for $l = l_{max}$ are also shown here as a legend, where LPs=1-4 and IMFs=5-24. The following results are evident: (i) As expected, the lower l-values contribute only towards σ_{LP} and at higher l-values the fission-like σ_{IMF} also starts to contribute. (ii) The σ_{LP} becomes zero at the *same* l_{max}=25$\hbar$ for the two entrance channels, a few units lower than the l_c-values. This result is a first clear signature of the independence of entrance-channel effects. In view of this result, we have presented our results in this figure up to l_{max} only, and in the following also we sum up the angular momentum l-values up to l_{max}, instead of l_c.

Figure 4.9 shows the variation of P_0 with ℓ for the energetically favored LPs and the even-A, N = Z IMFs (the contribution of the energetically unfavored odd-A IMFs being small at all $\ell^{'}s$. We notice that, whereas P_0 decreases for LPs with an increase of ℓ, it

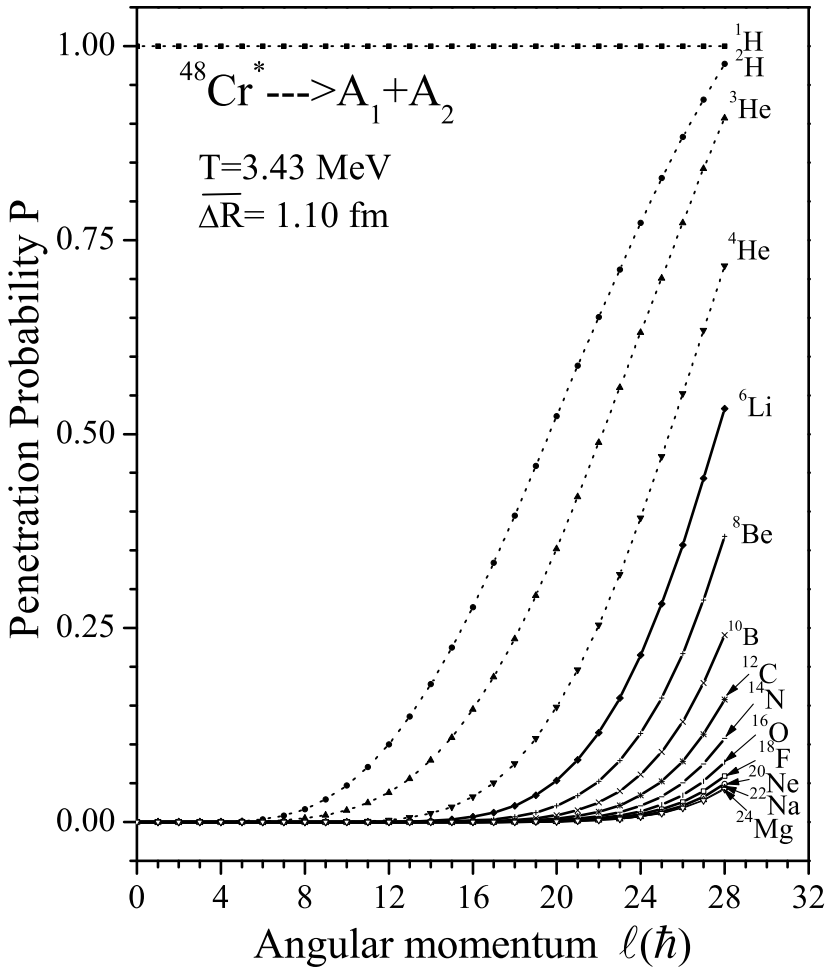

Figure 4.10: Variation of P with ℓ, for both the LPs and even-A,N = Z IMFs, using the scattering potentials of Fig. 4.1. For protons, there is no barrier at any ℓ value and hence P = 1.

increases for IMFs as ℓ increases and then starts to decrease at a large ℓ value. $P_0(\ell)$ shows that the behavior of all LPs is different from that of the IMFs. Also, for heavier IMFs (A≥16), P_0 is almost zero for $\ell \leq 20\ \hbar$. The P_0 for all the LPs becomes zero at the $\ell = 25\hbar$. In Fig. 4.10 (P as a function of ℓ), the P′s for LPs are also large. P = 1 for proton emission since there is no barrier corresponding to all ℓ-values. But for $\ell \leq 15\ \hbar$ the penetrabilities are nearly zero for all IMFs. Thus, for the penetrability P also, the behavior of LPs differs from those of the IMFs. These results for the cross sections (Fig. 4.8) means that the lower ℓ values contribute mostly to the LP cross section σ_{LP} and that the higher ℓ values ($\ell > 20\ \hbar$) contribute to the fission-like IMFs production cross section σ_{IMF}, also evident from the (decay) barrier heights $V_B(A_2, l)$ (Fig. 4.7).

Table 4.1 shows the l_{max}-summed up results of our calculated σ_{LP}, σ_{IMF} and σ_{Total},

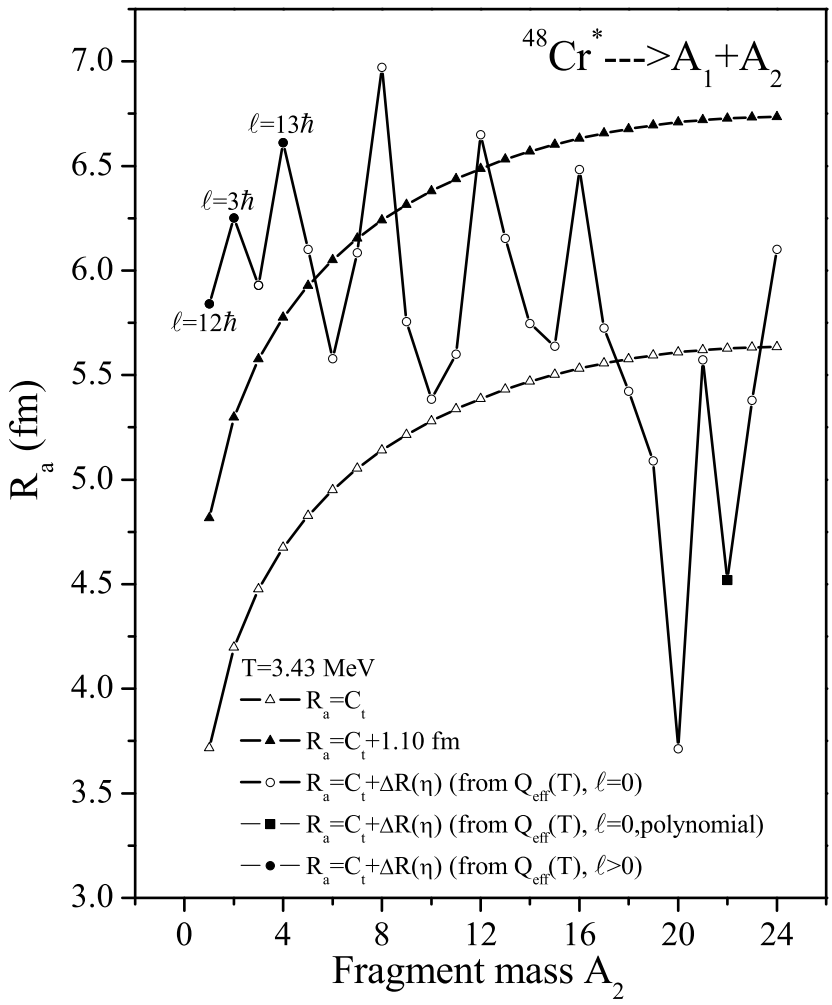

Figure 4.11: Variation of the first turning point R_a with light fragment mass A_2 for fixed $\overline{\Delta R}$=0 and 1.10 fm, and one determined from Q_{eff} at l=0, or l >0 (as mentioned in each case), or via a polynomial joining the minimum in $V(R)$ to $Q_{out}(T)$ for l=0 case.

compared with the experimental data [1, 2] and the transition-state model (TSM) calculations [1, 2] for the two entrance-channels. Here, we take for LPs, the A_2=1-4 (as above), and for IMFs, as observed in experiments, A_2=6-24 and their complimentary heavy fragments. For asymmetric-channel ^{36}Ar+^{12}C, the A_2=8 is not observed and hence is not included here too. Also presented in Table 4.1 are the results of another calculation where $R_a(\eta)$ or $\Delta R(\eta)$ are calculated from Q_{eff} (see Fig. 4.11 for $R_a(A_2)$). We find in Table 4.1 that the fits for DCM are of the same quality as for TSM, and it is nearly difficult to choose between the $\overline{\Delta R}$ and $\Delta R(\eta)$ results for DCM, though the constant $\overline{\Delta R}$ seems to work better on the whole. Another important result that follows from Table 4.1 is that the differences in the numbers for all the three cross-sections due to the two

Table 4.1: The decay cross-sections for LPs (A_2=1-4), IMFs (as observed in experiments, i.e., A_2=6-24 and their complimentary heavy fragments, excluding A_2=8 in case of asymmetric-channel) and the Total, calculated on DCM for $\overline{\Delta R}$=1.10 and $\Delta R(\eta)$ (in fm) for l_{max}=25$\hbar$ and compared with TSM calculations and experiment data [1, 2].

Reaction	$\sigma_{LP}(mb)$				$\sigma_{IMF}(mb)$				$\sigma_{Total}(mb)$			
	DCM		TSM	Expt.	DCM		TSM	Expt.	DCM		TSM	Expt.
	$\overline{\Delta R}$	$\Delta R(\eta)$			$\overline{\Delta R}$	$\Delta R(\eta)$			$\overline{\Delta R}$	$\Delta R(\eta)$		
^{24}Mg+^{24}Mg	1247	789	1100	1065±65	135	46	132†	150	1382	835	1232	1215±65
^{36}Ar+^{12}C	1179	746	970	1215±67	119	12	30	25††	1298	758	1000	1240±67

† This number is stated to be 112 mb in [1], but from their Fig. 6, we get it as 132 mb.
†† Determined from Fig. 4 of [2].

entrance-channels are very small, and are of the same order as in experiments. Note that the large differences in the case of IMFs are due the fact that different fragments are observed in the two reactions. In other words, we find a reasonably good entrance-channel independence for the decay of ^{48}Cr* formed in asymmetric or symmetric reactions.

As a further check on the DCM predictions, we have plotted in Figs. 4.12 and 4.13, the mass spectrum for IMFs, for the two entrance channels ^{24}Mg+^{24}Mg and ^{36}Ar+^{12}C, respectively, compared with the TSM and experimental data [1, 2]. The data is grouped in the same way, as in experiments, and the average values plotted. Since the DCM does not include the non-compound nucleus effects, as expected [18], its results are good only for light fragments ($Z < 9$). Also, no effects of secondary light-particle emission are included in DCM, though these effects are known to be small [2] and are included in TSM calculations. In Fig. 4.12, ^{8}Be is also included for DCM though it was not accessible in experiments. Considering all these points and the comparisons in Table 4.1, the DCM predictions could be termed as in reasonably good agreement with the data. Since ^{12}C yield is observed to be maximum in both the reactions, we have also attempted to fit this yield via $\overline{\Delta R}$, the only parameter in DCM. We get an improved fit for $\overline{\Delta R}$=1.30 fm, but then the other cross-sections get over-estimated.

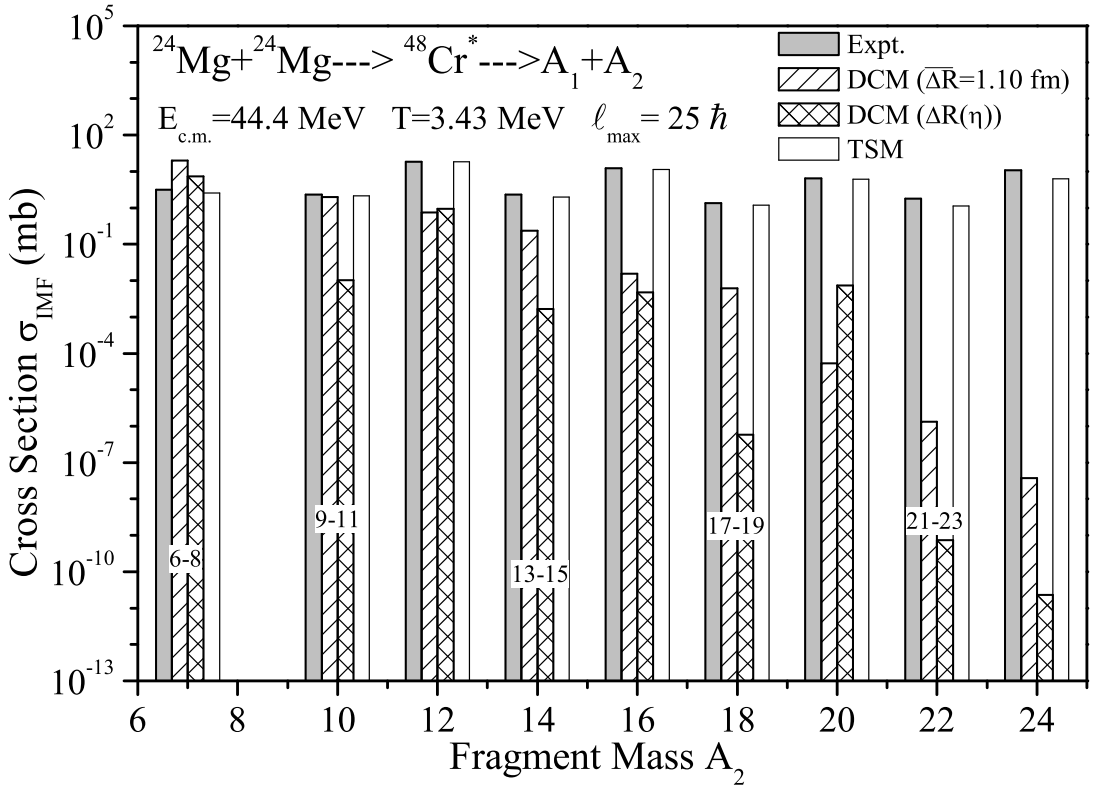

Figure 4.12: The calculated σ_{IMF} on DCM for decay fragments of ^{48}Cr* formed in symmetric entrance-channel ^{24}Mg+^{24}Mg, compared with the TSM and experimental data.

Finally, the calculated average TKE,

$$\overline{TKE}(A_2) = \sum_{l=0}^{l_{max}} \frac{\sigma_l(A_2)}{\sigma(A_2)} TKE(l, A_2);$$

with $\sigma = \sum_l \sigma_l$, is compared with the experimental data and TSM results [1, 2] in Fig. 4.14 for both the entrance channels. Apparently, our fits are as good as for TSM, but for $l_{max} < l_c$-values, and for the asymmetric-channel for two different l_{max}-values. However, this has always been the case for DCM predictions of average $\overline{TKE}$ [17], not evident why.

4.3 Summary

The entrance channel effects are studied and the dynamical cluster-decay model (DCM) applied for the first time to the decay of a light compound nucleus $^{48}Cr^{*}$ formed in sym-

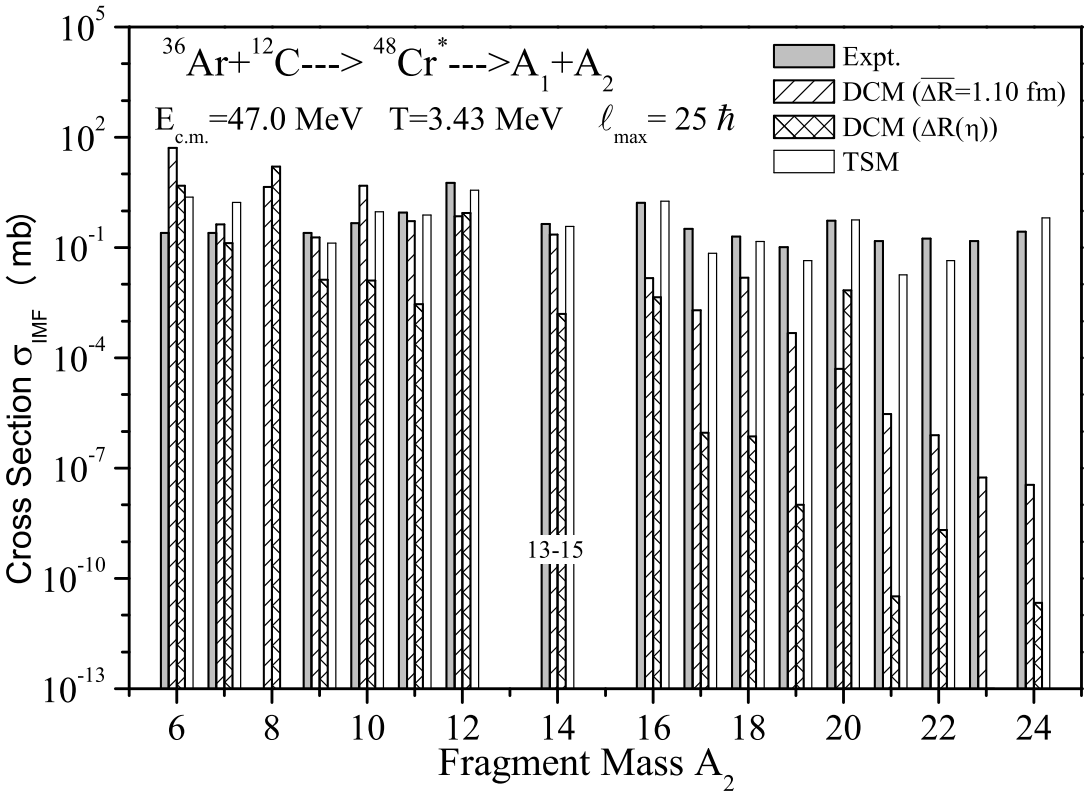

Figure 4.13: The same as for Fig. 4.12, but for asymmetric entrance-channel ^{36}Ar+^{12}C.

metric ^{24}Mg+^{24}Mg and asymmetric ^{36}Ar+^{12}C reactions, at incident energies E$_{c.m.}$=44.4 and 47.0 MeV, respectively, but with same excitation energy E^*_{CN} ≈60 MeV. The emission of both the LPs and IMFs is treated on the same footing. Though some of the characteristic quantities of the model do show entrance channel effects, the calculated cross-sections are found to be entrance-channel independent for the decay of the compound nucleus $^{48}Cr^*$.

Both the preformation factor and penetrability, as a function of angular momentum, behave differently for the LPs and the IMFs. The same result is also evident from the variation of both σ_{LP} and σ_{IMF} with angular momentum. The lower ℓ values contribute mostly to the LP cross section σ_{LP} and that the higher ℓ values contribute to IMFs production cross section σ_{IMF}.

The calculated decay cross-sections for different fragments (the LPs and IMFs) are found to contain the complete structure of the experimental data and are in reasonably good agreement with it, particularly for the IMFs of mass $A \leq 20$. The calculated aver-

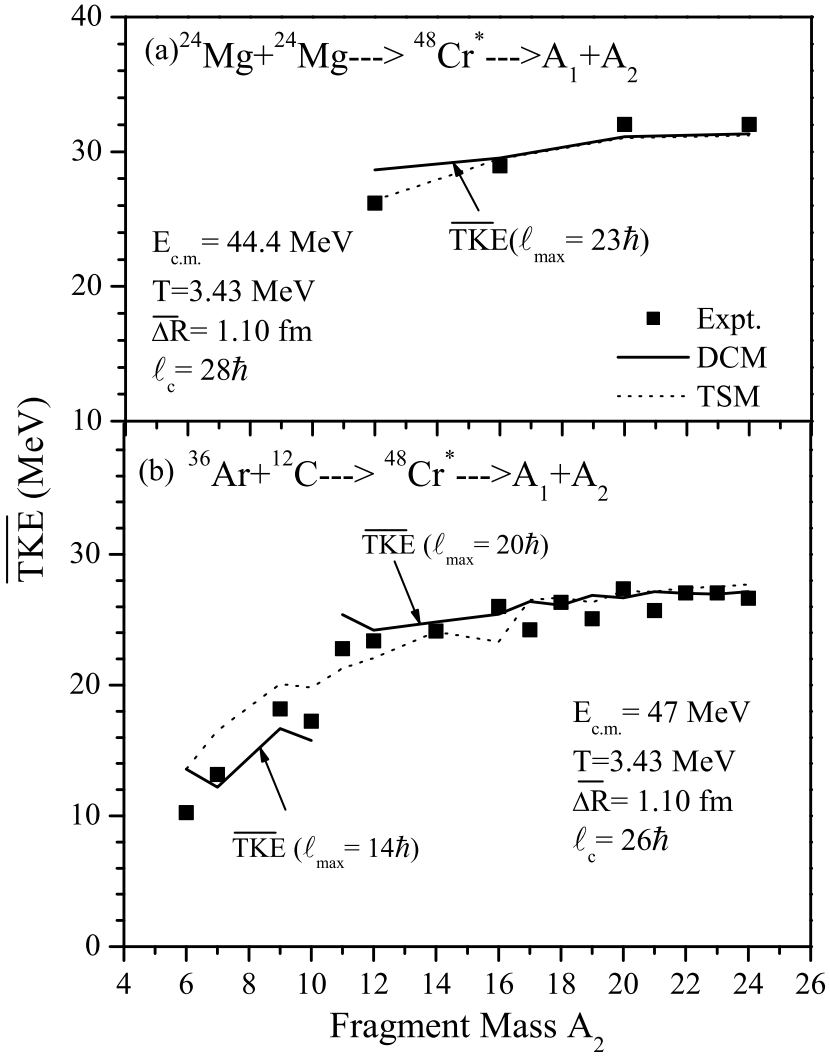

Figure 4.14: The average total kinetic energy $\overline{TKE}$, calculated on DCM and compared with the TSM and experimental data, for the decay of compound system ^{48}Cr* formed in (a) symmetric ^{24}Mg+^{24}Mg and (b) asymmetric ^{36}Ar+^{12}C entrance-channel.

age kinetic energies ($\overline{TKE}$s) are also comparable with experimentally measured average TKEs.

Bibliography

[1] A.T. Hasan, S.J. Sanders, K.A. Farrar, F.W. Prosser, B.B. Back, R.R. Betts, M. Freer, D.J. Henderson, R.V.F. Janssens, A.H. Wuosmaa and A. Szanto de Toledo, Phys. Rev. C **49** 1031 (1994).

[2] K.A. Farrar, S.J. Sanders, A.K. Dummer, A.T. Hasan, F.W. Prosser, B.B. Back, I.G. Bearden, R.R. Betts, M.P. Carpenter, B. Crowell, M. Freer, D.J. Henderson, R.V.F. Janssens, T.L. Khoo, T. Lauritsen, Y. Liang, D. Nisius, A.H. Wuosmaa, C. Beck, R.M. Freeman, Sl. Cavallaro and A. Szanto de Toledo, Phys. Rev. C **54** 1249 (1996).

[3] A.H. Wuosmaa, R.W. Zurmühle, P.H. Kutt, S.F. Pate, S. Saini, M.L. Halbert and D.C. Hensley, Phys. Rev. C **41** 2666 (1990).

[4] S.P. Barrow, R.W. Zurmühle, D.R. Benton, Y. Miao, Q. Li, P.H. Kutt, Z. Liu, C. Lee, N.G. Wimer and J.T. Murgatroyd, Phys. Rev. C **52** 3088 (1995).

[5] N. Bohr, Nature (London) **137** 344 (1936).

[6] S.J. Sanders, Phys. Rev. C **44** 2676 (1991) .

[7] A. Ruckelshausen, R.D. Fischer, W. Kühn, V. Metag, R. Mühlhans, R. Novotny, T.L. Khoo, R.V.F. Janssens, H. Gröger, D. Habs, H.W. Heyng, R. Repnow, D. Schwalm, G. Duchéne, R.M. Freeman, B. Haas, F. Haas, S. Hlavac and R.S. Simon, Phys. Rev. Lett. **56** 2356 (1986).

[8] B. Fornal, F. Gramegna, G. Prete, G. D'Erasmo, E.M. Fiore, L. Fiore, A. Pantaleo, V. Paticchio, G. Viesti, P. Blasi, F. Lucarelli, M. Anghinolfi, P. Corvisiero, M.

Taiuti, A. Zucchiatti, P.F. Bortignon, Ch. Ferrer, G. Nardelli and G. Nebbia, Phys. Rev. C **42** 1472 (1990).

[9] S. Flibotte, H.R. Andrews, T.E. Drake, A. Galindo-Uribarri, B. Haas, V.P. Janzen, D. Prévost, D.C. Radford, J. Rodriguez, P. Romain, J.P. Vivien, J.C. Waddington, D. Ward and G. Zwartz, Phys. Rev. C **45** R889 (1992).

[10] P. Twin, Nucl. Phys. A **574** 51c (1994).

[11] M. Thoennessen and J.R. Beene, Nucl. Phys. A**557** 247c (1993) .

[12] M. Thoennessen, E. Ramakrishnan, J.R. Beene, F.E. Bertrand, M.L. Halbert, D.J. Horen, P.E. Mueller and R.L. Varner, Phys. Rev. C **51** 3148 (1995) .

[13] R.K. Gupta, R. Kumar, N.K. Dhiman, M. Balasubramaniam, W. Scheid and C. Beck, Phys. Rev. C **68** 014610 (2003).

[14] M. Balasubramaniam, R. Kumar, R.K. Gupta, C. Beck and W. Scheid, J. Phys. G: Nucl. Part. Phys. **29** 2703 (2003).

[15] R.K. Gupta, Acta Phys. Hung. (N.S.) Heavy Ion Phys. **18** 347 (2003).

[16] R.K. Gupta, M. Balasubramaniam, R. Kumar, D. Singh and C. Beck, Nucl. Phys. A **738** 479c (2004).

[17] R.K. Gupta, M. Balasubramaniam, R. Kumar, D. Singh, C. Beck and W. Greiner, Phys. Rev. C **71** 014601 (2005).

[18] R.K. Gupta, M. Balasubramaniam, R. Kumar, D. Singh, S. K. Arun and W. Greiner, J. Phys. G: Nucl. Part. Phys. **32**, 345 (2006).

[19] B. B. Singh, M. K. Sharma, R. K. Gupta, and W. Greiner, Int. J. Mod. Phys. E **15**, 699 (2006).

[20] G. Royer, J. Phy. G : Nucl. Part. Phys. **21** 249 (1995).

Chapter 5

Role of deformations and orientations in the ^{208}Pb-daughter cluster radioactivity

5.1 Introduction

Cluster radioactivity is the spontaneous emission of fragments, heavier than alpha particles, from heavier nuclei and is an established phenomenon since its theoretical prediction in the early 1980 [1] and experimental confirmation in 1984 [2]. The ground state cluster decays of different nuclei in trans-lead region have been observed by many experimental groups around the world, which include ^{14}C, $^{18,20}O$, ^{22}Ne, ^{23}F, $^{24,26}Ne$, $^{28,30}Mg$ and $^{32,34}Si$. It is well established that these decays find their origin in the closed shell effects of daughter nuclei (^{208}Pb or its neighboring nuclei), understood via various theoretical studies including Preformed Cluster-decay Model (PCM) of Gupta and collaborators [3]-[5]. It means that the shell structure of the daughter nucleus or the Q-value ($B.E._{parent}$ - ($B.E._{daughter}$ + $B.E._{cluster}$)) of the reaction is the key factor in the cluster decay process.

In the present work, we intend to investigate the role of deformation and orientation of decaying nucleus and emitted fragment(s) in the ground state decay of parent nuclei, using Preformed Cluster-decay Model (PCM) of Gupta and collaborators. The study is confined to only those clusters in which daughter formed is always a ^{208}Pb which is

spherical due to its being a double closed-shell nucleus (Z = 82, N = 126). It is relevant to mention here that all the parents (^{222}Ra, $^{226,228}Th$, ^{231}Pa, $^{230,232,234}U$, $^{236,238}Pu$ and ^{242}Cm) and their respective emitted clusters (^{14}C, $^{18,20}O$, ^{23}F, $^{22,24,26}Ne$, $^{28,30}Mg$ and ^{34}Si) in to ^{208}Pb daughter decays considered here are deformed, except for ^{26}Ne and ^{34}Si which are spherical. Also all parent nuclei are prolate deformed whereas clusters ^{14}C, ^{23}F, ^{24}Ne, ^{30}Mg are oblate deformed and clusters $^{18,20}O$, ^{22}Ne, ^{28}Mg are prolate deformed. Another interesting point to be noted here is that all the parent nuclei chosen here for studying cluster decay have almost same N/Z ratio. Experimentally measured decay half lives are given in the ref. [4] for all the cluster decays studied here.

It is relevant to mention here that the first theoretical study of including deformation effects of clusters on WKB penetrability have been carried out by Gupta et al [6],[7] using the double folded Michigan-3 Yukawa (M3Y) potential for a spherical daughter and a quadrupole deformed emitted cluster. A similar study was carried out later on, accounting for the deformation of the daughter nucleus as well as including higher multipole deformations [8]. However in these studies the effects of orientation degrees of freedom in the cluster decay process are not included explicitly. Moreover, the empirically calculated preformation probability P_0, used in these works, do not contain the effects of deformation and orientations of clusters and daughters. In the present study we include all such effects in the ^{208}Pb-daughter cluster radioactivity.

The Dynamical Cluster-decay Model (DCM) of Gupta and collaborators have been recently developed successfully, with deformation and orientation effects of nuclei included in it, for studying the decay of excited compound nucleus ($\ell \neq 0$ and T $\neq$ 0)) formed in heavy ion reactions [9]. Basically, DCM is an extension of PCM of Gupta et al. [3]-[5] for studying ground state decays (i.e. ℓ=0 and T=0), which itself is based on the well-known Quantum Mechanical Fragmentation Theory (QMFT) [10],[11]. PCM is extended to include deformation and orientation effects of decay fragments [12],[13]. In PCM, we consider the preformation probability P_0 of the decaying fragments and their penetrability P across the nuclear interaction barrier which, together with the contribution of barrier assault frequency ν_0, allows defining the decay half-life $T_{1/2}$ as in equation (2.55), or the decay constant λ, equation (2.54). It has been shown explicitly that the inclusion

of deformation and orientation effects of the decaying fragments in the fragmentation potential changes the potential energy surface PES quite significantly. As a consequence of this the relative preformation probability P_0 for all the fragments changes in the ground state decay of parent nuclei. Similarly, the scattering potential (barrier position as well as its height) is also modified with deformation and orientation effects of outgoing fragments thereby affecting tunneling through barrier and penetrability P. We have used the ground state binding energies and deformation of nuclei as given by Möller-Nix [14]. For the ground state decay of parent nuclei we have considered optimum orientation for cold process from reference [15] i.e. deformed daughter and cluster in an elongated, non-compact configuration.

Section 5.2 gives our calculations for ground state decays of the chosen parent nuclei. Finally, the results are summarized in Section 5.3.

5.2 Calculations

Figure 5.1 shows the fragmentation potentials for the parent nucleus ^{232}U, for cases of spherical (β_2=0), quadrupole deformations alone (β_2), and the quadrupole, octupole, hexadecapole deformations (β_2, β_3 and β_4) taken into account for all the possible fragments. We find that the inclusion of deformation and orientation effects in the fragmentation potential change the potential energy surface (PES) quite significantly. As a result, the relative pre-formation probability P_0 for all the fragments changes accordingly. For example, the observed cluster ^{24}Ne is at the minimum in the fragmentation potential for only the spherical case. For the case of quadrupole deformations alone (β_2 only) ^{22}Ne and ^{28}Mg are found to compete with ^{24}Ne (but the ^{22}Ne has a smaller penetrability P in comparison to that for ^{24}Ne). However, the ^{28}Mg seems equally favoured for which only the upper limit of $T_{1/2}$ is measured experimentally. But, in case of higher multipole deformations (β_2, β_3, β_4), clusters other than ^{24}Ne, i.e., ^{24}F and ^{24}O are largely favoured for the mass A=24 cluster (though these clusters (both ^{24}F and ^{24}O) are prohibited by penetrability P). Moreover, deeper minima are found corresponding to other clusters which are not experimentally observed. This anomalous behaviour may be due to the

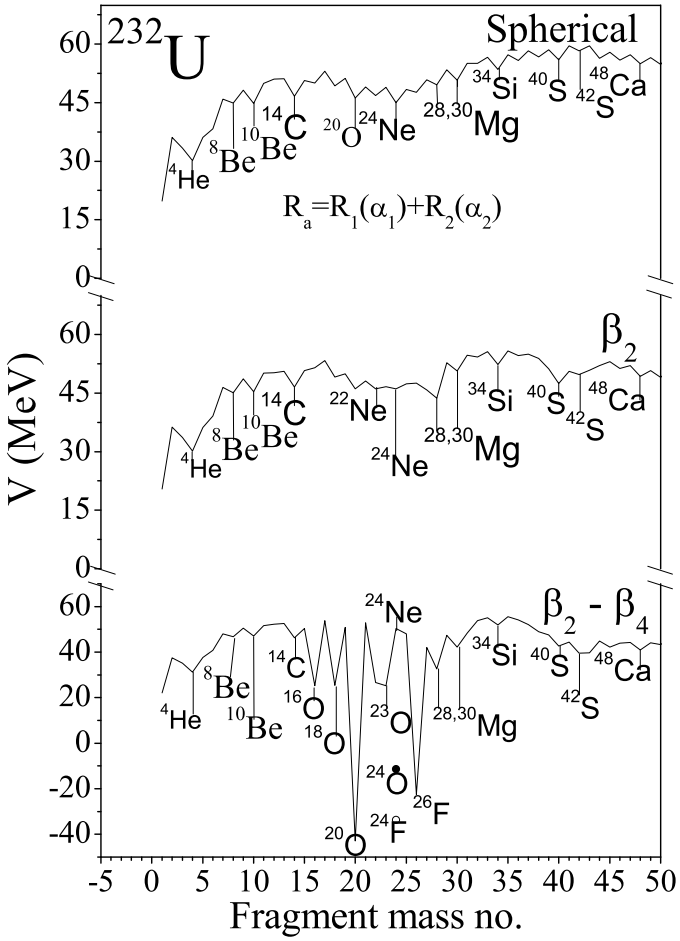

Figure 5.1: The fragmentation potential for the parent nucleus ^{232}U, for cases of spherical (β_2=0), quadrupole deformations alone (β_2) and quadrupole, octupole, hexadecapole deformations (β_2, β_3 and β_4), taken into account for all possible clusters.

use of extrapolated higher multi-pole deformations (the β_4-values) from [14], as only the ^{24}Ne cluster decay is so far observed in the ground state decay of ^{232}U. In this study we have made calculations only for experimentally observed clusters in the ^{208}Pb-daughter cluster radioactivity. Therefore, due to this anomalous behaviour of higher multipole deformation, we will mainly compare our results with the choice of quadrupole deformations alone (β_2) and spherical (β_2=0) considerations, except, in one case of ^{14}C cluster decay of ^{222}Ra, where the comparison with measured half life time becomes good only with inclusion of the higher multi-pole deformations. It is relevant to mention here that an earlier study [8] shows if daughter is spherical then the choice of quadrupole deformations alone (β_2) can reproduce the experimental value without taking into account higher multipole deformations.

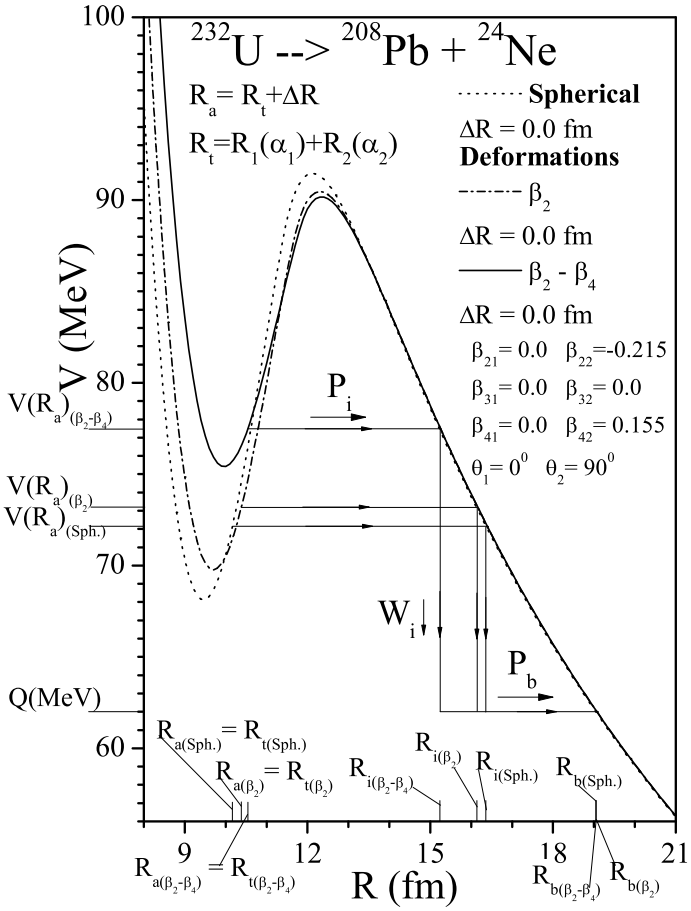

Figure 5.2: The scattering potentials for the ^{24}Ne cluster decay of parent nucleus ^{232}U daughter being ^{208}Pb i.e. ^{232}U$\rightarrow$^{208}Pb+^{24}Ne, for different cases of deformations for ^{24}Ne.

Figure 5.2 gives the scattering potential for ^{24}Ne cluster decay of ^{232}U, for cases of each spherical (β_2=0), quadrupole deformations alone (β_2) and quadrupole, octupole, hexadecapole deformations (β_2, β_3 and β_4). It shows that the barrier position as well as height are modified with the inclusion of deformation and orientation effects of the cluster ^{24}Ne (β_2 = -0.215, β_3 = 0 and β_4 = 0.155). The penetration path is considered to begin at R=R_t+$\triangle$R ($\triangle$R=0 in this case, the only free parameter of the model), which is different in each case thereby affecting the tunneling penetrability P.

A comparison between measured and calculated $log_{10}T_{1/2}$-values for the choice of quadrupole deformations alone (β_2) and spherical (β_2=0) considerations is shown in Figure 5.3(a). In Figure 5.3(b) the Q-values of the all observed clusters are plotted as a function of cluster mass. The structure seen here corresponding to $log_{10}T_{1/2}$-values in Figure 5.3(a), emphasizes again the well observed role of shell effects played in the phenomenon of cluster radioactivity. Moreover, the comparison of calculated and measured values of $log_{10}T_{1/2}$, for the two choices of deformed and spherical fragments of parent nu-

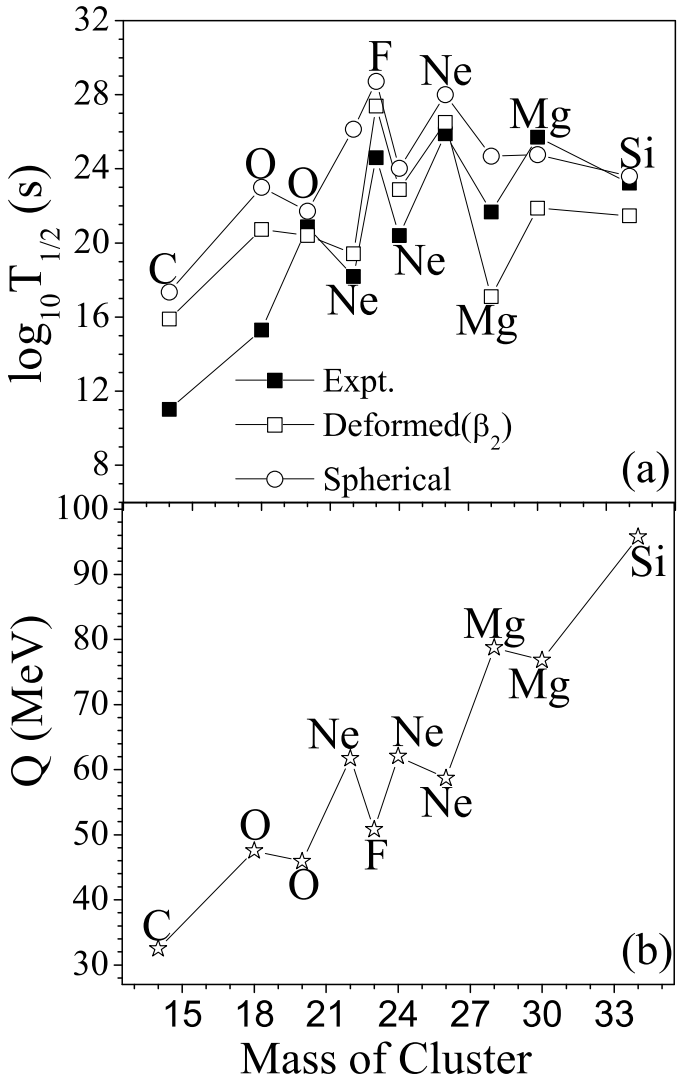

Figure 5.3: (a) Comparison of measured values of $log_{10}T_{1/2}$ for cluster decays ^{14}C, $^{18,20}O$, ^{22}Ne, ^{23}F, $^{24,26}Ne$, $^{28,30}Mg$ and ^{34}Si of parents ^{222}Ra, $^{226,228}Th$, ^{230}U, ^{231}Pa, $^{232,234}U$, $^{236,238}Pu$ and ^{242}Cm respectively having daughter ^{208}Pb in each case, with the calculated $log_{10}T_{1/2}$ for cases of spherical (β_2=0), quadrupole deformations alone (β_2) and quadrupole, octupole, hexadecapole deformations (β_2, β_3 and β_4). (b) Q-values of the cluster decays.

clei, points out the important role being played by deformed and oriented nuclei besides the role of well established shell effects. We observe that for almost all the cluster decays the comparisons become good with the choice of deformed and oriented nuclei, except for few heavier cluster decays. The heavier clusters may follow the experimental data if improved values of hexadecapole deformation β_4 are made available. The generalized orientation considerations may further add to the cause. Table 5.1 and 5.2 summarizes the above results and characteristic quantities in our calculations for the cluster decay of parents ^{222}Ra, $^{226,228}Th$, ^{230}U, ^{231}Pa, $^{232,234}U$, $^{236,238}Pu$ and ^{242}Cm. The results for all the three choices are compiled here in these tables i.e. for spherical (β_2=0), quadrupole

Table 5.1: Half-life times and other characteristic quantities for cluster decay of parent nuclei having daughter nuclei ^{208}Pb in each case, using the Preformed Cluster-decay Model (PCM) of Gupta and collaborators , extended to include deformation and orientation effects of decaying fragments [12],[13]. The calculations and comparisons have been made for cases of spherical (β_2=0), quadrupole deformations alone (β_2) and quadrupole, octupole, hexadecapole deformations (β_2, β_3 and β_4). The results are compared with the experimental data given in [4]. The impinging frequency is nearly constant, with $\nu \sim 10^{21} s^{-1}$ for each case.

Parent	Cluster	R_a	$Q_{M.N.}$	PCM Half-lives ($log_{10}T_{1/2}$)			Expt. Half-lives ($log_{10}T_{1/2}$)
				β_2	β_2,β_3,β_4	Sph.	
^{222}Ra	^{14}C	R_t+1.26	32.47	15.89	11.20	17.36	11.01
^{226}Th	^{18}O	R_t	47.55	20.73		23.00	>15.3
^{228}Th	^{20}O	R_t+0.50	45.91	20.40		21.72	20.87
^{231}Pa	^{23}F	R_t+0.25	50.81	27.38	09.28	28.73	>24.61
^{230} U	^{22}Ne	R_t	61.69	19.41	01.27	26.15	>18.2
^{232} U	^{24}Ne	R_t	62.03	22.88	11.19	24.04	21.05
^{234} U	^{26}Ne	R_t+0.50	58.65	26.49	16.15	28.00	25.06
^{236}Pu	^{28}Mg	R_t	78.75	17.11		24.68	21.67
^{238}Pu	^{30}Mg	R_t+0.50	76.82	21.87	32.57	24.77	25.70
^{242}Cm	^{34}Si	R_t	95.78	21.47	33.96	23.59	23.24

deformations alone (β_2), and the quadrupole, octupole, hexadecapole deformations (β_2, β_3 and β_4). The experimental results for $logT_{1/2}$ are given here for comparisons. The Q-value for each cluster decay is also given here along with the fitted $\triangle$R values in few cases, in remaining cases $\triangle$R is zero. One can clearly see here that β_2 alone gives decent comparisons with the experimental data among all the three choices. However, with the higher multipole deformations (β_2-β_4) included, the $log_{10}T_{1/2}$ is underestimated, possibly due to the in-appropriate calculated β_4 values, except in one case of ^{14}C cluster decay of ^{222}Ra, where the comparison with measured half life time becomes good only with inclusion of the higher multi-pole deformations. This result have been reported earlier also [12].

Table 5.2: The comparisons have been made for the preformation probability P_0 and penetration probability P of clusters in ^{208}Pb daughter cluster radioactive decay of the parent nuclei calculated using PCM, for the cases of quadrupole deformations alone (β_2), quadrupole, octupole, hexadecapole deformations (β_2, β_3 and β_4) and spherical (β_2=0).

Parent	Cluster	PCM					
		Preformation Probability P_0			Penetration Probability P		
		β_2	β_2,β_3,β_4	Sph.	β_2	β_2,β_3,β_4	Sph.
^{222}Ra	^{14}C	1.88x10^{-20}	9.16x10^{-16}	6.54x10^{-22}	1.59x10^{-18}	1.59x10^{-18}	1.55x10^{-18}
^{226}Th	^{18}O	3.59x10^{-23}	9.29x10^{-08}	2.42x10^{-25}	1.13x10^{-20}		9.03x10^{-21}
^{228}Th	^{20}O	8.44x10^{-23}	9.99x10^{-01}	4.20x10^{-24}	1.12x10^{-20}		1.06x10^{-20}
^{231}Pa	^{23}F	1.05x10^{-26}	4.13x10^{-09}	3.27x10^{-27}	9.61x10^{-24}	3.06x10^{-23}	1.39x10^{-24}
^{230} U	^{22}Ne	5.61x10^{-23}	8.52x10^{-08}	2.40x10^{-28}	1.48x10^{-19}	1.36x10^{-16}	6.28x10^{-21}
^{232} U	^{24}Ne	1.03x10^{-25}	5.51x10^{-15}	8.64x10^{-26}	2.87x10^{-20}	2.63x10^{-19}	2.38x10^{-21}
^{234} U	^{26}Ne	1.15x10^{-26}	2.52x10^{-16}	3.56x10^{-28}	6.70x10^{-23}	6.70x10^{-23}	6.70x10^{-23}
^{236}Pu	^{28}Mg	6.62x10^{-22}	6.32x10^{-17}	6.56x10^{-28}	2.55x10^{-18}		6.92x10^{-20}
^{238}Pu	^{30}Mg	3.24x10^{-26}	2.55x10^{-36}	2.74x10^{-28}	9.47x10^{-19}	2.42x10^{-19}	1.42x10^{-19}
^{242}Cm	^{34}Si	1.52x10^{-25}	4.94x10^{-38}	1.14x10^{-27}	4.85x10^{-19}	4.85x10^{-19}	4.85x10^{-19}

5.3 Summary

We find that the calculated decay half-lives using the PCM, for the cluster-decay observed in ^{208}Pb daughter cluster radioactivity process, are in good agreement with the measured data, with inclusion of deformation and orientation effects. In PCM, both P_0 and P are shown to be modified with the inclusion of deformation and orientation effects. Moreover, unlike P, the value of P_0 is not only affected by the shapes of parent, daughter and cluster, but also due to the shape of all other possible fragmentations of the decaying parent. The study clearly points out the role of deformations and orientations in the cluster radioactive decays. The role of higher multipole deformations (β_3,β_4), however, crucial for ^{14}C cluster decay of ^{222}Ra, needs a closer look on extrapolation process of β_4 values along with generalization of orientation degree of freedom, before reaching at any discrete conclusion. In the present study we find that calculated $logT_{1/2}$ values are in better agreement with the measured data even for the choice of β_2 alone. We notice an important role played by the deformations and orientations in cluster formation process besides known shell closure effects.

Bibliography

[1] A. Săndulescu, D.N. Poenaru, and W. Greiner, Sovt. J. Part. Nucl. **11**, 528 (1980).

[2] H.J. Rose and G.A. Jones, Nature **307**, 245 (1984).

[3] S.S. Malik and R.K. Gupta, Phys. Rev. **C 39**, 1992 (1989).

[4] R.K. Gupta and W. Greiner Int. J. Mod. Phys. E **3**, 335 (1994, Suppl.).

[5] S. Kumar and R.K. Gupta, Phys. Rev. **C 55**, 218 (1997).

[6] R.K. Gupta, M. Horoi, A. Sandulescu, M. Greiner and W. Scheid, J. Phys. G: Nucl. Part. Phys. **C 19**, 2063 (1993).

[7] A. Săndulescu, R.K. Gupta, F. Carstoiu, M. Horoi and W. Greiner, Int. J. Mod. Phys. E 1379 (1992).

[8] S. Misicu, D. Protopopescu, Acta Physcia Polonica B **C 30** 127 (1999).

[9] B. B. Singh, M. K. Sharma and R. K. Gupta, Phys. Rev. **C 77**, 054613 (2008).

[10] J. Maruhn and W. Greiner, Phys. Rev. Lett. **32**, 548 (1974).

[11] R. K. Gupta, W. Scheid and W. Greiner, Phys. Rev. Lett. **35**, 353 (1975).

[12] S. K. Arun and R. K. Gupta, DAE Nucl. Phys. (Sambalpur) **52**, 365 (2007).

[13] B.B. Singh, S. K. Arun, M. K. Sharma, S. Kanwar and R. K. Gupta, DAE Nucl. Phys. (Roorkee) **53**, 261 (2008).

[14] P. Möller, J. R. Nix,W. D. Myers, andW. J. Swiatecki, At. Data Nucl. Data Tables **59**, 185 (1995).

[15] R. K. Gupta, M. Balasubramaniam, R. Kumar, N. Singh, M. Mahhas, and W. Greiner, J. Phys. G: Nucl. Part. Phys. **C 31**, 631 (2005).

Chapter 6

Decay of $^{246}Bk^*$ formed in reactions of ^{11}B+^{235}U and ^{14}N+^{232}Th at low energies

6.1 Introduction

A compound nucleus (CN) formed in low energy heavy ion reactions, in general, decays by emitting multiple light particles (n, p, α) and γ-rays resulting in the evaporation residue (ER) cross section, and is accompanied by a small (5-10%) component of so-called intermediate mass fragments (IMFs) of masses 5≤A≤20 and charges $2 < Z < 10$ for both the light (A_{CN} ∼40-80) and medium mass (A_{CN} >100) compound systems. The production of IMFs in light compound nuclei is best understood in the extended Hauser-Feshbach (EHF) formalism of the BUSCO code [1] or the EHF method based on scission-point picture [2], and in medium mass nuclei as binary decay in the statistical fission model of Moretto [3]. For the lighter compound nuclei (A_{CN} <80), another fission model [4], called the saddle-point transition-state model, has also been successfully used. Apparently, in the above stated formalisms, the emission of light particles (LPs) is calculated within the Hauser-Feshbach method [5]. Alternatively, in the dynamical cluster-decay model [6]-[14], Gupta and collaborators treated both the LPs and IMFs on equal footings as the dynamical collective mass motions of preformed clusters through the barrier. The model

is applied to both the light and medium mass systems, namely, the $^{48}Cr^*$, $^{56}Ni^*$ and $^{116}Ba^*$ nuclei. In heavier CN (A_{CN} >200), like the $^{246}Bk^*$ nucleus studied here, the main decay mode is (symmetric and near symmetric) fission which in DCM can be considered as an extreme case of IMFs, the heavier mass fragments (HMFs), observed together with or without the LPs and IMFs. In other words, all the processes of ER (LPs), IMFs as well as fission, or a combination of these, or any one of them alone as a dominant mode, can occur in different mass regions of the Periodic Table. In addition, there can be effects of non-compound nucleus decays, like the pre-equilibrium fission, quasi-fission (qf) or deep inelastic collisions (DIC), etc., occuring mostly at higher incident center-of-mass (c.m.) energies.

The compound nucleus $^{246}Bk^*$ formed in $^{11}B+^{235}U$ and $^{14}N+^{232}Th$ reaction channels at sub- and near-barrier energies [15, 16] is highly fissile and decays almost totally by fission. Thus, fusion cross sections are nearly the same as the measured fission cross sections, which makes $^{246}Bk^*$ an ideal case to study the compound nucleus fusion-fission process in heavy mass nuclei formed in low energy heavy ion reactions. Furthermore, the measured fission fragment anisotropies in these experiments [15, 16] show the entrance channel effects for the anisotropy values of $^{11}B+^{235}U$ being consistent, but that of $^{14}N+^{232}Th$ anomalous, with respect to the statistical saddle-point model [4, 17]. In other words, a non-compound nucleus component seems to be present in the fusion cross section for $^{14}N+^{232}Th$ reaction. In this paper, we look for the dynamics of this effect with respect to different entrance channels of similar mass asymmetry on the basis of the dynamical cluster-decay model [6]-[14].

The effects of deformations and orientations of decay fragments are included in the calculations. Application of the model to fusion-fission of $^{246}Bk^*$ is discussed in Section 6.2. This is a positive Q-value (Q_{out}) system. Finally, Section 6.3 gives a summary of our results. Interestingly, in contrast to the results of experiments mentioned above, at higher incident c.m. energies we find the contributions of quasi-fission process in the decay of $^{246}Bk^*$ formed due to $^{11}B+^{235}U$ rather than due to $^{14}N+^{232}Th$ incoming channel. In other words, the calculations on DCM show the decay of $^{246}Bk^*$ formed via $^{14}N+^{232}Th$ reaction as an almost pure CN decay.

6.2 Calculations

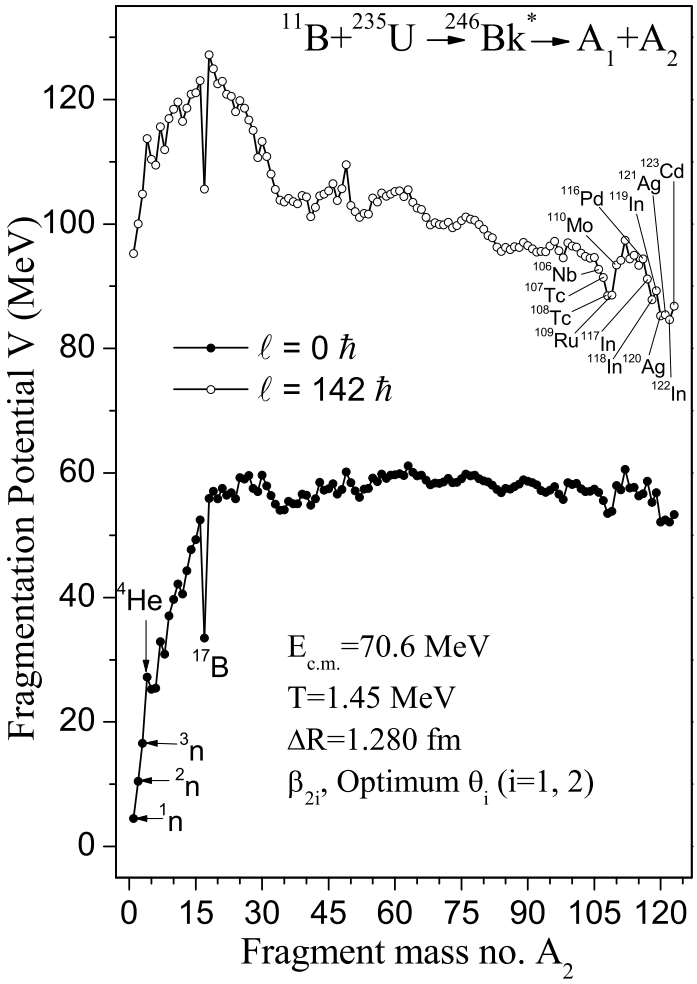

Figure 6.1: The fragmentation potential as a function of the light fragment mass A_2 for the decay of ^{246}Bk*, formed in ^{11}B+^{235}U reaction at $E_{c.m.}$=70.6 MeV (equivalently, T=1.45 MeV), calculated at two extreme ℓ-values.

As already mentioned above, fission cross sections for the decay of ^{246}Bk*, formed in ^{11}B+^{235}U and ^{14}N+^{232}Th reactions, have been measured [16] at various $E_{c.m.}$, which represent the sole contribution to the total fusion cross section ($\sigma_{fus}^{Expt} = \sigma_{fiss}^{Expt}$). No contribution due to the emission of LPs ($A \leq 4$), IMFs ($4 \leq A \leq 20$) or non-compound qf processes are explicitly recorded.

Figure 6.1 shows the calculated fragmentation potentials for the decay of ^{246}Bk* (formed in ^{11}B+^{235}U reaction at $E_{c.m.}$=70.6 MeV or T=1.45 MeV) at two extreme ℓ=0 and ℓ_{max}-values, using quadrupole deformations and optimally oriented hot configurations

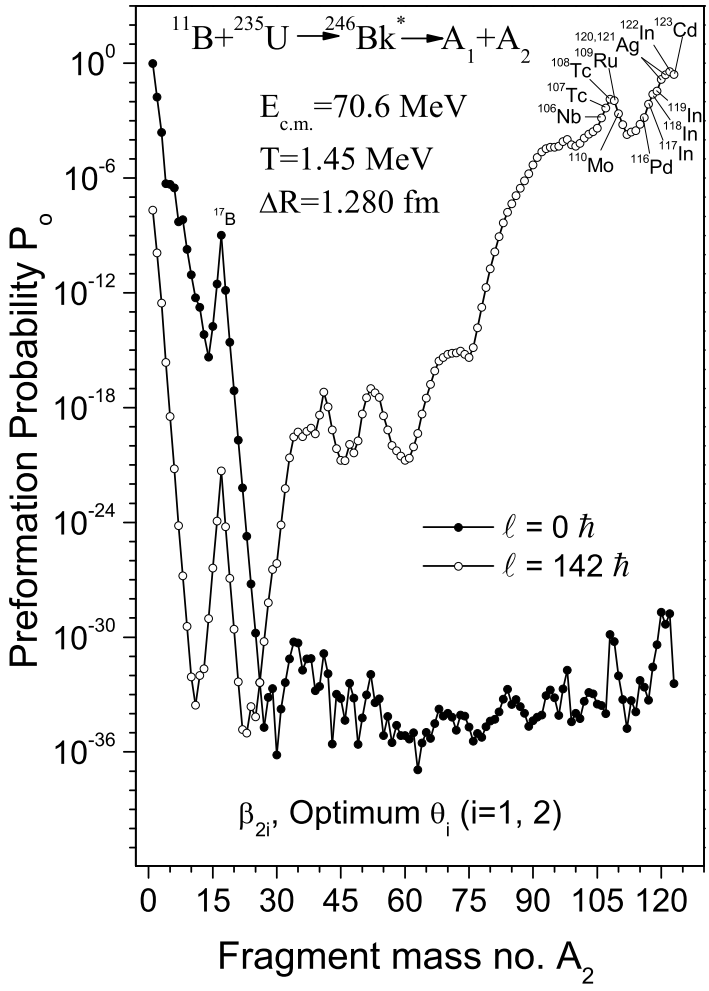

Figure 6.2: Same as for Fig. 6.1, but for the preformation probability P_0.

according to Table 1 of Ref. [18]. ℓ_{max}=142$\hbar$ is fixed for $\sigma_{LPs} \rightarrow$0 (see Fig. 6.4). We note that the LPs and IMFs are favored (lower in energy) at ℓ=0, but at higher ℓ-values the symmetric and near-symmetric fragments become more favored. At ℓ=142$\hbar$, a strong minima is obtained for symmetric fragments A=116-123, denoted as the symmetric fission (SF) window of mass $A_{CN}/2 \pm 7$. Also, another minima is seen in the immediate neighbourhood of the SF window, corresponding to heavy mass fragments A=106-110, referred to as the HMFs window. Thus, a sum of the SF and HMFs windows in Fig. 6.1 gives the (total) fission of compound nucleus. Since the reported fission cross sections correspond to assumed symmetric mass division only [16], without actually identifying the fragments, the presence of a new HMFs window, in addition to the SF window, allows us to look for the fine- or sub-structure of the fission of $^{246}Bk^{*}$ (see Fig. 6.8).

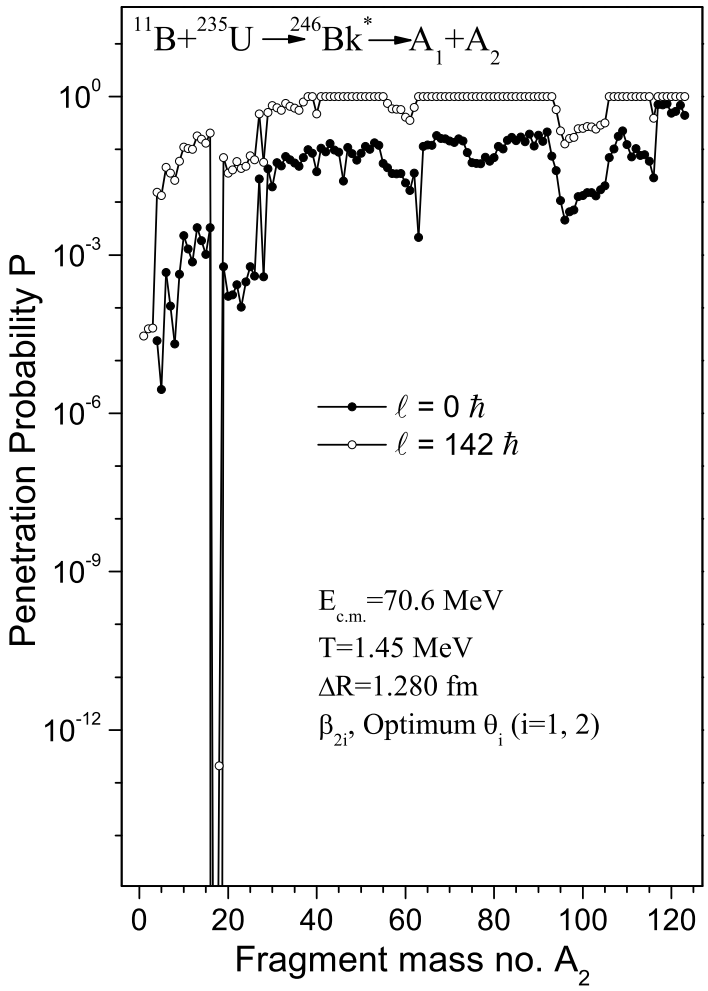

Figure 6.3: Same as for Fig. 6.1, but for the penetration probability P.

The above result of a favored asymmetric to a favored symmetric division with increase in ℓ-value is also depicted in Fig. 6.2 for the preformation factor $P_0(A_2)$, and in Fig. 6.3 for the penetration probability $P(A_2)$. In Fig. 6.3, we notice that, at higher ℓ-value, P$\rightarrow$1 (its highest value) for the symmetric fragments. P is very small for the emission of LPs, and also tends to zero for ^{17}B fragment (so also for ^{18}B) which occurs as a strong minimum in the fragmentation potential of Fig. 6.1 or as a maximum in the preformation probability of Fig. 6.2. In the following, we shall see that major contribution to fission (equivalently, fusion) cross section arises from the SF window, and that the HMFs window contributes to a maximum of $\sim 5\%$ and that too only for the first few higher c.m. (top three) energies. Furthermore, we shall see that the entrance channel also plays its role in terms of the quasi-fission contributing, at higher c.m. energies, due to the ^{11}B+^{235}U reaction and *not* due

to ^{14}N+^{232}Th reaction. Thus, in our calculations, respectively, for the case of negligible or zero contributions from LPs and IMFs, $\sigma_{fus}^{Cal} = \sigma_{HMF} + \sigma_{SF} + \sigma_{qf} = \sigma_{fiss}^{Cal} + \sigma_{qf}$, to be compared with experimentally measured σ_{fus}^{Expt} ($=\sigma_{fiss}^{Expt}$). Apparently, the quasi-fission component is obtained empirically [19] as the difference between the experimentally measured and our calculated fission comoponents, i.e., $\sigma_{qf} = \sigma_{fiss}^{Expt} - \sigma_{fiss}^{Cal}$.

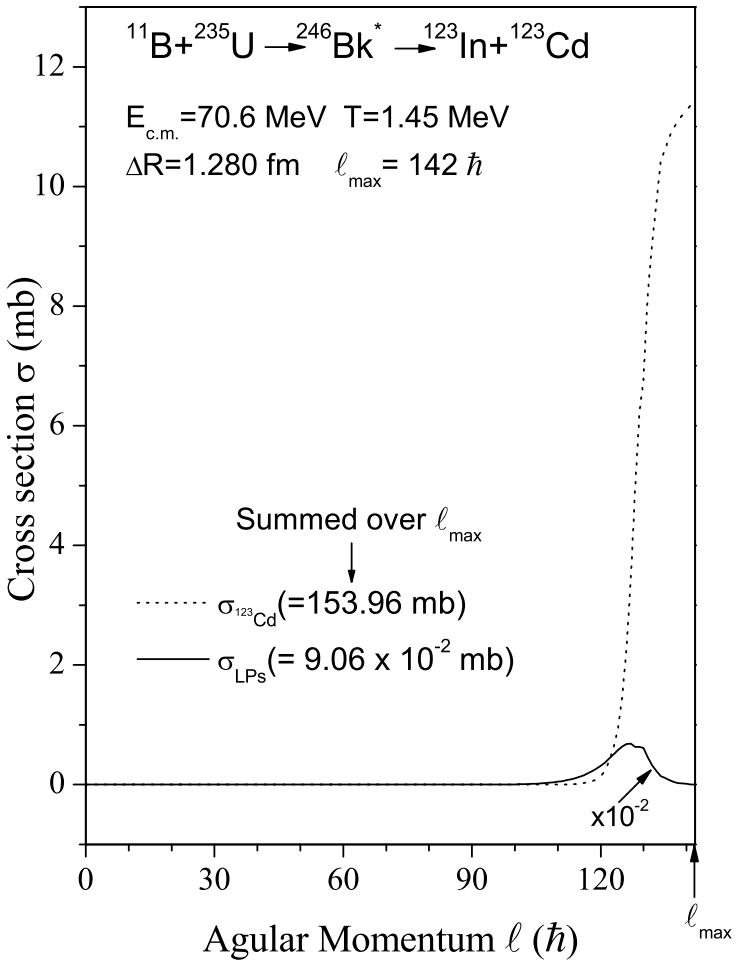

Figure 6.4: Variation of $\sigma_{A=123}$, the cross section for symmetric fission fragment of mass A=123, and the summed up cross section for LPs (A=1-4), the σ_{LPs}, as a function of the angular momentum ℓ for the decay of ^{246}Bk* (formed in ^{11}B+^{235}U reaction at T=1.45 MeV) up to point where $\sigma_{LPs} \rightarrow 0$.

Figure 6.4 presents the calculated cross section as a function of angular momentum for the LPs (A=1-4 summed) compared with the same for symmetric fragment A=A$_{CN}$/2=123 alone, up to ℓ_{max}=142 $\hbar$ where the $\sigma_{LPs}(\ell)$ goes to zero. We note that the contribution of light-particles cross section σ_{LPs}, summed up to ℓ_{max} (given in the

braces of the legend), is almost zero compared to the cross section of symmetric fragment alone.

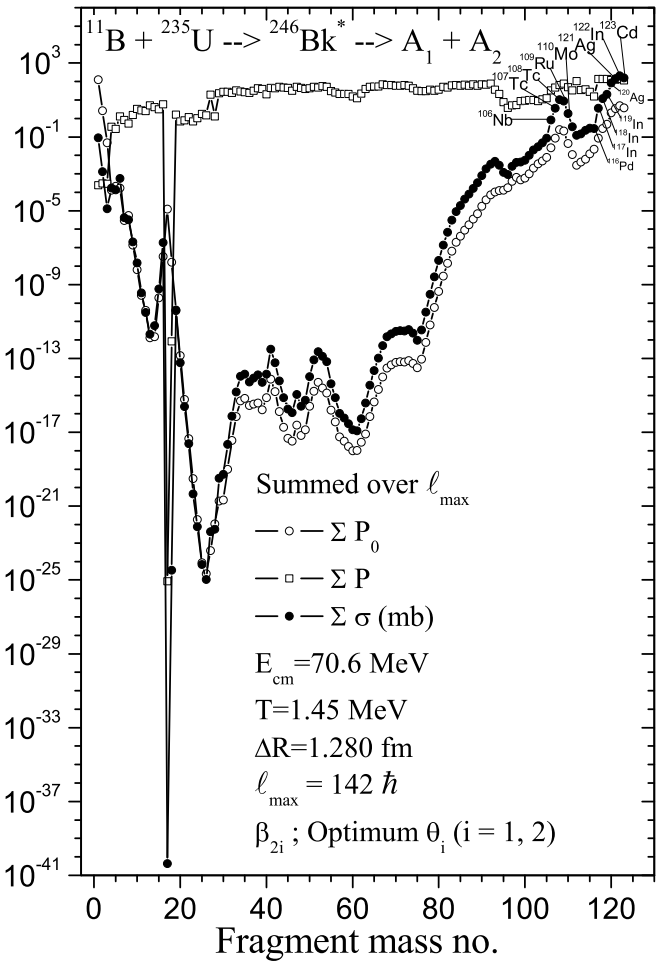

Figure 6.5: The ℓ-summed fragment preformation factor P_0, the penetrability P and the decay cross section σ, with summation over $\ell = \ell_{max} = 142\ \hbar$, as a function of light mass fragment A_2, for the decay of ^{246}Bk*.

Figure 6.5 shows the ℓ=ℓ_{max}-summed preformation factors P_0, the penetrability P and the cross section σ, as a function of the light fragment mass A_2. First, we note that the ℓ-summed P is almost constant ($\sim$10-50) as a function of A_2, except for ^1n where its value is $\sim$100. Hence, P contributes only to the magnitude but not to the structure of the cross section. On the other hand, the ℓ-summed P_0 shows an interesting structure with maximum preformation factor for SF and HMFs windows. This happens because of the inversion process noted in the fragmentation potential (Fig. 6.1) from a favoured asymmetric to favoured symmetric as ℓ increases, or, as is shown in Figure 6.2,

equivalently, for $P_0(A_2)$ plotted for some ℓ-values. Apparently for $\ell > \ell_{max}$, only the very heavy (SF and HMFs) fragments contribute. Thus, in terms of the cross sections in Figure 6.5, we note that, instead of the complete mass spectrum like in ^{48}Cr*, here the very light and the very heavy mass parts of the spectrum are shown to be of interest.

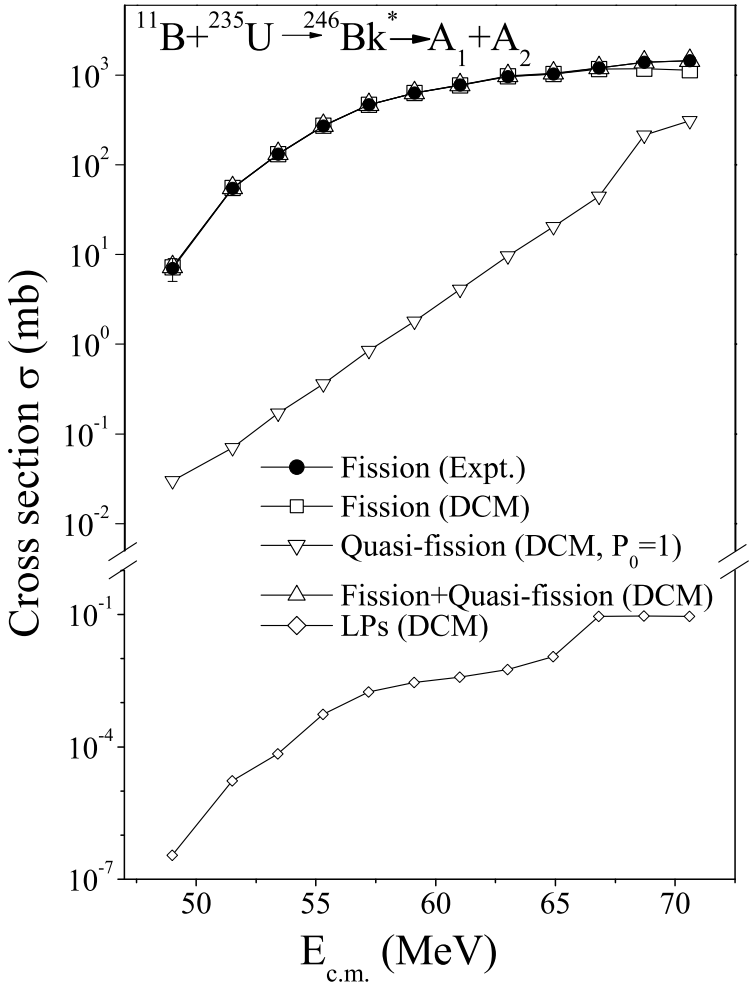

Figure 6.6: The calculated σ_{fus}^{Cal}, σ_{fiss}^{Cal} ($=\sigma_{SF} + \sigma_{HMFs}$), empirical σ_{qf} and σ_{LPs} on DCM for the decay of compound nucleus ^{246}Bk* formed in ^{11}B+^{235}U reaction at various E$_{c.m.}$, compared with experimental data [16] on σ_{fus}^{Expt} ($\equiv \sigma_{fiss}^{Expt}$).

Figure 6.6 gives a comparison of our DCM calculated fission cross sections σ_{fiss}^{Cal} ($=\sigma_{SF} + \sigma_{HMFs}$, hollow squares) at different center-of-mass energies, with the experimental data [16] on σ_{fiss}^{Expt} ($\equiv \sigma_{fus}^{Expt}$, filled circles) for ^{11}B+^{235}U reaction channel. The same result is also presented in Table 6.1 along with other calculated quantities and fitted parameters. With in one parameter fit, the comparison is clearly very good, except at the highest three energies. This discrepency is associated with the presence of a significant

non-compound, quasi-fission contribution at these three energies. This is explicitly calculated on DCM (P_0=1) for the best fit to the empirically estimated σ_{qf} ($=\sigma_{fiss}^{Expt} - \sigma_{fiss}^{Cal}$), also shown in Fig. 6.6 as open down-triangles. The sum of our calculated fission component σ_{fiss}^{Cal} and quasi-fission σ_{qf} is plotted here as σ_{fus}^{Cal} (open up-triangles) which shows an excellent comparison with experimental fusion cross section σ_{fus}^{Expt} ($\equiv \sigma_{fiss}^{Expt}$). Apparently, the quasi-fission cross section contributes only for the top three energies, and is negligibly small at all lower energies. We have also listed in Table 6.1, and plotted in Fig. 6.6, our calculated σ_{LPs} contribution which is also negligibly small at all energies, and decreases with decreasing c.m. energies in agreement with an earlier study [20].

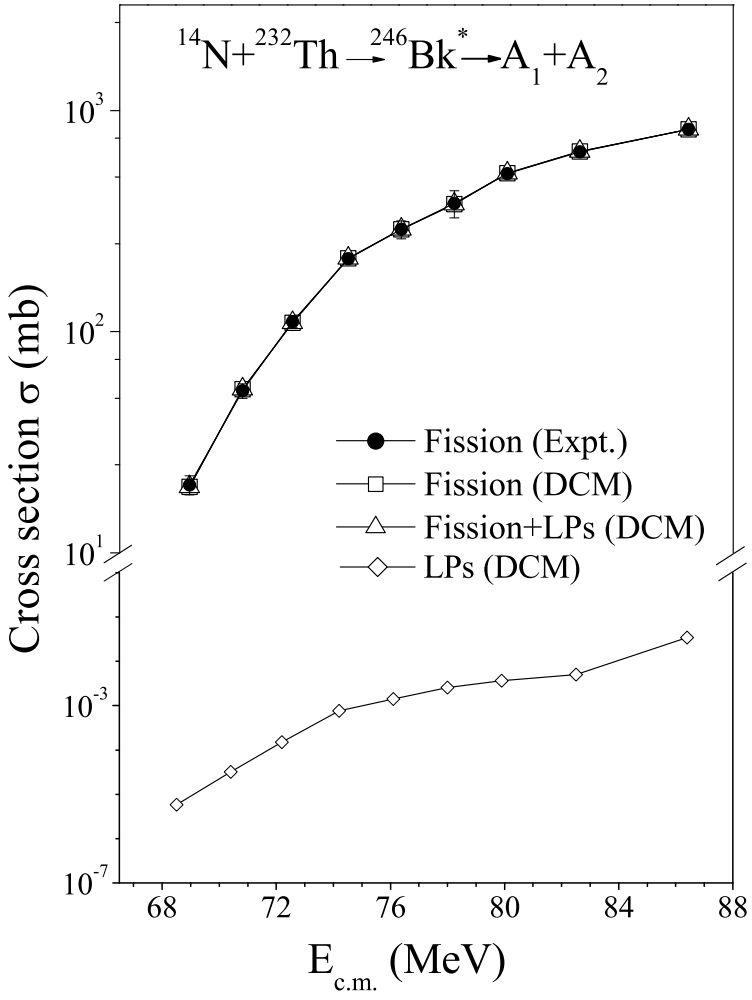

Figure 6.7: Same as for Fig. 6.6, but for $^{14}N+^{232}Th$ reaction.

For the incident channel $^{14}N+^{232}Th$, our results on DCM are presented in Fig. 6.7 and Table 6.2, compared with the experimental data of Ref. [16]. The important result

is that ^{14}N+^{232}Th is a pure CN reaction, showing no quasi-fission contribution, in disagreement with the anisotropy results of Behera *et al.* [16]. Hence, a further experimental check of this result is called for. For the calculated fission cross section, however, the two contributing windows (SF and HMFs) show nearly the same fine- or sub-structure effect, depicted in Fig. 6.8 for both the incoming channels. Here, peak 2 corresponds to fragment mass A=108 for the first three highest energies of channel ^{11}B+^{235}U and for only the first highest energy of channel ^{14}N+^{232}Th, and to fragment mass A=109 for the rest of the energies in both channels since the peak shifts between A=108 and A=109. Peak 1 corresponds to fragment mass A=122. The peaks for the two windows are marked, for example, in Fig. 6.2. An experimental verification of such a sub-structure of fission yields would also be interesting.

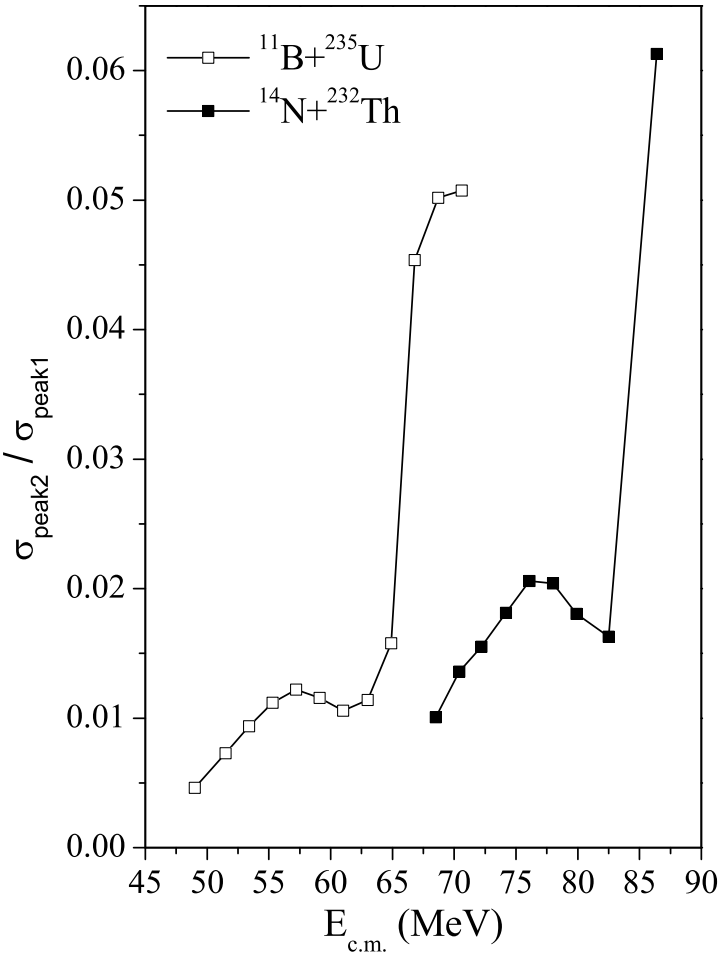

Figure 6.8: The ratios of the peak values of HMFs window and SF window as a function of the incident $E_{c.m.}$.

Finally, we look at the only free parameter of the model, the length parameter $\triangle$R and its connection to ℓ_{max}-value due to the use of the sticking or non-sticking moment of inertia. All the calculations presented above are for the sticking moment of inertia I_S where ℓ_{max} is fixed for $\sigma_{LPs} \rightarrow 0$, and is found to decrease slowly with decreasing $E_{c.m.}$ (see Tables 6.1, 6.2, and Fig. 6.9). Fig. 6.9 gives the variation of $\triangle$R with $E_{c.m.}$ for fission (dotted line with solid squares) and quasi-fission (dotted line with hollow circles) in the case of entrance channel ^{11}B+^{235}U, and for fission alone for the entrance channel ^{14}N+^{232}Th since the quasi-fission component is zero in this later case. We observe that $\triangle$R increases with increasing $E_{c.m.}$ for both the processes, showing a similar behaviour in the case of fission for the two entrance channels (the two straight line fits have nearly the same slope). The interesting result is that fission occurs earlier ($\triangle$R larger) than quasi-fission, and that qf is simply an additional contribution to fusion cross-section rather than a competing process of the type observed in, for example, ^{48}Ca induced reactions on deformed actinides for the synthesis of superheavy nuclei [21].

Next, as an illustrative case, we use for quasi-fission the non-sticking moment of inertia I_{NS} and find that for a similar fit as above for I_S, ℓ_{max} decreases considerably (ℓ_{max}=31 and 23$\hbar$, respectively, for $E_{c.m.}$= 70.6 and 49.0 MeV, instead of 142 and 137$\hbar$) but then $\triangle$R increases significantly (see solid line with crosses in Fig. 6.9(a)), approaching almost the value for fission for use of I_S (the dashed line with solid squares in Fig. 6.9(a)). The interesting result is that for qf, nearly the same $\triangle$R($E_{c.m.}$) variation is obtaned for I_S at ℓ_{max}=66$\hbar$ (solid line with open circles in Fig. 6.9(a)) as is obtained above (solid line with crosses) for I_{NS} at about half the ℓ_{max}-value. The ℓ_{max}=66$\hbar$ match exactly the value given by the finite-range liquid drop model (FRLDM) for mass A=246 compound nucleus (see Fig. 1 in [22]). For heavy ion collisions, however, we consider the sticking moment of ineria as more appropriate, which involves a larger limiting value for ℓ and hence a smaller neck length parameter $\triangle$R. Also, the data on TKE favours the use of I_S, as compared to I_{NS} (see Fig. 7 in [6]).

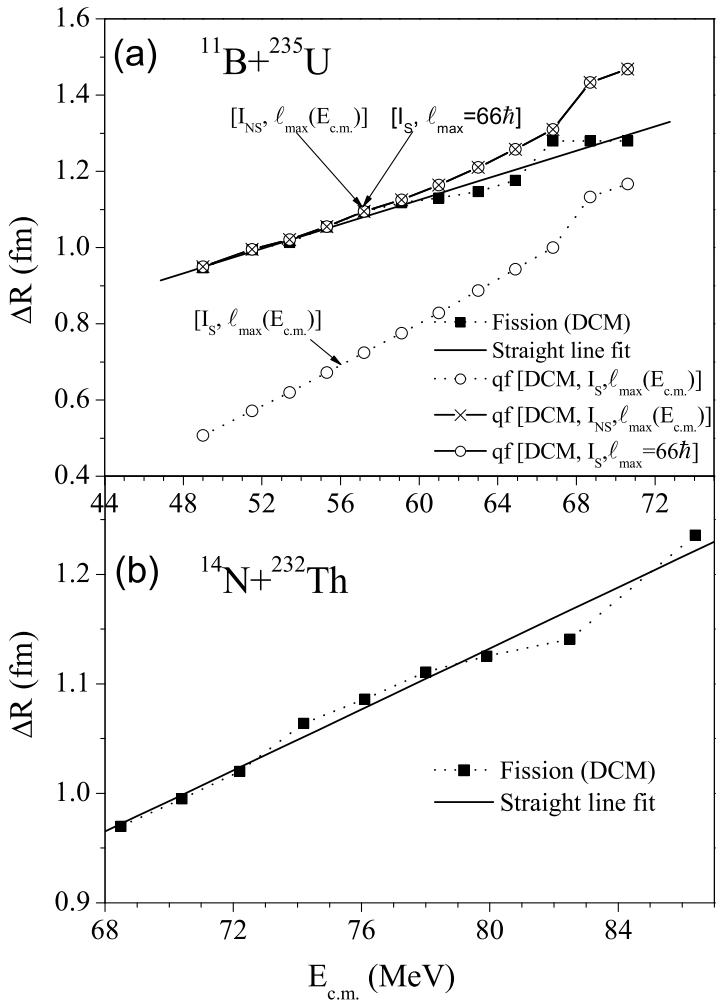

Figure 6.9: (a) The fitted parameter $\triangle$R for fission (dotted line with solid squares) and quasi-fission (dotted line with hollow circles) decays of the CN formed in ^{11}B+^{235}U reaction as a function of $E_{c.m.}$, and (b) the same for fission decay in the case of reaction ^{14}N+^{232}Th. Straight line fits $\triangle R = 0.162 + 0.016E_{cm}$ and $\triangle R = 0.018 + 0.014E_{cm}$, respectively, for ^{11}B+^{235}U and ^{14}N+^{232}Th are also shown as solid lines.

6.3 Summary

In this paper, we have studied the decay of ^{246}Bk* formed in reaction channels ^{11}B+^{235}U and ^{14}N+^{232}Th at different center-of-mass energies. The results of the DCM calculations, using hot (compact) configurations for quadrupole deformed nuclei, are compared with the experimental data [16]. Our calculations clearly demonstrate that, independent of the entrance channel, the decay of ^{246}Bk* in to symmetric and near-symmetric fragments are highly favoured over the light particles (LPs) and intermediate mass fragments (IMFs), in particular at higher angular momentum ℓ-values. At $\ell = \ell_{max}$, the preformation factor P_0

is large and penetration probability P approaches unity for all the symmetric and near-symmetric fragments. Thus, the main contribution to decay cross section comes from the fusion-fission fragments which consist of the symmetric fission (SF) window of mass $A_{CN}/2 \pm 7$ and a heavy mass fragments (HMFs) window of A=106-110 (and complementary fragments) in the immediate neighbourhood of the SF window. Interestingly, the prediction of two windows suggest a fine- or sub-structure of observed fission fragments, not yet analyzed experimentally.

For the entrance channel ^{11}B+^{235}U, the DCM calculations are in good agreement with the experimental data for all c.m. energies, except for the highest three energies. Allowing a contribution from the non-compound quasi-fission (qf) process, makes the comparison very good at all the experimental energies. The cross section for qf, σ_{qf}, is significant for only the top three energies. For the ^{14}N+^{232}Th entrance channel, however, contrary to the experimental observations (of anisotropy), the non-compound nucleus (quasi-fission) contribution is zero, i.e., the DCM calculated σ_{fiss}^{Cal} ($=\sigma_{SF} + \sigma_{HMFs}$) match the measured fission cross section σ_{fiss}^{Expt} ($\equiv \sigma_{fus}^{Expt}$) almost exactly without invoking any quasi-fission contribution. Note, however, that there is a parameter (the length parameter $\triangle$R) to be fitted in this model, which shows a simple linear dependence on the incident c.m. energy, with an almost constant slope for both the entrance channels. The role of sticking versus non-sticking moment of inertia for the limiting angular momentum ℓ_{max} is also studied, which results in an increase of $\triangle$R for the lower ℓ_{max}-value of I_{NS} used in experiments.

Table 6.1: The decay cross sections for LPs, σ_{LP}, the symmetric fission (SF) window (A=A_{CN}/2±7), σ_{SF}, the heavy mass fragments (HMFs) window (A=106-110, and their complementary fragments), σ_{HMFs}, and the quasi-fission (qf) component, σ_{qf}, and their sums σ^{Cal}_{fiss} (=σ_{SF} + σ_{HMFs}) and σ^{Cal}_{fus} (=σ_{qf} + σ^{Cal}_{fiss}), calculated on DCM for different $E_{c.m.}$ for ^{246}Bk* formed in ^{11}B+^{235}U reaction, compared with the experimental fusion (≡ fission) cross-sections [16], σ^{Expt}_{fus} (≡ σ^{Expt}_{fiss}).

				DCM					DCM (P$_0$=1)		DCM	Expt
$E_{c.m.}$	E^{*}_{CN}	T	ℓ_{max}	△R	σ_{LP}	σ^{Cal}_{fiss}(mb)			△R	σ_{qf}	σ^{Cal}_{fus} (= σ^{Cal}_{fiss} + σ_{qf})	σ^{Expt}_{fus} (≡ σ^{Expt}_{fiss})
(MeV)	(MeV)	(MeV)	($\hbar$)	(fm)	(mb)	σ_{SF}	σ_{HMFs}	Sum	(fm)	(mb)	(mb)	(mb)
70.6	55.9	1.449	142	1.2800	9.06×10^{-2}	1080.11	50.46	1130.57	1.167	310.93	1441.50	1440±138
68.7	54.0	1.424	142	1.2800	9.29×10^{-2}	1125.76	51.80	1177.56	1.133	214.44	1392.00	1390±128
66.8	52.0	1.398	141	1.2800	9.03×10^{-2}	1115.45	46.23	1161.68	1.000	44.33	1206.01	1200±112
64.9	50.1	1.372	140	1.1760	1.11×10^{-2}	1017.71	14.54	1032.25	0.943	20.35	1052.60	1030±72
63.0	48.2	1.346	140	1.1470	5.62×10^{-3}	954.51	10.62	965.13	0.887	9.64	974.77	960±95
61.0	46.3	1.320	140	1.1300	3.82×10^{-3}	761.18	8.41	769.59	0.828	4.08	773.67	772±54
59.1	44.4	1.293	140	1.1171	2.91×10^{-3}	621.96	7.31	629.27	0.775	1.81	631.08	630±40.0
57.2	42.5	1.266	140	1.0940	1.75×10^{-3}	461.40	5.32	466.73	0.724	0.85	467.58	465±33
55.3	40.6	1.237	139	1.0540	5.41×10^{-4}	269.36	2.70	272.06	0.672	0.36	272.42	270±20.0
53.4	38.7	1.208	139	1.0130	6.94×10^{-5}	130.88	1.06	131.94	0.620	0.17	132.11	132±14.0
51.5	36.8	1.179	137	0.9940	1.70×10^{-5}	54.78	0.35	55.13	0.572	0.07	55.20	54.6±5.3
49.0	34.3	1.139	137	0.9470	3.51×10^{-7}	7.20	0.03	7.23	0.507	0.03	7.26	7.00±2.0

Table 6.2: Same as for Table 6.1, but for the reaction ^{14}N+^{232}Th, and without the quasi-fission (qf) component.

				DCM					Expt
$E_{c.m.}$	E^*_{CN}	T	ℓ_{max}	$\triangle$R	σ_{LP}	σ^{Cal}_{fiss}(mb)			$\sigma^{Expt}_{fiss}(\equiv \sigma^{Expt}_{fus})$
(MeV)	(MeV)	(MeV)	($\hbar$)	(fm)	(mb)	σ_{SF}	σ_{HMFs}	Sum	(mb)
86.4	60.9	1.511	142	1.2360	3.45×10^{-2}	782.04	41.24	823.29	823±40
82.5	57.0	1.463	142	1.1410	5.05×10^{-3}	641.49	10.73	652.21	650±26
79.9	54.4	1.429	142	1.1255	3.65×10^{-3}	510.35	9.79	520.14	518±24
78.0	52.5	1.404	141	1.1110	2.58×10^{-3}	369.47	7.48	376.95	380±53
76.1	50.6	1.379	141	1.0860	1.41×10^{-3}	285.02	5.45	290.48	290±27
74.2	48.7	1.353	140	1.0640	7.57×10^{-4}	211.12	3.46	214.58	214±11
72.2	46.8	1.327	140	1.0200	1.51×10^{-4}	108.27	1.47	109.74	111±07
70.4	44.9	1.300	140	0.9950	3.20×10^{-5}	54.35	0.64	55.00	54±04
68.5	43.0	1.273	139	0.9700	5.77×10^{-6}	19.69	0.17	19.85	20.3±2

Bibliography

[1] J. Gomez del Campo, R. L. Auble, J. R. Beene, M. L. Halbert, H. J. Kim, A. D'Onofrio, and J. L. Charvet, Phys. Rev. C **43**, 2689 (1991).

[2] T. Matsuse, C. Beck, R. Nouicer, and D. Mahboub, Phys. Rev. C **55**, 1380 (1997).

[3] L. G. Moretto Nucl. Phys. A **247**, 211 (1975).

[4] R. Vandenbosch and J.R. Huizenga, *Nuclear Fission*, Academic, New York, 1973.

[5] S. J. Sanders, A. Szanto de Toledo, and C. Beck, Phys. Rep. **311**, 487 (1999).

[6] R. K. Gupta, R. Kumar, N. K. Dhiman, M. Balasubramaniam, W. Scheid, and C. Beck, Phys. Rev. C **68**, 014610 (2003).

[7] M. Balasubramaniam, R. Kumar, R. K. Gupta, C. Beck, and W. Scheid, J. Phys. G: Nucl. Part. Phys. **29**, 2703 (2003).

[8] R. K. Gupta, Acta Phys. Hung. (N.S.) Heavy Ion Phys. **18**, 347 (2003).

[9] R. K. Gupta, M Balasubramaniam, R. Kumar, D. Singh, and C. Beck Nucl. Phys. A **738**, 479c (2004).

[10] R. K. Gupta, M. Balasubramaniam, R. Kumar, D. Singh, C. Beck, and W. Greiner, Phys. Rev. C **71**, 014601 (2005).

[11] R. K. Gupta, M. Balasubramaniam, R. Kumar, D. Singh, S. K. Arun, and W. Greiner, J. Phys. G: Nucl. Part. Phys. **32**, 345 (2006).

[12] B. B. Singh, M. K. Sharma, R. K. Gupta, and W. Greiner, Int. J. Mod. Phys. E **15**, 699 (2006).

[13] S. K. Arun and R. K. Gupta, Phys. Rev. C (2008)- submitted.

[14] B. B. Singh, M. K. Sharma and R. K. Gupta, Phys. Rev. **C 77**, 054613 (2008).

[15] B. R. Behera, S. Jena, M. Satpathy, S. Kailas, K. Mahata, A. Shrivastava, A. Chatterjee, S. Roy, P. Basu, M. K. Sharan, and S. K. Datta, Phys. Rev. C **64**, 041602(R) (2001).

[16] B. R. Behera, M. Satpathy, S. Jena, S. Kailas, R. G. Thomas, K. Mahata, A. Chatterjee, S. Roy, P. Basu, M. K. Sharan, and S. K. Datta, Phys. Rev. C **69**, 064603 (2004).

[17] S. Kailas, Phys. Rep. **284**, 381 (1997).

[18] R. K. Gupta, M. Balasubramaniam, R. Kumar, N. Singh, M. Mahhas, and W. Greiner, J. Phys. G: Nucl. Part. Phys. **31**, 631 (2005).

[19] G. N. Knyazheva, E. M. Kozulin, R. N. Sagaidak, A. Yu. Chizhov, M. G. Itkis, N. A. Kondratiev, V. M. Voskressensky, A. M. Stefanini, B. R. Behera, L. Corradi, E. Fioretto, A. Gadea, A. Latina, S. Szilner,M. Trotta, S. Beghini, G. Montagnoli,F. Scarlassara, F. Haas, N Rowley, P. R. S. Gomes, and A. Szanto de Toledo, Phys. Rev. C **75**, 064602 (2007).

[20] H. Delagrange, C. Gregoire, F. Scheuter, and Y. Abe, Z. Phy A **323**, 437 (1986).

[21] M. G. Itkis, A. A. Bogatchev, I. M. Itkis, M. Jandel, J. Kliman, G. N. Kniajeva, N. A. Kondratiev, I. V. Korzyukov, E. M. Korzulin, L. Kruppa, Yu. Ts. Oganessian, I. V. Pokrovski, V. A. Ponomarenko, E. V. Prokhorova, A. Yu. Rusanov, V. M. Voskresenski, A. A. Goverdovski, F. Hanappe, T. Materna, N. Rowley, L. stuttge, G. Giardina, and K. J. Moody, J. Nucl. and Radiochem. Sciences **3**, 57 (2002).

[22] C. Beck and A. Szanto de Toledo, Phys. Rev. C **53**, 1989 (1996).

Chapter 7

Summary

In this thesis, we have studied the possible decay modes of various nuclear systems. The reaction dynamics of hot and rotating light as well as heavier compound systems at low energies have been studied extensively. The phenomenon of cluster radioactivity has also been investigated for the possible effects of oriented nuclei besides well established role of closed shells in the process. The preformed cluster-decay model (PCM) is used for this purpose. For the dynamics of excited compound systems, we have used the dynamical cluster decay model (DCM), including the deformations and orientations of nuclei. The DCM is an extension of PCM for the decay of excited nuclei.

An overview of the current status of research in the related aspects of nuclear physics and various models have been discussed in Chapter 1, specifically pertaining to heavy ion reaction dynamics and the process of cluster radioactivity. For successful formation of heavy nuclei, deep understanding of fusion-fission process of a compound nucleus formed in heavy ion reaction is essential. Nuclear shapes, i.e., the deformations and orientations of nuclei, during fusion reactions change the interaction barrier (its height as well as position) thereby affecting the dynamics of reaction process. In the fusion of deformed and oriented nuclei, the distance between mass centers of massive reaction partners relies on the orientation of the deformed nuclei. The compound nucleus (CN) is normally in an excited state depending upon the energy of reaction partners. It looses this excitation energy in various ways, depending upon the mass of CN formed. The role of angular mo-

mentum, excitation energy, entrance channel effects, together with the effects of deformed and oriented nuceli, are also significant in the process.

As a first step towards applying the DCM, for studying the decay of excited compound nucleus, we have carried out an extensive work for obtaining the temperature T-dependent binding energies. The T-dependent binding energy B of a nucleus is given as the sum of T-dependent liquid drop energy $V_{LDM}(T)$ and shell correction $\delta U(T)$. The macroscopic liquid drop energy V_{LDM} of the reaction partners or decaying fragments plays an important role in the the collective potentials used in DCM. All the potentials (Coulomb, proximity and the centrifugal) are temperature dependent and also include the effects of deformations and orientations of the interacting nuclei. So, temperature dependence of liquid drop energy $V_{LDM}(T)$ is essential, which has been calculated by using the T-dependent liquid drop model of Davidson et. al., based on the well established semi-empirical mass formula of Seeger. Large amount of data has become available since the inception of Seeger's formulae in 1961, which needed a revival now. In an effort towards this direction, we have refitted, the bulk $\alpha(0)$ and neutron proton asymmetry a_a constants of Seeger's formula at T=0. The fitted constants are compiled in Table 3.1. Here the deformation effects in V_{LDM} and in shell correction δU are also included to some extent since we essentially use the experimental binding energies split into two contributions (V_{LDM} and δU), and then temperature dependence is included explicitly. This work will surely help to reformulate the liquid drop energy in context of present day understanding i.e. refitting of all the constants and their temperature dependence.

As a first application, we have used the DCM to study the entrance-channel effects in the decay of hot and rotating CN ^{48}Cr, formed in a symmetric ^{24}Mg+^{24}Mg and very asymmetric ^{36}Ar+^{12}C reaction at E$_{c.m.}$=44.4 and 47.0 MeV, respectively. In this work, we took the shapes of nuclei as spherical, assuming the role of deformed nuclei being prominent in the heavy mass region. The decay of a hot and rotating CN, formed in light heavy-ion reactions, consists of multiple light particles, LPs (n, p, α and γ-rays) or evaporation residue and intermediate mass fragments, IMFs (with $2 < Z < 10$ and

5≤A≤20) emission. In DCM, both the LPs and IMFs in the decay of $^{48}Cr^*$ are treated identically as the dynamical collective mass motion of preformed fragments or clusters through a barrier, i.e. quantum mechanical tunneling of clusters that are considered preborn with different probabilities before they actually penetrate the barrier. Thus, the cluster preformation probabilities contain the structure effects of the CN, that are found to be important in the description of the measured yields in the experiments under study. Both the LPs and the IMFs, though treated on same footing, have different characteristics. At lower l-values, the LPs are energetically more favourable, whereas the same is true of IMFs at higher l-values. Also P_0 as function of ℓ-values shows that the behavior of all LPs is different from that of the IMFs. The lower ℓ values contribute mostly to the LP cross section σ_{LP} and that the higher ℓ values contribute to IMFs production cross section σ_{IMF}. Thus role of angular momentum is quite significant in the reaction dynamics of excited compound system.

Though some of the characteristic quantities of the model do show entrance channel effects, the calculated cross-sections are found to be entrance-channel independent for the decay of the compound nucleus $^{48}Cr^*$. The σ_{LP} becomes zero at the same l_{max}=25$\hbar$ for the two entrance channels, indicating channel independence. This study confirms the entrance-channel independence of the decay of compound nucleus $^{48}Cr^*$ formed due to different target-projectile combinations with similar excitation energies. The measured decay cross-sections are in good agreement with the experimental data (Table 4.1). The calculated $\overline{TKE}$ also reproduces the experimental data, though at an $\ell < \ell_c$-value. The calculations are worked out in terms of only one parameter, the neck-length parameter $\triangle R$, that depends on the total kinetic energy of the fragments TKE(T) at given temperature T of the CN. Note that the $\triangle R$ is taken to be η-dependent, whereas the average $\overline{\triangle R}$ (= 1.10 fm, taken in this study) assimilates the effects of both the deformations (if any) and η dependence. The calculations have been done for both the choices i.e. $\triangle R(\eta)$ and $\overline{\triangle R}$ (given in Table 4.1). It is nearly difficult to choose between the $\overline{\Delta R}$ and $\Delta R(\eta)$ results for DCM, though the constant $\overline{\Delta R}$ seems to work better on the whole.

Next, we look for the role of deformations and orientations of nuclei, first for the ground state decays of heavier nuclei. These effects are duly incorporated in PCM for investigating the cluster radioactive decays of parents which are deformed. Our study pertains to the spontaneous cluster decays of deformed ^{222}Ra and heavier actinide parents. The interesting feature of the study is that in all the chosen cluster decays, the daughter nucleus is always the spherical ^{208}Pb. The role of deformations and orientations has been investigated besides the shell closure effects. For the ground state decay of parent nuclei we have considered optimum orientations for deformed daughters and clusters in elongated, non-compact (cold) configuration. The calculated decay half-lives for all such cluster-decays are in good agreement with measured data. Both the key quantities of PCM, the preformation probability P_0 and penetrability P, show noticeable changes with and without invoking deformation and orientation effects as shown in Table 5.2. We find that results are reasonably good for quadrupole deformations (β_2) while with inclusion of higher multipole deformations (β_3, β_4) the results become anomalous, possibly due to the extrapolations used in extracting higher multi-pole deformations.

It is almost established that a light compound nucleus, CN (A_{CN} ~40-80) formed in low energy heavy ion reactions, decays by emitting LPs, and is accompanied by a small (5-10%) component of so-called IMFs. We have obtained equivalently small contribution of IMFs in comparison to LPs in decay of $^{48}Cr^*$. As a further application of DCM we have applied it to investigate the reaction dynamice of heavier CN (A_{CN} >200) for which fission is prominent. In order to do that, next, we have chosen to apply the DCM to a heavier nuclear system $^{246}Bk^*$ (formed in similar entrance channel reactions $^{11}B+^{235}U$ and $^{14}N+^{232}Th$, at different $E_{c.m.}$), where the deformation and orientation effects are almost indispensable. These calculations have been done using quadrupole deformations and optimally oriented hot (compact) configurations for decaying products. The main decay mode here is (symmetric and near symmetric) fission which in DCM have been taken as an extreme case of IMFs, the heavier mass fragments, HMFs ($A_{CN}/2 \pm 7$ and A=106-110 plus complementary fragments, taken in this case), observed together with or without the LPs and IMFs. In addition, there can be effects of non-compound nu-

cleus decays, like the pre-equilibrium fission, quasi-fission (qf) or deep inelastic collisions (DIC), etc., occuring mostly at higher incident center-of-mass (c.m.) energies. We note that the LPs and IMFs are favored (lower in energy) at ℓ=0, but at higher ℓ-values the symmetric and near-symmetric fragments become more favored. At ℓ=142$\hbar$, a strong minima is obtained for symmetric fragments $A_{CN}/2 \pm 7$ (SF Window) and corresponding to heavy mass fragments A=106-110 (and complementary fragments), referred to as the HMFs window. This result of a favored asymmetric to a favored symmetric division with increase in ℓ-value is also shown by the preformation factor P_0. Penetrability, P is very small for the emission of LPs. The ℓ-summed preformation factors P_0, the penetrability P and the cross section σ, shows that P contributes only to the magnitude but not to the structure of the cross section. On the other hand, the ℓ-summed P_0 shows an interesting structure with maximum preformation factor for SF and HMFs windows. We find that major contribution to fission (equivalently, fusion) cross section arises from the SF window, and that the HMFs window contributes to a maximum of $\sim 5\%$ and that too only for the first few higher c.m. (top three) energies (Table 6.1).

We see that entrance channel also plays its role in terms of the quasi-fission contribution specifically at higher c.m. energies, due to the ^{11}B+^{235}U reaction in contradiction with the measured anisotropy effects which indicate the other entrance channel ^{14}N+^{232}Th to contain the non-compound nucleus contribution. In our calculations, for the case of negligible or zero contributions from LPs and IMFs, calculated fusion cross-sections are given as sum of HMF cross-sections σ_{HMF}, SF cross-sections σ_{SF} and quasi-fission cross-sections σ_{qf} i.e. $\sigma_{fus}^{Cal} = \sigma_{HMF}+\sigma_{SF}+\sigma_{qf} = \sigma_{fiss}^{Cal}+\sigma_{qf}$, to be compared with experimentally measured fusion cross-sections σ_{fus}^{Expt} ($=\sigma_{fiss}^{Expt}$). The quasi-fission component is obtained empirically as the difference between the experimentally measured and our calculated fission comoponents, i.e., $\sigma_{qf} = \sigma_{fiss}^{Expt} - \sigma_{fiss}^{Cal}$. As given in Table 6.1, the quasi-fission cross section contributes only in case of ^{11}B+^{235}U reaction and for the top three energies only, and is negligibly small at all lower energies. Also, the calculated σ_{LPs} contribution is negligibly small at all energies, and decreases with decreasing c.m. energies. For the calculated fission cross section, the two contributing windows (SF and HMFs) show nearly

the same fine- or sub-structure effect for both the entrance channels. An experimental verification of such a sub-structure of fission yields could be extremely interesting.

In these calculations the fitted values of $\triangle R$ (Table 6.1 and 6.2) are not shown to be an average $\overline{\triangle R}$ value, unlike for the light CN $^{48}Cr^*$. The reason for the same is that for light CN studies we assumed spherical shapes of the fragments, but for heavier CN $^{246}Bk^*$ the deformation effects are indispensable and the value of R_t will not only depend upon deformation of complementary fragment but also on its orientation as well, which is not the case with $^{48}Cr^*$. For $^{246}Bk^*$, the value of $\triangle R$ (neck length parameter) is shown to depend on limiting angular momentum, which in turn depends on the use of sticking or non-sticking moment of inertia for angular momentum effects. All the calculations presented in Tables 6.1 and 6.2 are for the sticking moment of inertia I_S where ℓ_{max} is fixed for $\sigma_{LPs} \rightarrow 0$, and is found to decrease slowly with decreasing $E_{c.m.}$. We observe that $\triangle$R increases with increasing $E_{c.m.}$ for both the processes (fission and quasi-fission), showing a similar behaviour in the case of fission for the two entrance channels (the two straight line fits have nearly the same slope). The interesting result is that fission occurs earlier ($\triangle$R larger) than quasi-fission, and that qf is simply an additional contribution to fusion cross-section rather than a competing process of the type observed in, for example, ^{48}Ca induced reactions on deformed actinides for the synthesis of superheavy nuclei. As an illustrative case, we use for quasi-fission the non-sticking moment of inertia I_{NS} and find that for a similar fit as for I_S, ℓ_{max} decreases considerably (ℓ_{max}=31 and 23$\hbar$, respectively, for $E_{c.m.}$= 70.6 and 49.0 MeV, instead of 142 and 137$\hbar$) but then $\triangle$R increases significantly. The interesting result is that for qf, nearly the same $\triangle$R($E_{c.m.}$) variation is obtained for I_S at ℓ_{max}=66$\hbar$ as is obtained for I_{NS} at about half the ℓ_{max}-value. The ℓ_{max}=66$\hbar$ match exactly the value given by the finite-range liquid drop model (FRLDM) for mass A=246 compound nucleus. For heavy ion collisions, however, we consider the sticking moment of ineria as more appropriate, which involves a larger limiting value for ℓ and hence a smaller neck length parameter $\triangle$R.

Finally, it is relevant to mention here that the experimental studies have started an-

alyzing the role of orientation degrees of freedom for deformed nuclei in the measured fusion-fission cross-sections, though the use/identification of the actually polarized (or oriented at a particular angle) nuclei is still to be realized. Such studies will help explore the yet unknown landscapes in order to approach towards the "island of stability" and to extend the periodic table further.